Transcriptome profiles of porcine oocytes and their corresponding cumulus cells reveal functional gene regulatory networks

by

Katelyn Marie Kimble

A thesis submitted to the Graduate Faculty of
Auburn University
in partial fulfillment of the
requirements for the Degree of
Master of Science

Auburn, Alabama
August 4, 2018

Keywords: oocyte, cumulus cells, signaling, transcriptome, porcine

Approved by

Fernando Biase, Chair, Assistant Professor, Dept. of Animal Sciences
Paul Dyce, Assistant Professor, Dept. of Animal Sciences
Julie Gard, Professor, Dept. of Clinical Sciences
Jacek Wower, Professor, Dept. of Animal Sciences

Abstract

The oocyte acquires developmental competence as it progresses through folliculogenesis. It does so, by communicating with the surrounding cumulus cells in a bidirectional fashion. Analyses of single oocytes are essential for further clarification of these molecular mechanisms. Standard protocols to obtain RNA for single-cell RNA-Seq involve RNA extraction kits that select for mRNAs or cell lysis procedures, which present limitations when the oocyte is the cell of interest. We adapted the phenol-chloroform procedure for the purification of total RNA from single oocytes with modifications that included the use of Phasemaker™ tubes, a second chloroform wash, and the precipitation of the RNA with glycogen in microcentrifuge tubes. We profiled the total RNA of single oocytes (bovine and porcine), and observed distinct peaks for small RNAs, 18S, and 28S. We amplified the total mRNA and observed DNA fragments longer than 5000 bp in length, suitable for single-cell RNA sequencing. We applied this approach to sequence the transcriptome of 17 prepubertal porcine oocytes and their corresponding cumulus cells. We hypothesized that the transcript profiles of the cumulus cells and oocyte display distinct gene regulatory networks within the oocyte and cumulus cells. We quantified 7277 genes expressed in the cumulus-oocyte

complex. Independent clustering of co-expressed genes revealed critical biological functions for the oocyte, such as regulation of transcription, stem cell population maintenance, and insulin receptor signaling pathway. In cumulus cells translation, cellular response to insulin stimulus, and regulation of transcription emerged as critical functions among co-expressing genes. In summary, we developed an approach to extract total RNA from single oocytes. The sequencing of single oocytes and their surrounding somatic cells revealed coordinated expression of hundreds of genes that formed functional regulatory networks.

Acknowledgements

First and foremost, I would be remiss if I did not thank my mentor, Dr. Fernando Biase, for all of his insight, guidance, and support of my endeavors – future and present.

Secondly, I would like to express my utmost gratitude to Mr. Brian Anderson and his associates at the Auburn University Swine Research and Education Center and to Mr. Barney Wilborn and his associates at the Auburn University Lambert-Powell Meats Lab. Both managers and the corresponding facilities allowed us to obtain porcine ovaries, without which we would not be able to conduct this work.

I am eternally grateful to those who have invested years of their lives in me. At Southwestern University, Dr. Martín Gonzalez and Dr. Fay Guarraci. You taught me to love science and how to find the amazement on a molecular level. I hope I am making you proud.

To my family, thank you for instilling in me an insatiable curiosity and drive to learn more. I cannot imagine a day in my life where I will ever stop learning and my upbringing is heavily responsible for this.

To my lab mates both within the Biase lab and my adoptive lab mates from the Dyce lab, I have found forever friends in you and I can't wait to see where life takes us. To Brock Griffin, to my fellow Texan, thank you for being the Jim to my Dwight these last two years – it wouldn't have been the same without you. And finally, to my beautiful Luca and Svarta, I work hard so you can have the biggest back yard. Thank you for begrudgingly living in an apartment these last two years.

Table of Contents

List of Tables

List of Figures

List of Abbreviations

acDNA	Amplified cDNA
cDNA	Complementary DNA
CL	Corpus Luteum
COC	Cumulus-Oocyte Complex
DNA	Deoxyribonucleic Acid
E	Embryonic Day
ER	Endoplasmic Reticulum
ESC	Embryonic Stem Cells
GV	Germinal Vesicle
GVBD	Germinal Vesicle Breakdown
MI	Metaphase I
MII	Metaphase II
miRNA	micro RNA
mm	Millimeter

mRNA	messenger RNA
mtDNA	Mitochondrial DNA
MPF	Maturation Promoting Factor
MVB	Multivesicular Bodies
N	Number
nM	Nanomolar
nt	Nucleotide
OSF	Oocyte Secreted Factors
PGC	Primordial Germ Cell
polyA+	Polyadenylated
P4	Progesterone
RNA	Ribonucleic Acid
RNP	Ribonucleoprotein
rRNA	Ribosomal Ribonucleic Acid
SCNT	Somatic Cell Nuclear Transfer
tRNA	Transfer Ribonucleic Acid
TZP	Transzonal Projection
U	Units

UTR	Untranslated Region
WGCNA	Weighted Gene Correlation Network Analysis
ZP	Zona Pellucida
µl	Microliter
µM	Micromolar
µm	Micron

List of gene symbols according to the HUGO Gene Nomenclature Committee

ABHD4	Abhydrolase Domain Containing 4
AC3	Adenylate Cyclase 3
AGO2	Argonaute 2, RISC Catalytic Component
ALK	ALK Receptor Tyrosine Kinase
ALIX	Programmed cell death 6 interacting protein
AMH	Anti-Müllerian hormone
AQP3	Aquaporin 3
AREG	Amphiregulin
ARF6	ADP Ribosylation Factor 6
ARHGAP22	Rho GTPase activating protein 22
ARRDC1	Arrestin Domain Containing 1
BMP	Bone Morphogenetic Protein
BMP2	Bone Morphogenetic Protein 2

BMP4	Bone Morphogenetic Protein 4
BMP6	Bone Morphogenetic Protein 6
BMP8	Bone Morphogenetic Protein 8
BMP15	Bone Morphogenetic Protein 15
BMPRII	Bone Morphogenetic Protein Receptor Type 2
BTC	Betacellulin
BUB1	BUB1 Mitotic Checkpoint Serine/Threonine Kinase
cAMP	Cyclic adenosine monophosphate
CD63	CD63 molecule
cGMP	Cyclic guanosine monophosphate
CNP	C-type natriuretic peptide
COL18A1	Collagen type XVIII alpha 1 chain
COX2	Cytochrome c oxidase subunit II
CPE	Carboxypeptidase E
CPEB	Cytoplasmic polyadenylation element-binding protein
CX43	Connexin 43
CYP19A1	Cytochrome P450 family 19 subfamily A member 1
DPPA3	Developmental pluripotency-associated 3
eIF4E	Eukaryotic translation initiation factor 4E

eIF4G	Eukaryotic translation initiation factor 4G
eIF4F	Eukaryotic translation initiation factor 4F
EGF	Epidermal Growth Factor
EREG	Epiregulin
ERK	Extra-cellular signal related kinase
ESCRT	Endosomal sorting complexes required for transport
FGF	Fibroblast growth factor
FGF11	Fibroblast growth factor 11
FOXL2	Forkhead Box L2
FSH	Follicle Stimulating Hormone
FST	Follistatin
GDF9	Growth Differentiation Factor 9
GATA4	GATA Binding Protein 4
GLD2	Terminal nucleotidyl transferase 2
GPC4	Glypican 4
GnRH	Gonadotropin releasing hormone
G_s	G protein subunits alpha, group s
GTPase	Guanosine triphosphatase

H2A	Histone cluster 2 H2A family member c
HIF	Hypoxia Inducible Factor
HOXA1	Homeobox A1
HOXB1	Homeobox B1
hnRNPA2B1	Heterogeneous Nuclear Ribonucleoprotein A2/B1
HPG Axis	Hypothalamic–pituitary–gonadal Axis
HRS	Hepatocyte growth factor-regulated tyrosine kinase substrate
HSPA5	Heat shock protein family A (Hsp70) member 5
HSP90AB1	Heat shock protein 90 alpha family class B member 1
IGF-I	Insulin-like Growth Factor 1
IGFBP4	Insulin like growth factor binding protein 4
INHBA	Inhibin subunit beta A
KIT	KIT proto-oncogene receptor tyrosine kinase
KITLG	KIT ligand
LH	Luteinizing Hormone
LHR	Luteinizing Hormone Receptor
LHX9	LIM homeobox 9
LIF	Leukemia inhibitory factor

MAD2	Mitotic arrest deficient 2
MAPK	Mitogen-activated protein kinase
MLCK	Myosin light-chain kinase
MOS	*c-mos* pro-oncogene
mTORC1	mTOR Complex 1
MYS2	Y-box binding protein 2
NANOS3	Nanos C2HC-Type Zinc Finger 3
NPRB	Natriuretic peptide receptor-B
nSMase2	Neutral sphingomyelinase2
PARN	PolyA+-specific ribonuclease
PABP	PolyA+-binding protein
PAP	PolyA+ polymerase
PDCD6IP	Programmed Cell Death 6 Interacting Protein
PDE3A	Phosphodiesterase 3A
PGF2α	Prostaglandin F2alpha
PI3K	Phosphatidylinositol-3-kinase
PIP3	Phosphatidylinositol 3,4,5 trisphosphate
PKA	Protein kinase A

PLD	Phospholipase D
PLP	Pyridoxal-5'-phosphate
PRDM1	PR/SET Domain 1
PRDM14	PR/SET Domain 14
PTEN	Phosphatase and Tensin Homolog
PSAP	Prosaposin
SEPT7	Septin 7
SIAH2	Siah E3 Ubiquitin Protein Ligase 2
SF1	Splicing factor 1
SMAD1	SMAD family member 1
SMAD4	SMAD family member 4
SMAD5	SMAD family member 5
SNAP23	Synaptosome Associated Protein 23,
SNARE	Soluble NSF Attachment Protein Receptor
SPRY1	Sprouty RTK signaling antagonist 1
T	Brachyury (T-box transcription factor T)
TFR	Transferrin receptor protein 2
TGFβ	Transforming growth factor beta

TNFAIP6	TNF alpha induced protein 6
TSC1	Tuberous sclerosis 1
TSC2	Tuberous sclerosis 2
TSG101	Tumor susceptibility gene 101
VAMP1	Vesicle Associated Membrane Protein 1
VEGF	Vascular endothelial growth factor
WNT	Wingless-type MMTV integration site family
WT1	Wilms tumor 1
YY1	YY1 transcription factor

1.Introduction

1.1.An overview of the oocyte in the context of reproduction

Within the female reproductive system, the basis of life is formed around the egg or oocyte. The quality of these oocytes is, therefore, a critical determinant of life or death. The oocyte itself is positioned within an ovarian follicle, but the regulation of its physiology is controlled by factors resulting from the hormonal release of the hypothalamic-pituitary-gonadal (HPG) axis (Scaramuzzi et al. 2011). The delicate balance of these hormones dictates the progress of folliculogenesis, with the developmental competence of the oocyte, or the ability of the oocyte to be successfully fertilized and progress to the blastocyst stage, under constant influence from its environment (Monniaux 2016).

In most vertebrates, the propagation of offspring starts with the fertilization of a developmentally competent oocyte with one sperm, leading to the formation of an embryo, which will further develop into an adult form. Although a major player in the natural reproductive world, some specialized animals, such as the bonnethead shark (Edwards 2007), get around this fertilization requirement of sperm by participating in parthenogenesis. Artificial technologies, such as somatic cell nuclear transfer (SCNT) also circumvent the sperm requirement (Wilmut et al. 2015). Even presently, in a time when embryonic stem cells (ESCs) are being successfully differentiated into a number of specialized cells, a heavy emphasis in the field is being placed on generating oocytes or oocyte-like cells from ESCs which are then capable of producing viable offspring (Hayashi et al. 2017). Taken

together, advances in reproductive technologies, such as SCNT and production of oocyte-like cells from ESCs, signify that, with or without its naturally occurring counterpart of sperm, the oocyte is capable of, and responsible for producing a viable offspring. Furthermore, with the end goal of the majority of currently available assisted reproductive techniques being to produce viable offspring, modern advances in *in vitro* maturation, fertilization, and embryo culture production have greatly improved the ability to do so.

Even with the years of work behind us concerning reproduction, and specifically, oocyte developmental competence, the field is still lacking in knowledge surrounding the molecular events that control maturation and fertilization. Throughout folliculogenesis, the oocyte relies on a dialogue with the surrounding cumulus cells in order to successfully acquire developmental competence (Monniaux 2016). Furthermore, transcriptome profiling of both cumulus cells and oocytes across several species are associated with the developmental competence of the oocyte (Nivet et al. 2013; Biase 2017). Regardless of these connections, little is known of the molecular networks connecting the oocyte and cumulus cell gene products and their implications for the acquisition of developmental competence in oocytes.

1.2.Signaling between cumulus cells and oocyte

1.2.1.Folliculogenesis

Folliculogenesis is the growth and development of a pool of ovarian follicles. Within the follicle, oocytes undergo growth, ovulation, or atresia (Williams and Erickson 2000). During successful folliculogenesis, the follicles persist through the primordial, primary, secondary, and tertiary or antral follicular phases (Figure 1) (Clarke 2017). This process of folliculogenesis can be divided into two distinct phases: a gonadotropin-independent phase and a gonadotropin-dependent phase (Williams and Erickson 2000). The first phase encompasses the growth and differentiation of the oocyte from the primordial germ cells, being controlled by paracrine and autocrine factors, while the second phase involves the growth of the follicle itself, regulated by FSH and LH in addition to local growth factors (Williams and Erickson 2000).

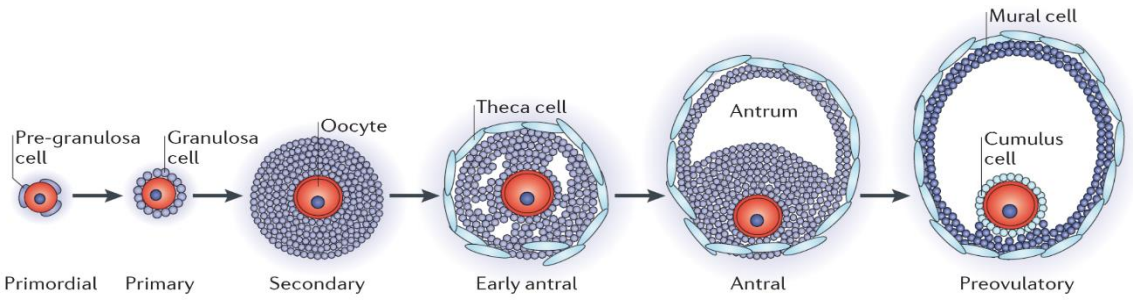

Figure 1. Stages of Folliculogenesis. Reproduced with permission from Li and Albertini (2013).

1.2.2.Primordial germ cells: proliferation, migration, differentiation

All oocytes originate from primordial germs cells (PGCs). These PGCs are diploid cells that have the potential to give rise to either a female or a male germline, the oocytes or the spermatozoa (Wear et al. 2016). In mice, the first signs of PGCs occur on embryonic day (E) 5 in the extraembryonic ectoderm, with PGC

proliferation continuing into E7 in the primitive streak of the cleft between the yolk sac and developing allantois (Mtango et al. 2008; Wear et al. 2016). In mice, the first sign of PGC presence is accompanied by an increase in bone morphogenetic protein (BMP) levels, as well as an increase in proto-oncogene wingless-type mouse mammary tumor virus integration site family member 3 (WNT3) levels (Sanchez and Smitz 2012; Aramaki et al. 2013; Wear et al. 2016). The proteins BMP2, BMP4, and BMP8 bind to SMAD1/4, as well as SMAD4/5 (Figure 2) (Wear et al. 2016). These factors play a role in PGC formation, and regulation of gene expression in PGCs.

To maintain the pluripotency of PGCs, and prevent differentiation at such an early embryonic stage, the canonical β-catenin pathway must be activated. To do so, on the surface of the PGCs, WNT3 binds the Frizzled-related receptor (FRIZZLED), which then activates the signaling cascade of the β-catenin pathway and promotes pluripotency by activating the expression of the gene *T* for production of the Brachyury protein (Rivera-Perez and Magnuson 2005; Aramaki et al. 2013). Brachyury promotes pluripotency and histone methylation by activating the repressor positive regulatory domain zinc finger protein 1 (PRDM1), which then represses the transcription of differentiation factors homeobox A1 (HOXA1) and homeobox B1 (HOXB1) and activates nanos homologue 3 (NANOS3). NANOS3 is a required precursor for the expression of pluripotency maintaining genes, such as sex determining region Y-box 2 (*Sox2*), octamer-binding transcription factor 4 (*Oct4*), and homeobox transcription factor (*Nanog*) (Tsuda et al. 2003; Ohinata et al. 2005; Saitou et al. 2005; Wear et al. 2016).

Together with SOX2, OCT4, NANOG, and NANOS3, the developmental pluripotency associated 3 (DPPA3) protein also contributes to the maintenance of pluripotency of the PGCs (Tsuda et al. 2003). Additionally, lin-28 homologue A (LIN28) assists in the maintenance of pluripotency by forming a complex with small inhibitory mRNAs, to allow transcription of *Prdm1*, thus perpetuating the pluripotency maintenance cycle (Wear et al. 2016). During this time, mitosis is occurring to further the PGC population.

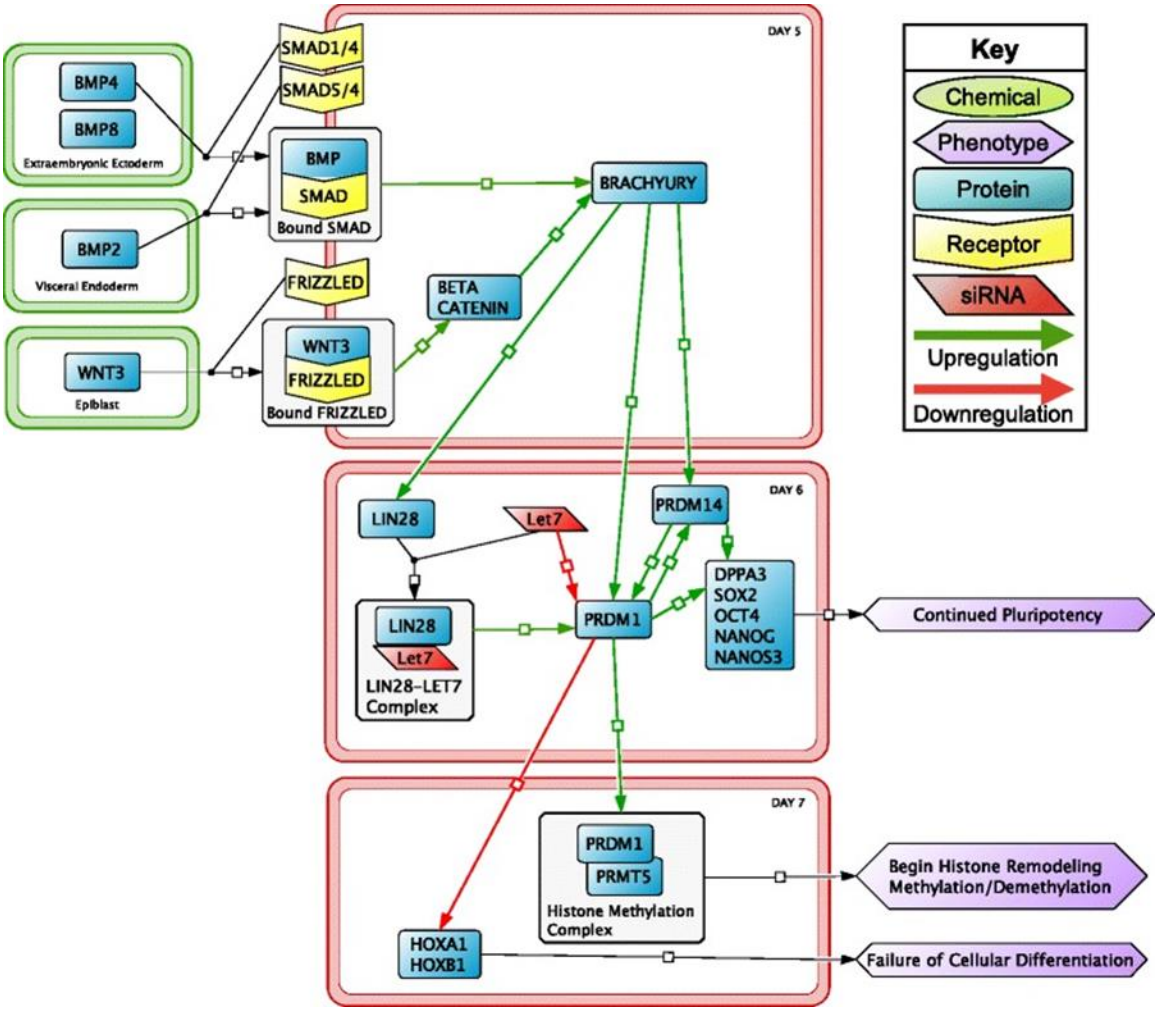

Figure 2. Signaling interactions in murine PGCs. Events with red connection depict molecular events from E5 to E7 occurring between PGCs. Events with green connection depict molecular events between embryonic tissues. Reproduced from

Wear et al. (2016) according to the Creative Commons Attribution 4.0 International License.

On E7.5 in mice, cellular adhesion decreases among PGCs, allowing PGC migration to the gonadal ridge by E8 (Wear et al. 2016). Migration of PGCs to the gonadal ridge is driven by the chemoattractant signaling interactions of the gonadal ridge secreted ligand, stromal cell-derived factor 1 (SDF1), and the chemokine receptor type 4 (CXCR4) which is present on the PGC (Molyneaux and Wylie 2004; Stebler et al. 2004). This chemoattraction process induces the PGC migration into the gonadal ridge (Molyneaux and Wylie 2004; Stebler et al. 2004; Wear et al. 2016). By E10 in the mouse, migration stops once PGCs interact with the somatic cells in the gonadal ridge (Sanchez and Smitz 2012; Wear et al. 2016).

Upon the cessation of migration, the somatic cells begin to express Wilms tumor protein homologue (WT1), thereby promoting the growth of the gonadal ridge region and female differentiation (Wilhelm et al. 2007; Wear et al. 2016). PGC differentiation continues by transcription factor influence from the somatic cell derived factors GATA4, FOXL2, LHX9, WNT4, and SF1 (Elvin and Matzuk 1998; Wilhelm and Englert 2002; Sanchez and Smitz 2012).

Immediately following the invasion of the gonadal ridge, the PGCs undergo a phase of intense mitosis from E10 to E13.5 in mice, and are now classified as oogonia, with a rising population of around 3000 cells (Pepling 2006; Wear et al. 2016). These mammalian oogonia develop into clusters called cysts, which remain surrounded by the somatic epithelial pregranulosa cells (Pepling 2006). During the mitotic phase, the cysts and associated epithelial pregranulosa cells begin to

organize and form the ovarian cords, where they remain until primordial follicles form (Pepling 2006). By E14.5 in mice, the oogonia pool has grown to more than ~18000 cells and mitosis halts, allowing for meiosis to begin, thus transitioning the oogonia to primary oocytes (Pepling 2006; Sanchez and Smitz 2012; Wear et al. 2016). These primary oocytes proceed through meiosis, and by E17.5 through day 5 post birth in mice, most primary oocytes have halted at the diplotene stage of prophase I and the germ cell cysts have broken down to form primordial follicles (Pepling 2006; Rimon-Dahari et al. 2016). This transition from PGC to primordial follicle is often associated with a notable loss of oogonia and oocytes, with 33% of the population reaching the primordial follicle stage (Pepling and Spradling 2001; Rimon-Dahari et al. 2016; Wang et al. 2017).

1.2.3.Primordial follicle

The primordial follicle in a quiescent state has an average diameter of ~35 microns in cattle and pigs (Kanitz et al. 2001; Hyttel 2012). It exists in a state that contains the primary oocyte arrested in diplotene of prophase I and is surrounded by flattened, simple squamous epithelial pregranulosa cells. It is distinguishable by its larger size (~25 microns in diameter in humans and cattle) compared to those present in a cyst (Williams and Erickson 2000; Hyttel 2012; Rimon-Dahari et al. 2016; Wear et al. 2016). Gap junctions exist between pregranulosa cells. Between the pregranulosa cells and the primary oocyte exist both gap junctions and adherens junctions (Hyttel 2012). These gap junctions allow for direct diffusion of ions and small molecules between cells (Perez-Armendariz et al. 2003;

Goodenough and Paul 2009). Additionally, the primordial follicle presents evidence of endocytosis through the presence of vesicles and numerous coated pits around its periphery (Hyttel 2012). In this follicular stage, the oocyte nucleolus is transcriptionally silent, consisting of a granular component interspersed with vacuoles, rather than a fibrillar one (Fair et al. 1997a; Hyttel 2012).

These primordial follicles make up the pool of quiescent oocytes which have the potential for fertilization upon sexual maturity. To remain in arrest and inhibit follicular activation, the primordial follicles require TSC1 or TSC2 and mTORC1. The TSC1/2 complex negatively regulates mTORC1, thereby maintaining a dormant state for the primordial follicles (Sanchez and Smitz 2012; Rimon-Dahari et al. 2016). Another mechanism in which the primordial follicle remains inactive is through Anti-Müllerian hormone (AMH) (McLaughlin and McIver 2009). AMH represses the expression of the TGFβ pathway, halting the transition of primordial to primary follicle (Nilsson et al. 2007). SDF1 also inhibits follicle activation in neonatal ovaries (Holt et al. 2006), though the mechanism is yet to be elucidated.

In mice, there are two distinct classes of primordial follicles. The first primordial follicle group is simultaneously activated shortly after birth in the medulla of the ovary. The second group, which are slowly activated in the adult phase of life, in the cortex of the ovary (Wang et al. 2017). The processes involving activation of primordial follicles into primary follicles and initiation of folliculogenesis take ~15 days in mice, whereas it may take six months in humans (Sanchez and Smitz 2012). This initial development is independent of gonadotropins and can occur before the onset of puberty.

The first stage of the activation and differentiation process requires activation of the PTEN/PI3K signaling pathway (Figure 3) (Sanchez and Smitz 2012; Monniaux 2016). Within this pathway, mTORC1 activates the differentiation of flattened pregranulosa cells into cuboidal granulosa cells. This morphological change of the somatic cells marks the transition from primordial to primary follicles. Additionally, as the somatic cells transition from a flattened shape to a cuboidal one, the zona pelucida (ZP) (a glycoprotein layer) forms between them and the oocyte (Da Silva-Buttkus et al. 2008). The oocyte and granulosa cells maintain contact with each other through transzonal projections (TZPs) of the somatic cells that reach the oocyte plasma membrane (Da Silva-Buttkus et al. 2008; Macaulay et al. 2014). The TZPs most commonly possess an actin back bone, while few TZPs have a tubulin backbone (Clarke 2018). The TZPs have two primary functions: to enable and maintain a contact-dependent communication between the cumulus cells and oocyte, as well as to keep the somatic cells bound to the oocyte through adherens junctions (Clarke 2018). The cuboidal granulosa cells now have the ability to express KITLG, which binds to KIT on the membrane of the adjacent oocyte and activates the PI3K pathway in the oocyte (Monniaux 2016). The signaling between the somatic granulosa cells and oocyte constitutes an important and essential communication at such an early stage. During this time, the mTORC2 complex acts to ensure the survival of the growing follicles (Monniaux 2016).

During the latter and final stages of activation in the oocyte, the oocyte derived TGFβ ligands GDF9 and BMP15, as well as the SMAD signaling pathway work to control the growth and differentiation of the surrounding pregranulosa cells into granulosa cells (Figure 3) (McLaughlin and McIver 2009; Sanchez and Smitz 2012; Persani et al. 2014; Monniaux 2016).

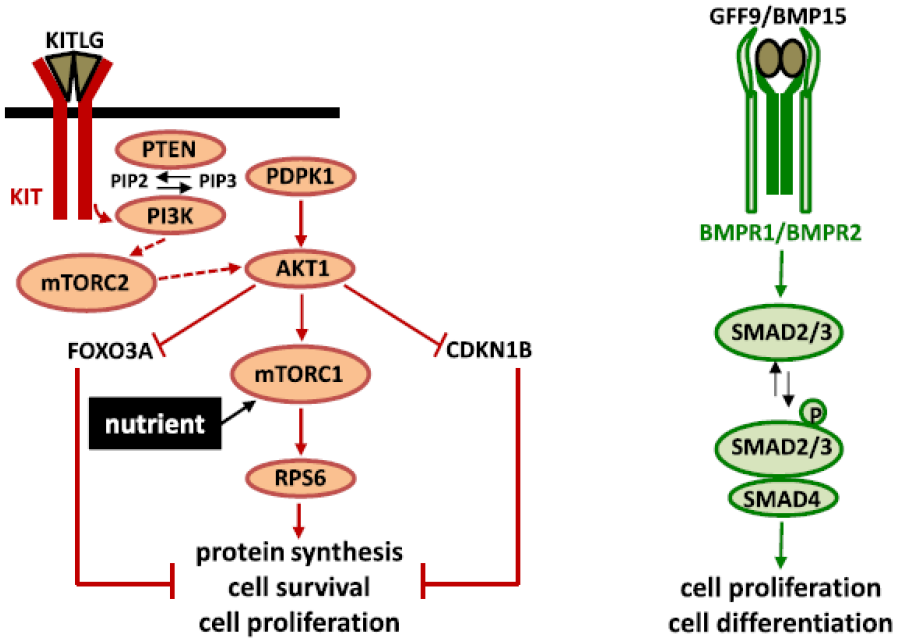

Figure 3. Primordial Follicle Activation. Left panel (red) depicts the early stages of activation in granulosa cells and oocytes. Right panel (green) depicts regulatory pathways for granulosa cell proliferation and differentiation during the latter stages. Reproduced with permission from Monniaux (2016).

1.2.4.Primary follicle

Primary follicles can range from 40 to 52.2 microns in diameter in cattle to an average of 64.9 microns in pigs (Griffin et al. 2006; Hyttel 2012). The oocyte diameter in the follicles averages around 32 microns in cattle and 37.5 microns in

pigs (Griffin et al. 2006; Hyttel 2012). The oocyte contains an eccentrical nucleolus, containing both fibrillar centers and granules, suggesting that the oocyte is slowly becoming transcriptionally active (Fair et al. 1997a; Fair et al. 1997b; Hyttel 2012). Primary follicles contain a single layer of cuboidal granulosa cells surrounding the oocyte (Williams and Erickson 2000). Within the cuboidal granulosa cells FSH receptor expression is initiated, which is not required for primary follicle development, but is essential for the signaling that contributes to the growth of the preantral follicles amongst a variety of mammalian species (human, mice, and monkeys) (Wright et al. 1999; Williams and Erickson 2000; Kreeger et al. 2005; Xu et al. 2009; Hsueh et al. 2015). Further activation of primary follicles is often stimulated by CNP (C-type natriuretic peptide) (Sato et al. 2012). CNP, expressed in the granulosa cells, activates its receptor, NPRB, present in the granulosa cells as well, which signals the production of cGMP (Hsueh et al. 2015). The cGMP then passes through the gap junctions into the oocyte, where it inhibits the hydrolysis of cAMP by PDE3A (Norris et al. 2009; Hsueh et al. 2015). The high intracellular levels of cAMP maintain the oocyte in meiotic arrest (Norris et al. 2009). Additionally, treatment of primary follicles with CNP promote follicle development in the absence of exogenous FSH (Sato et al. 2012).

1.2.5.Secondary follicle

The secondary follicle is marked by its larger size than its primary predecessor. On average, a secondary follicle in both cattle and pigs has a diameter of 102 microns with at least a bilayer of cuboidal granulosa cells

surrounding the oocyte, which is now ~46 microns in diameter in cattle and ~74.2 microns in diameter in pigs (Fair et al. 1997b; Griffin et al. 2006; Hyttel 2012). The oocyte of a secondary follicle in cattle is transcriptionally active, has a fibrillo-granular nucleolus, and the cytoplasm presents cortical granules, as well as a greater occurrence of lipid droplets (Fair et al. 1997a; Hyttel 2012). The oocyte and granulosa cells have established gap junctions and transzonal projections, allowing for direct cell to cell communication via signaling rather than through the utilization of endocytosis (Hyttel 2012; Macaulay et al. 2014). With the change in communication mechanism there is a decrease of coated pits and vesicle formation in the oocyte (Hyttel 2012). The secondary follicle development coincides with the formation of the theca cells. Thecal cells are recruited from the surrounding stromal layer beyond the granulosa cells. Once differentiated, the theca cells begin producing LH receptors, steroidogenic enzymes, and androgens (Young and McNeilly 2010). The differentiation of theca cells from surrounding stromal tissue is accomplished by peptides expressed by the pregranulosa and granulosa cells, including KITLG and leukemia inhibiting factor (LIF) (Knight and Glister 2006). The theca cells develop outside of the granulosa-oocyte complex forming two layers, namely the theca interna and theca externa (Young and McNeilly 2010). The theca interna surrounds the growing follicle, containing vasculature, fibroblasts, immune cells, as well as steroidogenic cells, and is primarily used to produce androgens, which are aromatized by the granulosa cells, and to supply the growing follicle with nutrients and growth factors (Hatzirodos et al. 2014). The theca externa is composed primarily of non-steroidogenic fibroblast

and smooth muscle-like cells, in a loosely arranged fashion (Magoffin 2005; Hatzirodos et al. 2014).

1.2.6.Tertiary follicle

Early tertiary follicles have a diameter of about 1 mm in cattle, while in pigs, the developing tertiary follicle has a mean diameter of ~360 microns (Griffin et al. 2006; Hyttel 2012). The follicle contains the developing antrum, and with the onset of the formation of this antrum, appears the differentiation of the granulosa cells into either cumulus granulosa cells (cumulus cells) or mural granulosa cells (Georges et al. 2014). Factors controlling this differentiation involve primarily the oocyte secreted factors BMP15 and GDF9. In mice, the ability for cumulus cells to undergo cellular proliferation can be triggered by oocyte secreted factors (OSFs) in response to EGF (Diaz et al. 2007). Within early tertiary follicles, the oocyte is present within the cumulus oophorus (Hyttel 2012). The oocyte of an antral follicle is immediately surrounded by the *corona radiata* formed by the cumulus cells with projections that transverse the fully developed ZP into the oolemma, and further surrounded by cumulus cells (Fair et al. 1997b; Hyttel 2012). The mural granulosa cells surrounding the antrum and on the inner line of the follicle wall are critical for steroidogenesis and have distinct physiology compared to the cumulus cells (Scaramuzzi et al. 2011; Rimon-Dahari et al. 2016). Surrounding the mural granulosa cells is the basil lamina followed by the theca cells in their distinct layers (Erickson 1983). The mural granulosa cells hold a higher density of LH receptors than their cumulus counterparts (Palermo 2007). Additionally, in the early tertiary

follicle the oocyte is transcriptionally active, with a fibrillo-granular nucleolus containing an even distribution of fibrillar centers. The cytoplasm of an early tertiary follicle presents a greater quantity of cortical granules, vesicles, and lipid droplets compared to earlier follicular stages (Fair et al. 1997b; Hyttel 2012). At this point in folliculogenesis, the antrum has formed, expanded, and filled with follicular fluid (Rodgers and Irving-Rodgers 2010). The fluid which fills the antrum is drawn in by osmotic potential created by the glycosaminoglycans and the proteoglycans secreted by the granulosa cells (Clarke et al. 2006).

In tertiary follicles, a much larger size follicle reaches 3 mm in diameter in cattle (a follicle diameter of ~630 microns in pigs) and contains an oocyte ranging from 80 to 110 microns in diameter (an oocyte diameter of ~77 microns in pigs) (Griffin et al. 2006; Hyttel 2012). The nucleolus differs depending on the size of the oocyte in the tertiary follicle. In follicles with an oocyte of less than 100 microns in diameter, the oocyte is transcriptionally active, and the nucleolus is still fibrillo-granular, with the development of electron dense granules around the fibrillar centers (Fair et al. 1997a; Lodde et al. 2008; Hyttel 2012). The nucleus, by this time, moves from an eccentrical position to the periphery (Fair et al. 1997b). Oocytes ranging from 100 to 110 microns in diameter contain a nucleus that is positioned even further towards the periphery and a nucleolus in a variable state of condensation (Hyttel 2012). In some of the nucleoli at this stage, accumulation of electron dense deposits around the fibrillar centers is common, demonstrating a decrease in transcriptional activity of rRNAs (Hyttel 2012). In other nucleoli at this stage, the fibrillar centers are peripherally stationed, forming lentiform

structures with the granular portion and thereby relinquishing the synthesis of rRNA from the oocyte (Hyttel 2012). In both instances, the transcription of rRNAs and mRNAs is diminished, as demonstrated by H3-uridine labeling (Lodde et al. 2008; Hyttel 2012). By this point in the growing tertiary follicle, the oocyte organelles have moved towards the periphery, and cortical granules are present in clusters (Fair et al. 1997b; Hyttel 2012).

Late tertiary follicles are those in which the bovine oocyte has a dimeter of 110 microns or greater and the porcine oocyte a mean diameter of 105 microns (Griffin et al. 2006; Hyttel 2012). Within this later tertiary follicle, the number of lipid droplets, vesicles, and cortical granules have increased, and the cumulus cells are still attached to the oocyte through TZPs (Hyttel 2012; Macaulay et al. 2014). The nucleus is now peripherally located, and the nucleolar condensation can vary. In some oocytes at this stage, the nucleolus will have completely transitioned the fibrillar centers to a single lentiform structure, whereas in others, the nucleolar inactivation process will have already begun, resulting in a nucleolus packed tightly with fibrils, attached to a fibrillar center (Hyttel 2012). The oocyte is now transcriptionally repressed, and the growth phase of the oocyte is considered complete (Lodde et al. 2008; Hyttel 2012). Additionally, as the growth phase of the oocyte concludes so does the gonadotropin-independent phase of folliculogenesis. With the onset of the tertiary follicle, the transition from the gonadotropin-independent phase of folliculogenesis to the gonadotropin-dependent phase occurs (Williams and Erickson 2000).

Pigs are a polytocus species and have one wave of follicular activity (Kanitz et al. 2001; Schwarz et al. 2008). In pigs, the follicular phase follows the luteal phase and spans a total of five to seven days of the estrous cycle (Soede et al. 2011). During the follicular phase the largest tertiary follicles are recruited for further development, growing from their current size of 2 to 4 mm in diameter to 7 to 8 mm in diameter (Soede et al. 2011).

After ovulation, the recruitment of a new cohort of follicles begins. Recruitment of these follicles occurs when the granulosa cells of the early tertiary follicles bind FSH, stimulating the synthesis of aromatase (CYP19A1), which then converts the theca-originating (in response to LH) androgens, specifically, androstenedione into estrone and 17β-estradiol (Young and McNeilly 2010; Barbieri 2014). When a threshold concentration of 17β-estradiol is produced by the granulosa cells within the tertiary follicles, a positive feedback is activated in the hypothalamus, resulting in pulses of gonadotropin releasing hormone (GnRH), allowing it to bind its receptor on the gonadotroph cell surface of the anterior pituitary gland, which in turn, stimulates the synthesis and release of FSH and LH (Guthrie et al. 1990; Kanitz et al. 2001; Soede et al. 2011; Barbieri 2014).

The recruitment of follicles, or the follicular phase, following the end of the luteal phase and the regression of corpus luteum function, coincides with a decline in 17β-estradiol, progesterone (P4), and inhibin A (Palermo 2007; Soede et al. 2011). This decline results in a change in GnRH; the GnRH and GnRH induced LH pulses transition over from less frequent pulses with greater amplitude to more frequent pulses with a lesser amplitude, resulting in a rise of FSH concentrations

(Palermo 2007; Soede et al. 2011). Not all tertiary follicles can be recruited and therefore only the ones which contain more FSH receptors on their granulosa cells, and are therefore more sensitive to FSH, will enter into the gonadotropin-dependent phase of folliculogenesis (Palermo 2007).

Under this initial rise in FSH, the recruited follicles grow rapidly and begin to secrete 17β-estradiol, causing a negative feedback effect on the hypothalamus, directly reducing the levels of GnRH being secreted, reducing the secreted levels of FSH and LH (Soede et al. 2011). Additionally, during this time, inhibin works to suppress the levels of FSH secretion (Russell and Robker 2007). In poly-ovulatory species, such as the pig, the number of recruited follicles, ~50, is considerably higher than the follicles selected for ovulation, ~15 to ~25 (Kanitz et al. 2001). However, the mechanism by which suppression of follicles occurs is still not entirely clear. One aspect of this mechanism is the reduction in FSH levels by inhibin and the forced transitional gonadotropin dependence on LH, causing the smaller follicles which have insufficient LH receptors on their theca and mural granulosa cells to undergo atresia. The remaining follicle population is now composed of larger, LH-dependent follicles (Russell and Robker 2007; Noguchi et al. 2010; Soede et al. 2011). The presence of LH on the selected follicles is required to continue the follicle growth and development until it reaches the pre-ovulatory size, varying from 5 to 8.5 mm in pigs (Soede et al. 1998; Kanitz et al. 2001). Within the growing follicle cohort, the levels of 17β-estradiol also increase, triggering a pre-ovulatory LH surge resulting in ovulation (Noguchi et al. 2010;

Soede et al. 2011). Follicular size during ovulation reaches between 4 to 9.5 mm in pigs (Soede et al. 1998).

After ovulation, and in the early stages of the luteal phase, angiogenesis begins, and with the assistance of angiogenic factors, such as VEGF and IGF-I, the ovulated follicular granulosa and theca cells undergo luteinization and form a corpus luteum (CL) (Soede et al. 2011). Corpora lutea reach their matured form, allowing the luteal cells to functionally secrete P4, at approximately seven days after ovulation (Soede et al. 2011). In the absence of viable embryos in the uterus, the CL begins to regress (Przygrodzka et al. 2016). Luteolysis is initiated with prostaglandin F 2-alpha (PGF2α) secreted by the endometrium, disrupting P4 synthesis and promoting the deterioration of the luteal and endothelial cells in the CL (Przygrodzka et al. 2016).

1.3.Maturation and acquisition of meiotic and developmental competence

In oocytes, developmental competence is acquired through maturation and is the ability of the oocyte to be successfully fertilized and sustain the early stages of embryogenesis (Nunes et al. 2015). Developmental competence in the oocyte relies on the presence of the bidirectional communication of the cumulus cells and the oocyte (Russell et al. 2016). The signaling between these two cell types is dynamic, altering during the different stages of oocyte growth and follicular growth (Russell et al. 2016). The oocyte maturation occurs during folliculogenesis through interconnected events that can be didactically split into meiotic, cytoplasmic, and molecular maturation for better comprehension.

1.3.1.Meiotic maturation

Meiotic maturation of an oocyte encompasses the transition from prophase I to metaphase II (MII), as well as the germinal vesicle breakdown (GVBD) and the condensation of the chromatin. The oogonia enter into meiosis shortly after colonization of the fetal gonad is established (Rimon-Dahari et al. 2016). Shortly after this, they are arrested in prophase I of meiosis and remain quiescent until their meiotic re-activation (Vaccari et al. 2009). The defining feature of a germ cell arrested in prophase I is the presence of the germinal vesicle nucleus containing a distinguishable nucleolus and partial condensation of the chromosomes (Vaccari et al. 2009). The surrounding somatic cells are a vital part of the prophase I arrest, as they drive the maintenance of it through intercellular communication. The primary modulator of the prophase I arrest is cGMP from the surrounding cumulus cells to the oocyte via gap junctions (Norris et al. 2009). It is known that cGMP works to maintain this arrest by inhibiting the hydrolysis of cAMP by phosphodiesterase 3A (PDE3A) within the oocyte, resulting in a high intracellular cAMP concentration of ~700nM in mice (Norris et al. 2009). Meiosis I resumption is triggered by the surge of LH prior to ovulation (Li and Albertini 2013). This resumption is marked by the breakdown of the nuclear membrane and the condensing of chromosomes (Li and Albertini 2013).

Luteinizing Hormone acts upon the follicle, binding to the receptors on the theca and mural granulosa cells and stimulating G_s, which then activate adenylyl cyclase (AC3) and increase the production of cAMP (Figure 4) (Mehlmann et al.

2006; Norris et al. 2009). The increase of cAMP activates protein kinase A (PKA) in the mural granulosa cells causing a release of factors, specifically amphiregulin (AREG), epiregulin (EREG), and betacellulin (BTC), that activate epidermal growth factor (EGF) receptors, which activate mitogen activated protein kinase (MAPK) (Panigone et al. 2008). Present in the cumulus cells, MAPK phosphorylates certain serine residues on connexin 43 (CX43), closing the gap junctions connecting cumulus cells (Norris et al. 2008; Tripathi et al. 2010). The closure of the CX43 gap junctions results in reduced diffusion of cGMP and cAMP from cumulus cells to the oocyte. The gap junctions remain closed for 0.5 to 2 hours in mice after the LH initiation (Norris et al. 2008; Norris et al. 2009). Within the oocyte, the reduced levels of cGMP (from ~1 μM pre-LH to ~40 nM post-LH in mice) allow for the activation of PDE3A, hydrolyzing cAMP within the oocyte and reducing its cAMP levels to ~140 nM in mice (Norris et al. 2009; Tripathi et al. 2010).

Reduction of cAMP levels inactivates PKA within the oocyte. Next Cdc25B phosphatases are activated and the kinases Wee1B/Myt1 are deactivated (Oh et al. 2010). Active Cdc25B dephosphorylates and activates CDK1, a catalytic subunit of Cdc2-cyclin B or the maturation promoting factor (MPF). Active CDK1 promotes germinal vesicle breakdown, resumption of meiosis from the prophase I arrest, chromosome condensation, and spindle formation (Han and Conti 2006; Bhattacharya et al. 2007; Tripathi et al. 2010).

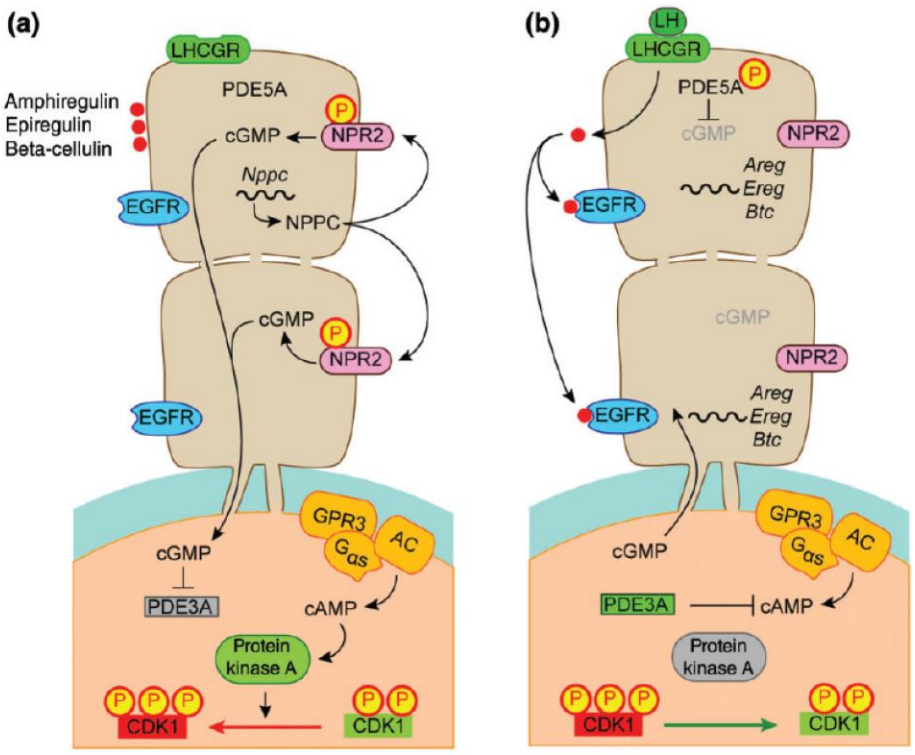

Figure 4. Meiotic Maturation. (a) Before the onset of meiotic maturation and (b) after the onset of meiotic maturation. Reproduced with permission from Clarke (2018).

1.3.2.Cytoplasmic maturation

Cytoplasmic maturation involves the rearranging of organelles, as well as the accumulation of mRNAs, proteins, and nutrients that are required for the oocyte to become developmentally competent, successfully undergo fertilization, and enter early embryogenesis (Watson 2007; Ferreira et al. 2009). The reorganization of organelles within the oocyte occurs during the transition from the germinal vesicle stage to the metaphase II stage (Ferreira et al. 2009).

Mitochondria are organelles that reorganize, changing their overall positioning and numbers within the oocyte over time. Prior to migration, germ cells have ~ten or less mitochondria, while oogonia have ~200, primary oocytes have ~20000, and during cytoplasmic maturation, the numbers can increase up to ~100000 with each holding one or two copies of mtDNA (Cummins 1998; Tarazona et al. 2006). Mitochondria move to areas of higher energy needs during cytoplasmic maturation, including areas which require more ATP to support the maturation and development processes (Stojkovic et al. 2001). In the oocyte, the mitochondria take on a more peripheral distribution before the pre-ovulatory LH surge; whereas, after the surge and, in the final stages of meiotic maturation, they begin to display clustered cortical formations, and ~19 hr post LH surge in cattle, the mitochondria disperse, following the displacement of the polar body (Kruip et al. 1983; Ferreira et al. 2009). By the time metaphase II is reached, the mitochondria occupy a more central location in the oocyte (Figures 5 & 6) (Hyttel et al. 1996).

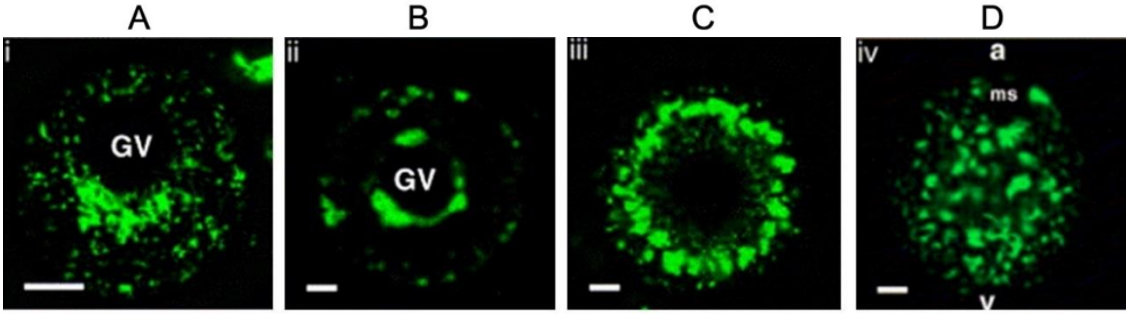

Figure 5. Distribution of mitochondria throughout murine cytoplasmic maturation. Mitochondria are marked by a green fluorophore. (A) Meiotically incompetent oocyte; (B) Fully grown GV-stage oocyte; (C) Maturing oocyte immediately following GV breakdown, (D) Mature metaphase-II-arrested oocyte.

Scale bars = 10 µm. GV = germinal vesicle; a = animal pole; ms = meiotic spindle; v = vegetal pole. Reproduced with permission from Mao et al. (2014).

The nucleolus changes composition during the maturation of an oocyte to conform to the oocyte's changing protein synthesis needs. Beginning in primordial follicles of cattle, the nucleolus of the oocyte is composed of strictly granular portions, reflecting the quiescence of transcription that is carried into the primary follicle, as well as an absence of ribosomal synthesis (Hyttel et al. 2001). In secondary follicles, transcription is initiated and the nucleoli present fibrillar centers that become embedded into the superficial layer of the granular component, this activates the genome which then allows for synthesis of both rRNA and mRNA (Hyttel et al. 2001). These fibrillar centers are likely associated with rRNA genes. Therefore, when the granular component is invaded by the fibrillar center, the nucleolus begins the transition to actively transcribe rRNA and process it to its ribosome form (Hyttel et al. 2001). Early tertiary follicles have high rates of transcription within the oocyte's nucleoplasm and nucleolus, with the nucleolus presenting a fibrillo-granular composition (Hyttel et al. 2001). The latter tertiary follicles present a nucleolus, or rather a nucleolus precursor body (NPB), with electron-dense fibrillar spheres and a fibrillar center attached but missing a granular component (Chouinard 1971; Hyttel et al. 2001; Fulka and Langerova 2014). These NPBs are devoid of ribosome synthesis (Hyttel et al. 2001; Kyogoku et al. 2014). Just prior to the LH surge, changes in the germinal vesicle occur; the nuclear envelope swells and the NPB begins to disperse (Hyttel et al. 2001; Kyogoku et al. 2014). This dramatic disassembly of the NPB is associated with the

resumption of meiosis in oocytes (Hyttel et al. 2001). During the transition into metaphase II, transcripts are necessary from the cumulus-oocyte complex (COC) (Hyttel et al. 2001). During the first few hours post LH surge, transcription is present within the COC, including a small number of genes in the oocyte (Sirard et al. 1989; Memili et al. 1998).

The Golgi apparatus also undergoes changes during cytoplasmic maturation (Figure 6). The Golgi apparatus plays a crucial role in processing and delivering proteins, as well as molecules within the cell (De los Reyes et al. 2012; Racedo et al. 2012). In murine and human germinal vesicle stage oocytes, the Golgi apparatus resides dispersed throughout the ooplasm in a continuous pattern, with vesicles present and a higher population density occurring towards the interior, rather than at the cortex (Mao et al. 2014). At the breaking down of the germinal vesicle, the Golgi apparatus fragments, moving towards a cortical distribution as meiosis resumes (De los Reyes et al. 2012; Mao et al. 2014). Essential for this fragmentation is cyclin-dependent kinase 2A (CDC2A), which associates as a heterodimer with cyclin B to form MPF (Racedo et al. 2012). At the onset of metaphase I, the Golgi fragments move once more and are disperse throughout the ooplasm (Racedo et al. 2012).

The endoplasmic reticulum (ER) remains physiologically active during oocyte maturation and functions in the folding and degradation of proteins, as well as in lipid metabolism, nucleus compartmentalization and organization, regulation and storage of calcium ions, and membrane synthesis (Ferreira et al. 2009; Mao et al. 2014). At the germinal vesicle stage of murine oocytes, the ER is consistently

distributed across the ooplasm. However, following GVBD into MII, the ER forms clusters (1 – 2 microns wide) throughout the ooplasm, localizing, specifically, to the cortical regions of the oocyte (Figure 6) (Ferreira et al. 2009; Mao et al. 2014). The ER plays an essential role in intracellular signaling by storing and releasing calcium from their cytoplasmic stores (Kline 2000). During oocyte maturation the signaling pathways of Ca^{2+} are remodeled to prepare for future fertilization events (Machaca 2007).

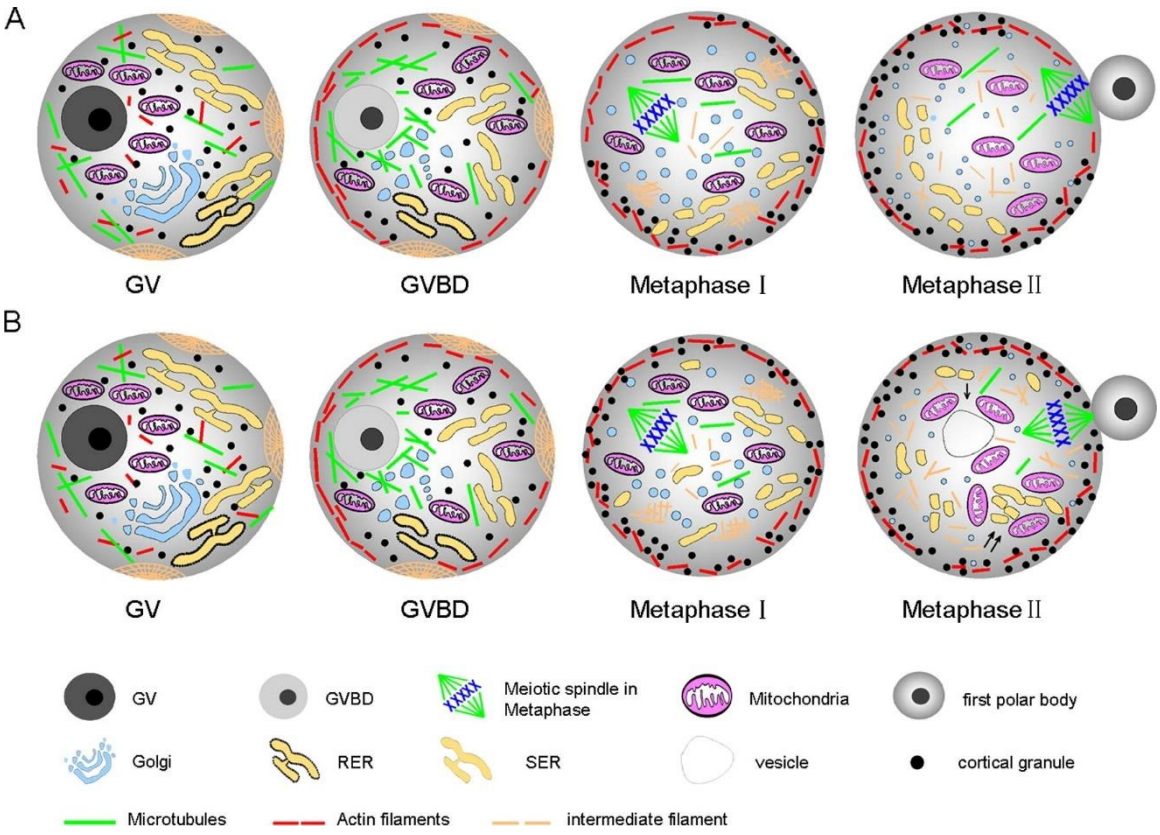

Figure 6. Cytoplasmic Maturation. Depiction of events in (a) mouse and (b) human oocyte as it undergoes cytoplasmic maturation. Reproduced with permission from Mao et al. (2014).

Cortical granules are produced by the Golgi apparatus as a result of hypertrophy and proliferation experienced during cytoplasmic maturation (Mao et

al. 2014). This happens when vesicles form on the hypertrophied Golgi apparatus, migrate towards the subcortical region, and eventually merge to form the mature state of cortical granules (~0.5 microns in diameter) that are separate entities from the Golgi apparatus (Gulyas 1980; Liu 2011). During oocyte maturation, from GVBD to MII, the cortical granules migrate from a dispersed fashion to a more cortical position, with their final resting position being in the cortex (Figure 6) (Mao et al. 2014). Oocyte specific SNARE proteins, SNAP-23 and VAMP1, are required to establish the cortical granules to the oolemma, working to prevent the spontaneous release of the cortical granules. Additionally, these proteins function with complexin, a *trans*-SNARE complex-stabilizing protein (Tsai et al. 2011). The primary function of cortical granules is to exocytose, transferring contents from the oocyte to the perivitelline space following fertilization, a calcium dependent process known as the cortical reaction (Mao et al. 2014). Upon exocytosis of these cortical granules, the cortical reaction causes the ZP to undergo a reaction as well, known as the zona reaction (Sun 2003). The zona reaction occurs when the ZP becomes resistant to sperm binding and penetration, effectively preventing polyspermy (Sun 2003). When the cortical reaction occurs, a concurrent endocytosis also occurs, releasing complexin and clathrin into the ooplasm, further stimulating the endocytosis of vesicles containing the SNARE proteins (Tsai et al. 2011).

During cytoplasmic maturation, the cytoskeletal filaments reorganize. The three main types of cytoskeletal filaments within eukaryotic cells are microfilaments, intermediate filaments, and microtubules (Mao et al. 2014).

Microtubules, consisting of both a globular and compacted tubulin component, microfilaments, consisting of both a globular and compacted actin component, and intermediate filaments, consisting of both a fibrous and elongated polypeptide component, are bound by noncovalent interactions, rapidly and frequently breathing from their set structures (Mao et al. 2014). During cytoplasmic maturation, the microtubules, bound to dynein, dynactin, and kinesin, are the most directly involved in moving organelles (Steffen et al. 1997; Sun and Schatten 2006).

In GV stage oocytes, microtubules and microfilaments are evenly dispersed throughout the ooplasm, while the intermediate filaments occupy large cortical aggregates (Mao et al. 2014). Upon GVBD, the microtubules form asters and appear around the condensing chromosomes (Figure 6 & 7) (Ferreira et al. 2009). Simultaneously, the microfilaments begin to densely populate the subcortical region of the oocyte, compacting into clumps, but remaining separate from the microtubules (Li et al. 2005; Mao et al. 2014).

As meiosis progresses, reaching MI, the masses of intermediate filaments break up, organizing themselves into smaller bundles, while the microtubules, now nucleated by tubulin polymerization, form the meiotic spindles and the metaphase plate (Ferreira et al. 2009; Petry and Vale 2015). Although microfilaments are absent among the microtubules, their interaction drives the microfilament-dependent polarized movement of the chromosomes (Ferreira et al. 2009). Approaching anaphase I, the chromosomes begin to separate, exposing the microtubules between them. Additionally, the microtubule spindles begin to

elongate, exposing the microfilaments which have congregated around the chromosomes (Ferreira et al. 2009). By the time the oocyte reaches telophase I, the microtubule spindles form a tapering structure, with the wider portion of the microtubules connected to the chromosome set which is bound to become the polar body. The tapered end is associated with the chromosome set entering MII and thus forms the metaphase plate, this shape of microtubules at telophase I is drastically different compared to the barrel-shape present at MI (Li et al. 2005; Ferreira et al. 2009). In preparation for MII, the chromatin has rapidly condensed and the microfilaments and microtubules of the spindle have dispersed, a process known as interkinesis. By the time the oocyte reaches MII, the metaphase plate has reformed, with the intermediate filaments uniformly distributing themselves throughout the ooplasm. During this time, the microfilaments distribute themselves in the cortical regions, and the meiotic spindles are fully forming adjacent to the extruded polar body (Mao et al. 2014).

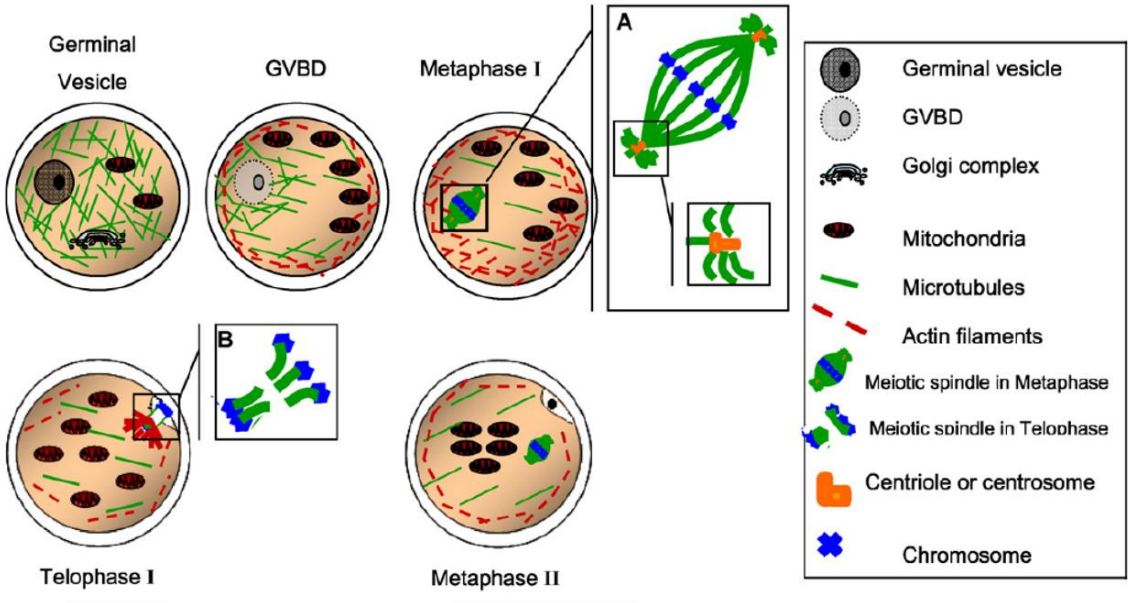

Figure 7. Cytoskeletal filaments during cytoplasmic maturation in bovine. Reproduced with permission from Ferreira et al. (2009).

1.3.3.Molecular maturation

Molecular maturation occurs throughout the life of the oocyte and refers to the transcription, processing, and storing of mRNAs within the oocyte that are used during maturation, fertilization, and early cleavages. After the resumption of meiosis, transcriptional activity is repressed in the oocyte, therefore, leaving only those transcripts accumulated during oocyte growth. The nascent mRNA transcripts produced during the growth phase prior to meiotic resumption are either processed and used quickly or stored in a stable, temporarily inactive form, packaged into ribonucleoprotein (RNP) particles (Sirard 2001; Gosden and Lee 2010; Zhang et al. 2017). In the normal mRNA life cycle, as it exits the nucleus, the cap-binding protein 20 (CBP20)/CPB80 complex begins the processing of

RNAs for translation, removing the exon-junction complexes from the mRNA strand, and eventually replacing the CBP20/CBP80 complex with the major cytoplasmic cap-binding protein eukaryotic translation initiation factor 4E (eIF4E), thereby promoting the recruitment of the translation initiation complex, consisting of ribonucleoproteins, proteins, and small noncoding RNAs (Moore 2005; Anderson and Kedersha 2009). Together with mRNA, this initiation complex is the messenger RNP (Moore 2005). These mRNPs are packaged to prevent their own degradation and to remain in storage until the oocyte resumes meiosis and the signals for translation are initiated (Figure 8) (Ferreira et al. 2009).

To promote storage, the spliced transcripts are recognized by the CPE-binding protein (CPEB) (Moore 2005). CPEB recognizes the cytoplasmic polyadenylation element (CPE) in the 3' untranslated region (UTR) and interacts with other factors including PARN, GLD2, and symplekin to remove the polyA+ tail (Richter 2007). PARN and GLD2 are both very active factors in both maintaining storage of the transcript and initiating translation. PolyA+ ribonuclease (PARN), deadenylates the transcripts as soon as it is added by GLD2, a polyA+ polymerase (Richter 2007). By further interacting with Maskin, a protein which competes with eIF4G for binding to eIF4E, the transcript cannot recruit cytoplasmic polyA+ binding proteins (PABPCs) or the 40S subunit of the ribosome to the start codon, effectively inhibiting translation (Moore 2005; Richter 2007; Gosden and Lee 2010).

Initiating translation of the stored transcripts is contingent on the polyadenylation of the 3' end of the fragment; stored mRNAs are prevented from

translation by protecting or “masking” their 3’ ends, as well as shortening them (Meric et al. 1996). Translational activation is dependent upon CPE, which lies upstream of the processing signal in the 3’ UTR, a CPEB, which recognizes the CPE in conjunction with symplekin, PARN, GLD2, and maskin (Richter 2007).

When the oocyte is induced to complete meiosis, translational activation proceeds after a progesterone-dependent signal cascades from the oocyte surface, activating Aurora kinase A and phosphorylating CPEB at Ser174, forcing PARN from the mRNP and allowing GLD2 to extend the polyA+ tail (Moore 2005; Kim and Richter 2006; Richter 2007). The now longer polyA+ tail recruits and binds to PABPCs, further binding with eIF4G to begin translation (Moore 2005). Maskin remains bound while the polyA+ tail is short (20 to 40 bp from the active 200 to 250 bp), but after PARN has left and both mRNP and GLD2 have the opportunity to extend the tail, polyA+ binding protein is recruited to the tail and maskin dissociates, prompting translational initiation (Moore 2005; Richter 2007). In mice, up to 90% of the stored transcripts are degraded by the first cellular division, and maternal mRNAs are no longer present in mammalian blastocysts (Gosden and Lee 2010).

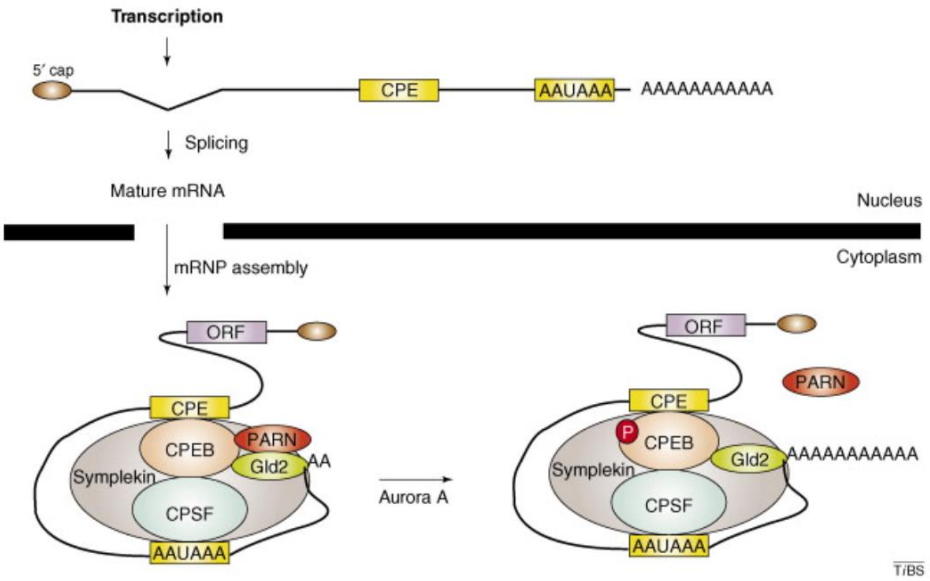

Figure 8. Regulation of Polyadenylation via CPEB. Reproduced with permission from Richter (2007).

1.4.Paracrine signaling

The communication between the oocyte and its surrounding cumulus cells is essential for the normal development and maturation of the oocyte and follicle to occur, as well as the differentiation of the surrounding somatic cells. One such method of communicative signaling is paracrine signaling (Gilchrist et al. 2008). Paracrine signaling from the oocyte to the cumulus cells, driving cumulus cell differentiation and function is often via the OSFs (Russell et al. 2016). The most commonly recognized OSFs are members of the TGFβ family: GDF9, BMP6, BMP15, and FGFs (Emori and Sugiura 2014).

Within the ovary growth differentiation factor 9 (GDF9), bone morphogenic factor 15 (BMP15), and BMP6 are produced only in the oocyte, with expression of the mRNA appearing in small primary follicles and persisting throughout

folliculogenesis in the oocytes and even after ovulation in the COC (Elvin et al. 1999). Oocyte produced BMP15 and GDF9 are required for cumulus cells competence acquisition in order to undergo expansion prior to ovulation (Emori and Sugiura 2014). GDF9 promotes expansion of cumulus cells by stimulating the synthesis of hyaluronan synthase 2 (HAS2) and suppressing urokinase plasminogen activator (uPA) (Elvin et al. 1999). Additionally, estrogen interacts with these two OSFs and contributes to the cumulus expansion just prior to ovulation (Sugiura et al. 2010). Together, the OSFs contribute to the regulation of the follicular somatic cell proliferation and differentiation, steroidogenesis, promotion of glycolysis in the cumulus cells, regulation of gene expression (including KITLG and cyclooxygenase-2 (COX2)) in the surrounding somatic cells, inhibition of luteinization, prevention of apoptosis, and induction of EGF responsiveness in the cumulus cells – a defining feature of developmental competence (Joyce et al. 1999; Joyce et al. 2001; Eppig et al. 2002; Hickey et al. 2005; Sugiura et al. 2007; Gilchrist 2011; Ritter et al. 2015).

The OSFs BMP15 and GDF9 act in a paracrine fashion from the oocyte to the granulosa and cumulus cells through their receptors, bone morphogenetic protein receptor type-II (BMPRII), and activin receptor-like kinases (ALKs), activating SMAD2/3 intracellular signaling pathways (Gilchrist 2011). Additionally, OSFs function in a gradient manner, with noticeable differences detected between, not only the concentration of transcripts present, but also the specificity of transcripts present in the cumulus and mural granulosa cells (Wigglesworth et al. 2015). For example, OSFs promote cumulus cell differentiation, leading to the

occurrence of a cumulus phenotype in a gradient within the follicle starting at the oocyte, whereas FSH has an opposite gradient promoting the mural granulosa phenotype (Wigglesworth et al. 2015).

Very few paracrine factors have been identified with a granulosa origin. One of the most studied is KITLG and KIT tyrosine kinase-receptor. KITLG and the receptors for KIT are expressed in growing and preovulatory follicles alike, with KITLG expressed in the granulosa cells and KIT expressed in oocytes of varying follicular developments (Kidder and Vanderhyden 2010). Evidence suggests that KITLG is required to induce the primordial follicle development, as well as the follicular growth (Kidder and Vanderhyden 2010). This was demonstrated by using oocytes taken from E15.5 – E16.5 murine embryos and exposing them to KITLG, which prompted oocyte growth, but failed to fully initiate the key pathways and mechanisms required to acquire meiotic competence (Klinger and De Felici 2002). From the evidence that oocyte growth and development control the rate of growth and development of the follicle, the notion can stand that KITLG activating KIT on the oocyte may control the proceeding molecular events in the oocyte such as growth and development, OSF production, and cytoplasmic, molecular, and meiotic maturation (Eppig et al. 2002; Kidder and Vanderhyden 2010).

1.5.Small molecular transfer

Gap junctions exist between cumulus cells and the oocyte containing predominantly Cx37, as well between cumulus cell and cumulus cell containing predominantly Cx43 (Kidder and Mhawi 2002). Gap junctions are oligomers

composed of six connexin proteins, forming hemi-channels, with the adjoining of two hemichannels on adjacent cells forming the actual gap junction and many clustered gap junctions on the plasma membrane forming a plaque (Clarke 2018). Gap junctions are situated at the tip of the TZPs at the oolemma, working to maintain the meiotic arrest of the oocyte by allowing the transfer of molecules permeable to gap junctions (<1kDa) between cells (Clarke 2018). The particles which transfer through Cx37 gap junctions include ions, metabolites, and amino acids (Gilchrist et al. 2008). Oocytes do not have the ability to synthesize certain amino acids directly and uptake via gap junction from the cumulus cells is essential (Clarke 2018). Additionally, molecules that are necessary for oocyte maturation, such cGMP, pass through the gap junctions (Gilchrist et al. 2008; Clarke 2018). Another molecule which passes readily though the gap junctions is Pyruvate (Clarke 2018). Glucose is one major energy source that is not efficiently utilized by oocytes due to the lack of expression of key glycolytic enzymes within it, but cumulus cells can readily metabolize glucose to its downstream product pyruvate and transfer it to the adjacent oocyte through gap junctions, where it can then be utilized it as a substrate for energy production (Clarke 2018).

1.6.Large molecular transfer

Large molecules transfer between the cumulus cells and oocyte via the TZPs (Macaulay et al. 2014). Cumulus derived mRNA transcripts, both nascent and established, can pass through them and result in deliverance to the oocyte (Macaulay et al. 2014). In canine GV stage oocytes, organelles such as

mitochondria, vesicles, and lipid droplets localize in TZPs, but their transfer to oocytes has not been demonstrated yet (De Lesegno et al. 2008).

It has been hypothesized that vesicular secretion at the oolemma allows transfer of larger molecules to enter into the oocyte, a short distance of communication rather than the usual long-distance communication which vesicles normally participate in (Macaulay et al. 2014). The vesicles containing the large molecular material bud off of the TZPs almost immediately adjacent to coated pits, which have been possibly implicated as to where the material is deposited from the vesicles (Macaulay et al. 2014). The opportunity for large molecule transfer in TZPs is transient and slowly concludes upon the resumption of meiosis, which, in cattle, is a window of approximately 9 hr after the resumption of meiosis (Macaulay et al. 2014). Furthermore, vesicular release has been suggested to occur from nanotubule like structures with origins in the plasma membrane (Abels and Breakefield 2016). This is important in the oocyte-cumulus cell relationship as the TZPs resemble nanotubules.

1.7.RNA stores in the oocyte

In eukaryotic cells, active mRNAs can exist for a short life span of minutes to several days (Yu and Russell 2001). However, like previously mentioned, these molecules can also be stored until a later time for translational activity. To regulate this activity, the nascent transcripts are sorted into RNA granules that further regulate the translation and decay of the transcripts, as well as the corresponding function associated with them (Anderson and Kedersha 2009). In germ cells, the

nascent transcripts compile themselves into these RNA granules, often called polar – granules. Once in the granule, they associate with the nuclear envelope of the cell, maintaining the dormant state until the developmental state of the cell requires their translation abilities (Anderson and Kedersha 2009).

1.7.1.RNAs affecting developmental competency

1.7.1.1. RNAs expressed in the oocyte which are associated with developmental competence

It is well known that, just as the ovarian reserve diminishes over age, the developmental competence of the oocyte diminishes too. The developmental competence of oocytes is associated with the housing of specific transcripts, with those transcripts varying as the developmental competence of the oocyte varies, for example with age. In humans, 30 mRNAs and over 160 non-coding RNAs were differentially expressed between oocytes collected from women of differing ages (women around 21 years of age to women around 34 years of age) (Barragan et al. 2017). These results by Barragan and others (2017) demonstrate that RNAs affect and are related to developmental competence in oocytes. Additionally, these results are further confirmed by the finding of spindle checkpoint genes, *MAD2* and *BUB1*, encoding the conserved kinetochore-associated proteins, had less abundant transcripts in oocytes from women > 36 years of age compared to women < 36 years of age (Steuerwald et al. 2001). Along the same lines, when comparing oocyte pools from women > 40 years of age to oocytes from women <

32 years of age, a total of 608 genes were differentially expressed, specifically annotated with functional categories relating to cell cycle, DNA damage and response, energy pathways and mitochondrial function, as well as transcription and protein transport and trafficking, amongst others (Steuerwald et al. 2007). Differences were noted in the transcriptome of oocytes from women aged 37 to 39 years old compared oocytes from to women ≤ 36 years old. It was demonstrated that, of the total 7470 genes detected within the single human oocyte samples, 342 genes were differentially expressed between the two age groups, with noteworthy genes being involved in cell cycle regulation, alignment of the chromosomes, and chromatid separation (Grondahl et al. 2010). Collectively, the results show that maternal age is associated with RNA expression profile in oocytes which affects developmental competence.

When looking at the differentially expressed genes in oocytes from adult Japanese Black cattle (24 - 35 months of age) compared to pre-pubertal animals (9 – 10 months of age), a total of 333 genes were differentially expressed between the two oocyte age groupings (Dorji et al. 2012). Additionally, within the cattle model, a positive association of inhibin/activin (the βA and βB subunits) and follistatin arises within the adult GV stage oocyte when compared to pre-pubertal oocyte (Patel et al. 2007). Similar results were demonstrated in mice. When murine oocytes aged ~5 to 6 weeks and 6 to 12 weeks were compared to those aged 42 to 45 weeks and 60 to 70 weeks, there was statistically significant differential expression in ~5% of all the transcripts detected (Hamatani et al. 2004; Pan et al. 2008). Additionally, these differentially expressed transcripts were involved with

mitochondrial function and oxidative stress, as well as chromatin structure DNA methylation, genome stability, and RNA helicase function (Hamatani et al. 2004).

In vitro maturation also affects the transcriptome of the oocyte, thereby affecting their developmental competence. In bovine, following microarray analysis, ten genes were differentially expressed after a group of MII oocytes was subjected to IVM compared to control oocytes, which were allowed to mature under *in vivo* conditions (Katz-Jaffe et al. 2009). Within these differentially expressed genes were *AQP3, SEPT7*, *ABHD4,* and *SIAH*2, which included gene ontology clusters involving metabolism, energy pathways, cell organization and biogenesis, as well as cell growth and maintenance (Katz-Jaffe et al. 2009). Additionally, in human, oocytes ranging in stages from immature, GV, GVBD/MI, MII, and mature MII, that were matured *in vitro* presented over 2000 genes upregulated (> 2-fold) compared to their *in vivo* control (Jones et al. 2008). Many of these differentially expressed genes were functionally annotated with gene ontology terms related to transcription, cell cycle regulation, as well as transport and cellular protein metabolism (Jones et al. 2008). Having different and unique transcription patterns in one form of maturation when compared to another, signifies a response of the oocyte to its environment, by which the differences from an *in* vivo to *in vitro* environment could cause the compensation in the transcriptome affecting developmental competence for the oocyte.

Another aspect that has been extensively looked at when comparing RNA to oocyte developmental competence is the size of the follicle from which the oocyte emerges. When comparing the expression of different transcripts in bovine

oocytes and their corresponding cumulus cells across a variety of follicular diameters, increasing levels of *H2A* expression coincide with an increase in follicular diameter (from < 6 mm to ≥ 8 mm) (Caixeta et al. 2009). Within the same study, blastocyst formation rate was highest for oocytes taken from follicles of > 6 mm in diameter, demonstrating that, within oocytes, *H2A* is an indicator of developmental competence in oocytes (Caixeta et al. 2009).

Along the same lines, the stage of follicular development impacts the transcriptome and oocyte developmental competence. When looking at how persistence of a follicle affected the transcriptome of the bovine oocyte, it was demonstrated that oocytes gathered from growing follicles (follicles on days 6 or 8 of the estrous cycle) had significantly higher relative abundances of *MSY2, PARN,* and *YY1*, whereas oocytes collected from the persistent follicles (follicles present of days 13 or 15 of the estrous cycle) had increased relative abundances of *PAP* and *eIF4E* (Lingenfelter et al. 2007). Additionally, in mice it was demonstrated, that in terms of follicular development (i.e.: primordial, primary, secondary, small, and large antral follicles), the greatest change in gene expression profiling exists between the primordial and primary follicle, probably representative of the dramatic structural change of the follicle and of the beginning of a major period of growth, development, and maturation for the oocyte (Pan et al. 2005).

1.7.1.2. RNAs expressed in the cumulus cells which are associated with developmental competence

Much like the oocyte itself, the cumulus cells have the ability to harbor transcripts which are associated with oocyte developmental competence. When exposed to different maturation conditions, *in vivo* or *in vitro,* the cumulus cells taken from matured COCs showed distinctly different transcript profiles (Tesfaye et al. 2009). In cattle, the cumulus cells attached to COCs matured *in vivo* were abundant in transcripts related to the regulation of oocyte maturation (*INHBA, FST*) and cumulus expansion (*TNFAIP6*), while the corresponding cumulus cells from COCs matured *in vitro* showed an abundance in transcripts related to stress response (*HSPA5, HSP90AB1*) (Tesfaye et al. 2009).

Additionally, comparing COCs of different developmental competence via follicle size in bovine, may lead to the identification of biomarkers of developmental competence in cumulus cells. Comparing the developmentally competent follicle ≥ 8.0 mm and the less developmentally competent follicle ranging 1 – 3 mm in size, Melo et al. (2017) demonstrated over 4000 genes differentially expressed in the cumulus cells between the two groups, with 143 genes upregulated and 80 genes downregulated at a fold change ≥ 2.5 in the developmentally competent cumulus cells. From their list, Melo et al. (2017) validated three up-regulated genes (*FGF11, IGFBP4, SPRY1*) and three down-regulated (*ARHGAP22, COL18A1, GPC4*) as potential biomarkers in cumulus cells of developmental competence in oocytes.

Even when considering *in vitro* development potential of the oocyte, cumulus cells have differential gene expression across bovine COCs with low and high potential from follicles ranging in sizes 3 mm to 8 mm (Kussano et al. 2016). When quantifying gene expression in cumulus cells from either COCs which had

the potential to either develop to the blastocyst stage, cleaved and arrested development, or remained uncleaved, the expression levels of *GPC4* was overexpressed in the cumulus cells taken from COCs resulting in an embryo compared to those from COCs which cleaved and arrested development (Kussano et al. 2016). Furthermore, in bovine COCs collected from 2 – 5 mm follicles, the expression of *CX43*, *LHR*, and *CYP19A1* was significantly higher in the cumulus cells associated with COCs leading to a morula/blastocyst formation, displaying higher developmental competence, versus their counterparts whose embryos arrested at the two-cell stage (Read et al. 2018).

From these studies, it is evident that cumulus cells are essential for viability of an oocyte, and they can be used as a noninvasive source of samples for testing the developmental potential of the oocyte they surround. Although, this cellular relationship and communication network is necessary for a successful development of the oocyte, much is still to be discovered regarding this essential aspect of mammalian reproduction.

2.Extraction of total RNA from single oocytes and single-cell mRNA sequencing of swine oocytes

2.1.Abstract

Analyses of single oocytes are essential for a fine dissection of molecular features governing developmental competence. Collecting oocytes and the downstream preparation for single-cell RNA-Seq is dependent upon human handling. RNA can be obtained from single oocytes through extraction kits or exposed by cellular lysis and used for reverse transcription. However, two problems emerge from these approaches: First, RNA extraction kits work by selecting poly-adenylated (polyA+) RNAs and/or using columns to retain RNA and eliminate cellular debris and small RNAs. Second, oocytes store massive amounts of RNAs, proteins, and lipids; by lysing the cells with detergents, cellular debris likely reduce the efficiency of downstream assays such as reverse transcription. Here, we adapted the phenol-chloroform procedure for the purification of total RNA from single oocytes to circumvent these problems. Key modifications include the use of Phasemaker™ tubes, a second chloroform wash of the aqueous phase, and the precipitation of the RNA with glycogen in a 200 µl micro-centrifuge tube. Assessment of the RNA profile from single oocytes showed distinct peaks for 18S and 28S ribosomal subunits. This approach permitted the extraction of small RNAs from single oocytes, which was evident by the presence of 5S and 5.8S rRNAs and tRNAs around 122-123 nucleotides long. The amplification of polyadenylated RNA resulted in detectable DNA products ranging from ~500 to ~5000 bp. We

used the amplified DNA as template for single-cell mRNA-sequencing of five swine oocytes and quantified the expression levels of 9587 genes with complete coverage of transcripts over 10000 nucleotides in length. The coverage was similar in all oocytes sequenced, demonstrating consistent high RNA quality across samples. We isolated total RNA from single oocytes and demonstrated that the quality was appropriate for single-cell mRNA-sequencing.

2.2. Introduction

The abundance of specific ribonucleic acids (RNAs) stored in the female gamete, namely the oocyte, has a direct relationship with the acquisition of developmental competence (Biase et al. 2010; Biase et al. 2014b; Biase 2017). With the recent advances of next generation sequencing, single oocyte RNA sequencing data have been generated for mice (Tang et al. 2009; Xue et al. 2013; Biase et al. 2014a), cattle (Reyes et al. 2015), goats (Yin et al. 2017), and humans (Liu et al. 2016). Analyses of single oocytes are essential for a fine dissection of molecular features governing developmental competence, however, technical challenges must be overcome for the generation of data from oocytes compatible with massive single-cell sequencing.

In mammals, the collection of oocytes and downstream preparation for single-cell RNA sequencing is dependent on human handling. The RNA from single oocytes can be obtained through extraction kits (Reyes et al. 2015) or by direct cellular lysis (Picelli et al. 2014) and used in enzymatic assays. However, three critical problems emerge from current approaches: First, most extraction kits

dedicated to limited amounts of RNA work by selecting polyadenylated (polyA+) RNAs and/or using columns to selectively eliminate cellular debris and small RNAs. Second, it is unclear how much of the RNA is lost when small volumes of eluent are used to recover limited amounts of RNA. Third, oocytes store massive amounts of RNAs, proteins, and lipids and by lysing the cells with detergents, cellular debris can reduce the efficiency of downstream assays such as reverse transcription and polymerase chain reaction (Schrader et al. 2012). Improving the methods for extraction of RNA from single oocytes is necessary for us to generate next-generation sequencing data from different RNA species (i.e.: micro RNA, or mRNA) from single oocytes.

Motivated by the above mentioned limitations, we describe modifications to the phenol-chloroform (Chomczynski and Sacchi 2006) procedure that made the purification of total RNA from single oocytes possible. We demonstrate that the total RNA is suitable for the preparation of libraries for single-cell mRNA sequencing. The approach we report can be applied to extract total RNA from single oocytes from any mammalian species.

2.3.Material and Methods

No live animals were handled specifically for this study and ovaries were handled postmortem, thus the study was not submitted for approval by the institutional animal care and use committee (IACUC) at Auburn University. Swine (*Sus scrofa*) and bovine (*Bos taurus*) ovaries were obtained from slaughterhouses and transported to the laboratory in saline solution for manual aspiration of follicles

and collection of cumulus-oocyte complexes. Single germinal vesicle oocytes were manually denuded of cumulus cells (Figure 9a) and deposited into 5 µl of 1 X phosphate-buffered saline (AMRESCO), supplemented with Ribonuclease inhibitor (0.5 U/µl) (AMRESCO), snap frozen in liquid nitrogen, and stored at -80 ºC. For the total RNA extraction from single oocytes (Figure 9b), the incubation times and centrifugation steps were performed as recommended by the TRIzol™ (ThermoFisher) and Phasemaker™ (ThermoFisher) protocols. We thawed the oocyte by adding 150 µl of TRIzol™ followed by the addition of 30 µl of chloroform. The mixture was transferred to a Phasemaker™ tube for centrifugation at 12000 x g for 5 minutes at 4 °C. We then mixed the aqueous solution with 20 µl of chloroform followed by a second centrifugation at the same parameters. The aqueous solution was collected and mixed with 1 µl of Glycoblue™ (ThermoFisher) and 150 µl of isopropanol in a 200 µl tube, then subjected to a centrifugation at 12000 x g for 10 minutes at 4°C. The RNA pellet was washed twice with 75 % ethanol followed by centrifugation at 7500 x g for 5 minutes at 4 °C. The pellet was air dried and eluted in 1 µl of nuclease free water to profile the RNA length distribution in an Agilent 2100 Bioanalyzer (Agilent) following the manufacturer's protocol.

To generate RNA-sequencing data from five swine oocytes, we eluted the RNA pellet in 4 µl of a solution containing oligo(dT) (Promega) and deoxynucleotide triphosphates (Promega) to assay full-length polyA+ RNA amplification following the SMART-seq2 procedure (Picelli et al. 2014). Following cleanup and quantification of the amplified complementary deoxyribonucleic acid

(cDNA) on a Qubit 3.0 fluorometer (Thermo Fisher), one ng was used as template for next generation sequencing libraries, prepared with Nextera XT DNA library Prep Kit (Illumina, Inc) (Picelli et al. 2014). The libraries were pooled and assayed on a HiSeq2500 instrument (Illumina, Inc) to generate pair-end reads.

The sequences were aligned to swine cDNAs obtained from Ensembl (Sscrofa11.1, release 90) using Bowtie2 (Langmead and Salzberg 2012) with the "--very-sensitive" option. Analyses to characterize the data properties were conducted in R software (Ihaka and Gentleman 2012).

2.4.Results and Discussion

We assessed the distribution of total RNA from single bovine (N = 25) and swine (N = 22) oocytes (Figure 9c). We observed distinct peaks for 18S ($\bar{x}_{peak} = 1740$ nucleotides (nt), bovine oocytes; $\bar{x}_{peak} = 1749$ nt, swine oocytes) and 28S ($\bar{x}_{peak} = 3481$ nt, bovine oocytes; $\bar{x}_{peak} = 4523$ nt, swine oocytes - respectively) ribosomal subunits. Additionally, we recorded RNA integrity number values between 5.1 and 7.3.

This procedure allowed us to profile small RNAs of single oocytes. The signal for small RNAs (5S, 5.8S, transfer RNAs (tRNAs)) is commonly observed in preparations using the phenol-chloroform without further column purification (Cirera 2013). The peaks were averaged on 123 and 122 nt in the bovine and swine oocytes, respectively. The observations were consistent with the RNA length of the 5S ribosomal subunit (Smirnov et al. 2008).

Amplification of polyA+ RNA via polymerase chain reaction resulted in amplified cDNA (acDNA) products detected between ~500 and ~5000 nucleotides (Figure 9d). The acDNA was used as input for library preparation and sequencing. We generated RNA-sequencing data from five swine single oocytes averaging 9.6 million pair-end reads per sample. The alignment of the reads to the swine cDNA sequences resulted in of 9587 Ensembl genes detected in all five oocytes with fragments per kilobase of transcript per million reads mapped > 0.3.

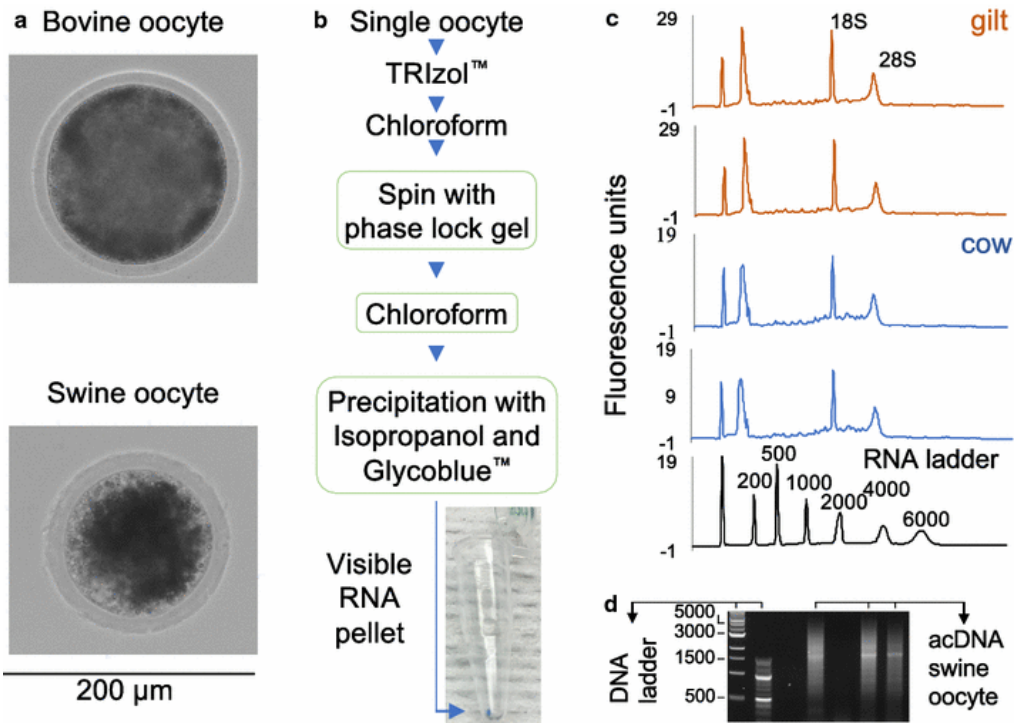

Figure 9. Total RNA extraction from single oocytes. (a) Representative images of bovine and swine oocytes. The scale bar is used for both images (b) Diagram of the RNA extraction flow. The green boxes indicate key adaptations to the standard TRIzol™ protocol. (c) Representative Bioanalyzer electropherograms of the total RNA extracted from single oocytes, and a ladder for reference. (d) Representative full-length cDNA amplification of swine oocytes.

The RNA-sequencing data revealed the quantification of short and long transcripts in single swine oocytes with a distribution similar to the observed in the Ensembl transcriptome database (Figure 10a) with approximately 75 % of the transcripts composed of ≤ 5000 nucleotides. Overall, there was a skewed distribution of reads towards 5' end of the cDNA (Figure 10b), which was probably caused by the tagmentation step of library preparation (Gertz et al. 2012). This tendency, however, was more prominent on transcripts whose length ranged between 5000 to 10000 nucleotides, while, transcripts with less than 5000 nucleotides presented a more homogeneous read distribution across the transcripts (Figure 10c). Most importantly, the overall distribution of read coverage on the transcripts was reproducible across five oocytes sequenced (Figure 10c).

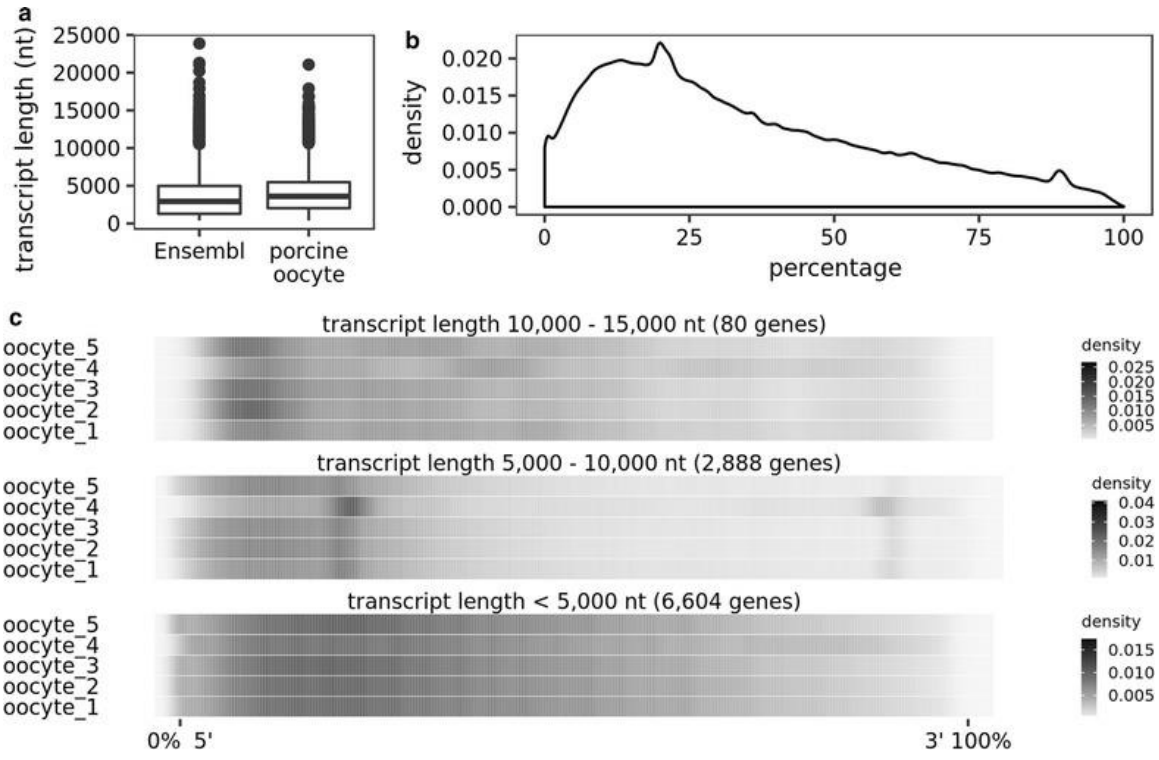

Figure 10. Single-cell mRNA sequencing of swine oocytes. (a) Length distribution of the transcripts sequenced in nucleotide units. The boxes represent

the 25th, 50th, and 75th quantiles of the distribution. The lower error bar represents the lowest value > (-1.5 x interquartile range) + 25th quantile. The upper error bar represents the greatest value < (1.5 x interquartile range) + 75th quantile (b) Overall transcript coverage. (c) Transcript coverage for each oocyte in three different ranges of transcript length.

We adapted the phenol-chloroform protocol to extract total RNA from single oocytes. Our adaptations to the phenol-chloroform protocol permit non-selective extraction of total RNA from single oocytes. The extracted RNA is compatible with downstream enzymatic assays needed for the generation of single-cell mRNA sequencing data. The transcripts of 9587 swine genes were sequenced from single oocytes with nearly full coverage.

3.Transcriptome profiles of porcine oocytes and their corresponding cumulus cells reveal functional gene regulatory networks

3.1.Abstract

The successful development and progression of an oocyte hinges upon its ability to effectively acquire developmental competence as it progresses through folliculogenesis. Hormones and small molecules, such as calcium, govern a heavy component of the oocyte's fate, but much is left to be elucidated concerning the role of transcripts. We hypothesized that the transcript profiles of the cumulus cells and oocyte of gilts (*Sus scrofa*) display distinct gene regulatory networks within the oocyte and cumulus cells. Here, by analyzing the expression of genes within oocyte and cumulus cell samples, we demonstrated 7277 of genes expressed in the cumulus-oocyte complex (COC). Independent clustering and enrichment analyses of gene ontology molecular functions and biological processes revealed significantly enriched (FDR < 0.05) and biologically relevant categories for folliculogenesis, such as "positive / negative regulation of transcription from RNA polymerase II promoter", "insulin receptor signaling pathway", "translation", and "protein transport". Our analysis revealed coordinated expression of hundreds of genes that formed functional regulatory networks in oocyte and cumulus cells.

3.2.Introduction

During gametogenesis the oocyte is surrounded by somatic cells. These somatic cells maintain their close knit positionings throughout gametogenesis,

folliculogenesis, and even ovulation. As the female gamete progresses through folliculogenesis, both the oocyte and surrounding somatic cells undergo vast cellular and physiological modifications, including differentiation of the somatic cells at the occurrence of a tertiary follicle from granulosa cell to either a cumulus granulosa cell (or cumulus cell) immediately adjacent to the oocyte within the follicle or a mural granulosa cell positioned on the periphery on the follicle (Georges et al. 2014). These differentiations are critical for the successful acquisition of developmental competence of the oocyte (Dumesic et al. 2015).

As the oocyte progresses through folliculogenesis and matures, it accumulates an abundance of gene transcripts and proteins, which leads to an increase in cell volume and dynamic organelle rearrangements, encompassing cytoplasmic and nuclear maturation (Gosden and Lee, 2010). The cumulus cells (CCs) are an essential piece of the puzzle which makes up oocyte developmental competence, as they provide the oocyte with nourishment through a bidirectional exchange involving ions, metabolites, small molecules (such as cAMP), and large molecules, such as transcripts (Macaulay et al. 2016; Russell et al. 2016).

Thus far, studies have been developed and conducted concerning the transcriptomes of both oocytes and cumulus cells across a variety of conditions, looking at their effect on oocyte developmental competence (Tesfaye et al. 2009; Ma et al. 2013; Takeo et al. 2013). Additionally, studies have been conducted to isolate biomarkers related to oocyte developmental competence in the pig (Yuan et al. 2011), but the functional gene regulatory networks have yet to be mapped within oocytes and CCs.

For this study, we hypothesized that the functional profiles of the cumulus cells and oocyte of prepubertal porcine would display distinct differences based on their subsequent transcriptomes. The objectives of this study were to elucidate the gene regulatory networks in the cumulus-oocyte complexes (COCs) within the oocyte and cumulus cells individually. Here, by analyzing the expression of genes within oocyte and cumulus cell samples, we demonstrated that oocytes and cumulus cells have distinctly different functional transcriptomes. Furthermore, within these transcriptomes, networks were formed which demonstrate genes as hubs in specific functions critical for the acquisition of developmental competence.

3.3.Material and Methods

3.3.1.Sample collection from single cumulus-oocyte complexes

Immediately following removal from the animal, ovaries from one gilt (*Sus scrofa*), ~150 days of age, were placed into a vial containing a 0.8% saline solution at room temperature and transported to the laboratory. Follicles on the ovaries measuring between 3 and 5 mm in diameter were aspirated with an 18-gauge needle. The follicular fluid containing the COCs was diluted with 1 X PBS (AMRESCO) and the COCs were selected and washed in 1 X PBS 0.02 % BSA (Akron). The COCs were selected based on morphological characteristics indicative of a greater developmental potential (Reader et al. 2017). The COCs collected contained an oocyte with a non-granulated cytoplasm and zona pelucida surrounded by a full cumulus cell layer, at least three layers deep. The selection

of uniform follicles and uniform COCs out of the follicular fluid limited the possibility of outside influences that could negatively impact the RNA within the oocyte.

Upon selection and post-wash, the COCs were individually placed in a 5 µl droplet of 1 X PBS 0.02 % BSA. In a consecutive fashion, the COCs were then transferred to a 5 µl droplet containing 1 X Trypsin (HyClone Laboratories) for removal of the cumulus cell layer with the assistance of gentle pipetting (Figure 11). With the removal of the cumulus cells, the remaining denuded oocyte was quickly transferred to a new droplet containing 1X PBS 0.02% BSA. The cumulus cell sample, still in the 1 X Trypsin droplet, was then immediately collected, flash frozen in liquid nitrogen, and stored at -80 °C. The remaining denuded oocytes were transferred over to a fresh droplet of 1 X PBS 0.02% BSA, avoiding carry over of cumulus cells, and individually collected and flash frozen in liquid nitrogen in a 0.2 ml containing 5 µl of 1 X PBS and RNase inhibitor (0.5 U/µl) (AMRESCO). All samples were stored at -80 °C until use for RNA extraction.

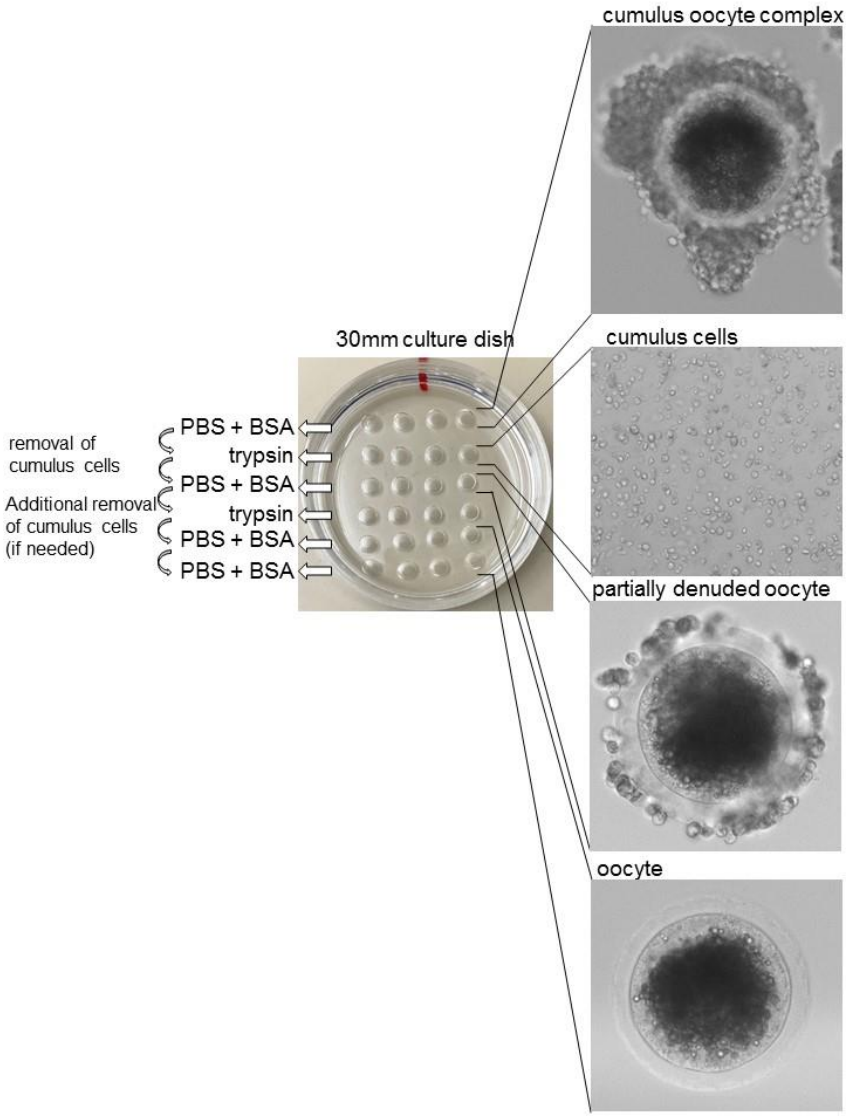

Figure 11. Sample collection schematic. For each COC, two sets of samples were obtained: cumulus cells and the corresponding oocyte.

3.3.2.Library preparation and RNA sequencing

We extracted total RNA from single oocytes or cumulus cell samples using TRIzol® (Thermo Fisher) protocol, with the aid of Phasemaker™ tubes (Thermo

Fisher) and the addition of 0.5 µl the co-precipitant GlycoBlue™ (Thermo Fisher) to pellet the RNA as described elsewhere (Kimble et al. 2018).

We eluted the RNA with 4 µl of a solution containing dNTPs (10 mM, Promega) and oligo(dT)$_{30}$VN (10 µM, Promega) and proceeded with reverse transcription and cDNA amplification according to the SMART-seq2 protocol (Picelli et al. 2014). The cumulus cell samples were subjected to 12 cycles of PCR amplification, while the oocyte samples were subjected to 14 cycles. For each sample, one ng of acDNA was used as starting material for the Nextera XT DNA library prep Kit (Illumina, Inc.) as described in the SMART-seq2 protocol (Picelli et al. 2014). Quantification of the libraries was performed on the Qubit 3.0 fluorometer (Thermo Fisher), while the quality of the libraries was evaluated on a 2100 Bioanalyzer System (Agilent). Sequencing of the libraries was conducted at the Genomic Services Lab at HudsonAlpha (Huntsville, AL) using the HiSeq2500 platform (Illumina, Inc.) to produce paired-end reads of 125 nucleotides in length.

3.3.3.Quantification of gene transcript abundance

Sequencing reads were aligned to the *Sus scrofa* genome (Sscrofa11.1 (Kinsella et al. 2011; Flicek et al. 2013)) downloaded from Ensembl (Flicek et al. 2013) using HISAT2 (v2.1.0, (Kim et al. 2015)) software. Reads aligned to the genome at less than 5 positions and presenting less than four mismatches were retained for further analysis. On average per sample, 6.9 and 9.6 million pairs of reads were mapped to the porcine genome (Sscrofa11.1 (Kinsella et al. 2011;

Flicek et al. 2013)) for cumulus cells and oocytes, respectively. We used the bam files as input to HTSeq (Anders et al. 2015) for counting of the reads according to the Ensembl gene annotation Sscrofa 11.1.90.

We quantified the gene transcript levels to obtain FPKM values (Law et al. 2016) using the 'rpkm' function of the 'edgeR' package (Robinson et al. 2010) in R software (Ihaka and Gentleman 2012), according to the gene transcript lengths obtained from Ensembl. To assure that downstream analyses were carried with genes whose transcript levels were robustly quantified, we only retained genes whose FPKM > 0.3 and CPM > 1 in $\geq$ 15 samples.

3.3.4. Analysis of gene co-expression in oocytes and cumulus cells

We performed weighted gene correlation network analysis (WGCNA) in each of the sample types (oocytes, cumulus) using the WCGNA package (Langfelder and Horvath 2008). We used $\log_2$(FKPM+1) values to calculate signed adjacency, followed by the calculation of topological overlap similarity to identify patterns of interconnectivity among genes (Langfelder and Horvath 2008). The topological overlap matrix (TOM) was converted into a distance matrix (1-TOM) for clustering, using the average method and the Euclidian distance, with the flashClust package (Langfelder and Horvath 2012). The modules were identified using the dynamic tree cutting approach (Langfelder et al. 2008), and modules were merged at the similarity threshold 0.15 to obtain a minimum of 25 genes per

cluster. We tested the genes in each module (test set) for enrichment of GO (Ashburner et al. 2000) biological processes and molecular functions with GOseq package (Young et al. 2010) considering the genes expressed in either oocyte or cumulus cells as background (Timmons et al. 2015).

3.3.5.Differential gene expression between oocyte and cumulus cells

We employed the raw read count to compare gene expression levels between samples with the packages edgeR (Robinson et al. 2010) using the TMM normalization (Robinson and Oshlack 2010) and DeSeq2 (Love et al. 2014) using sample- and gene-specific normalization factors (Love et al. 2014). The model considered the two cell types being compared (oocyte vs. cumulus cells). We inferred differential gene expression if the Benjamini-Hochberg (Benjamini and Hochberg 1995) FDR was < 0.01 in the results obtained using both packages (Dickinson et al. 2018).

3.3.6.Analysis of differential co-expression between oocytes and cumulus cells

We performed differential co-expression analysis according to the framework detailed elsewhere (Tesson et al. 2010). First, we calculated the adjacency matrix for oocytes and cumulus cells independently using Pearson's coefficient of correlation and a soft power of two to reduce the noise due to low

correlation values. Second, we subtracted the adjacency produced by the cumulus' data from the adjacency produced oocyte's data and raised the resulting matrix to the power of four. Next, we calculated the topological overlapping matrix and used 1-TOM as distance matrix input for clustering.

We established a threshold for identification of clusters and tested the genes in each module (test set) for enrichment of GO (Ashburner et al. 2000) biological processes and molecular functions with GOSeq package (Young et al. 2010) considering all genes quantified in oocyte or cumulus cells as background (Timmons et al. 2015).

3.3.7.Heat maps and network visualization

We used the ComplexHeatmaps package (Gu et al. 2016) to draw annotated heatmaps and Cytoscape software (Cline et al. 2007) to visualize the networks.

3.4.Results

3.4.1.Experimental Overview

We collected 17 prepubertal porcine (*Sus scrofa*) COCs from abattoir-sourced ovaries and separated each individual COC into a cumulus cell sample, consisting

of all CCs surrounding the oocyte, and an oocyte sample, consisting of a denuded oocyte. Additional COCs were collected and the diameters of the oocytes were measured. Out of a sample size of 63 oocytes, the mean diameter was 115 μm with a standard deviation of 5.5 (Figure 12), indicating the majority of the oocytes we sampled had reached a growth plateau by the time of collection (Lucas et al. 2002).

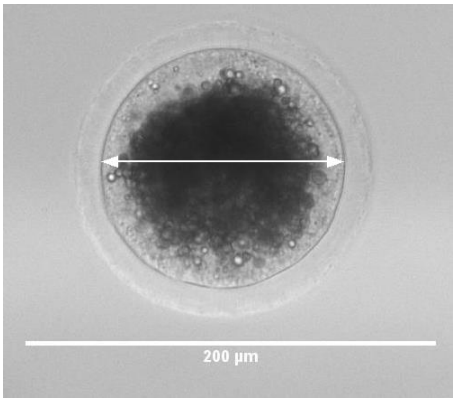

Figure 12. Porcine oocyte. The double headed arrow represents the axis used to measure the diameter. Scale bar: 200 μm

We separated the cumulus cells and the corresponding oocytes from 17 individual COCs and generated RNA-sequencing data from both components of the COCs (oocytes and cumulus cells, Figure 13a). On average per sample, 6.9 and 9.6 million pairs of reads were mapped to the porcine genome (Sscrofa11.1 (Kinsella et al. 2011; Flicek et al. 2013)). We applied a 'dual filter' strategy for a more robust estimation of gene transcript abundance and retained genes whose FPKM > 0.3 and CPM > 1 in ≥ 15 samples. This filtering strategy allowed us to quantify 3593 and 6811 genes in CCs and oocytes, respectively (Figure 13b). As

expected, the oocyte and cumulus samples clustered separately by a dimensionality reduction of their transcriptome data (t-SNE, Figure 13c).

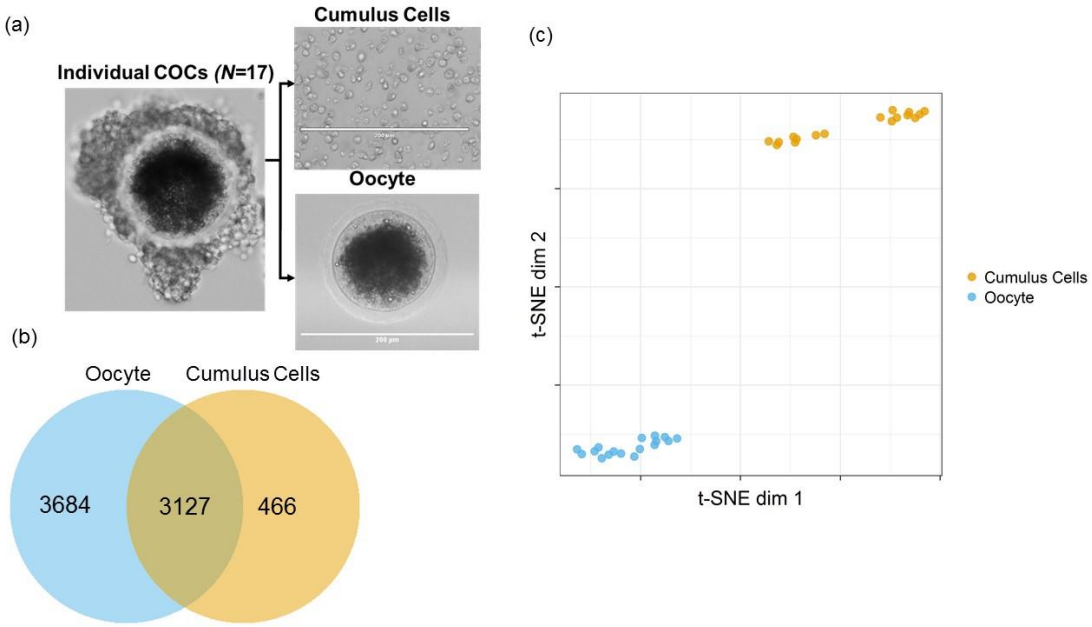

Figure 13. RNA Sequencing of single oocytes and cumulus cells. (a) Schematic of samples collected (scale bar: 200 μm). (b) Representation of unique and overlapping gene expression between cell types. (c) t-Distributed Stochastic Neighbor Embedding (t-SNE) of the transcriptomes of oocytes (blue) and CCs (orange).

3.4.2.Functional transcriptome profiles of single porcine oocytes through co-expression analysis

WGCNA and Gene Ontology (GO) enrichment analyses were used to determine the gene clusters, as well as the functional profiles of each of the two sample types independently. In oocytes, there were a total number of 3702 genes

annotated for biological processes across 11 clusters (0, 2, 5, 8, 9, 11, 13, 18, 19, 20 and 24). On average, the following number of genes per biological process occurred in each cluster: 33, 18, 8, 15, 16, 16, 6, 23, 8, 7, and 8 in clusters 0, 2, 5, 8, 9, 11, 13, 18, 19, 20, and 24, respectively. Additionally, the number of genes annotated for GO biological process in each cluster were as follows: 1407, 259, 35, 308, 105, 449, 6, 1100, 15, 10, and 8, in the same corresponding clusters noted above.

After applying an FDR filter of < 0.05, 248 co-expressed genes formed seven clusters with significant enrichment (FDR < 0.05) of numerous GO terms (Figure 14 a & b). The biological process “negative regulation of transcription from RNA polymerase II promoter” showed the greatest number of genes (66 genes in clusters 2, 9, and 24), followed by “positive regulation of transcription from RNA polymerase II promoter” (49 genes in cluster 2), “protein phosphorylation” (32 genes in clusters 2), and “translation” (32 genes across cluster 8). Another notable annotation for genes co-expressed in oocytes was the biological process "protein transport" (19 genes in cluster 8, Table 1).

Additionally, there were 3915 genes in the oocyte samples annotated with molecular functions across 16 clusters (0, 2, 5, 8, 9, 11, 13, 14, 18, 19, 20, 24, 28, 29, 30, and 37). On average, the following number of genes per category occurred in each cluster: 76, 22, 15, 37, 15, 37, 7, 9, 52, 14, 7, 9, 8, 6, 6, and 7 respectively. Additionally, the number of genes annotated for GO in each cluster were as

follows: 1377, 265, 81, 348, 132, 492, 16, 39, 1054, 36, 26, 22, 8, 6, 6, and 7 in the same corresponding clusters described above.

After applying an FDR filter of < 0.05, 227 annotated genes were co-expressed amongst five clusters with significant enrichment (FDR < 0.05) of numerous GO terms (Figure 14 a & b). The molecular function with the greatest number of annotated genes was “RNA binding” (113 genes in cluster 8), followed by “catalytic activity” (33 genes in cluster 11), “structural constituent of ribosome” (23 genes in cluster 11), and “unfolded protein binding” (17 genes across cluster 11, Table 2).

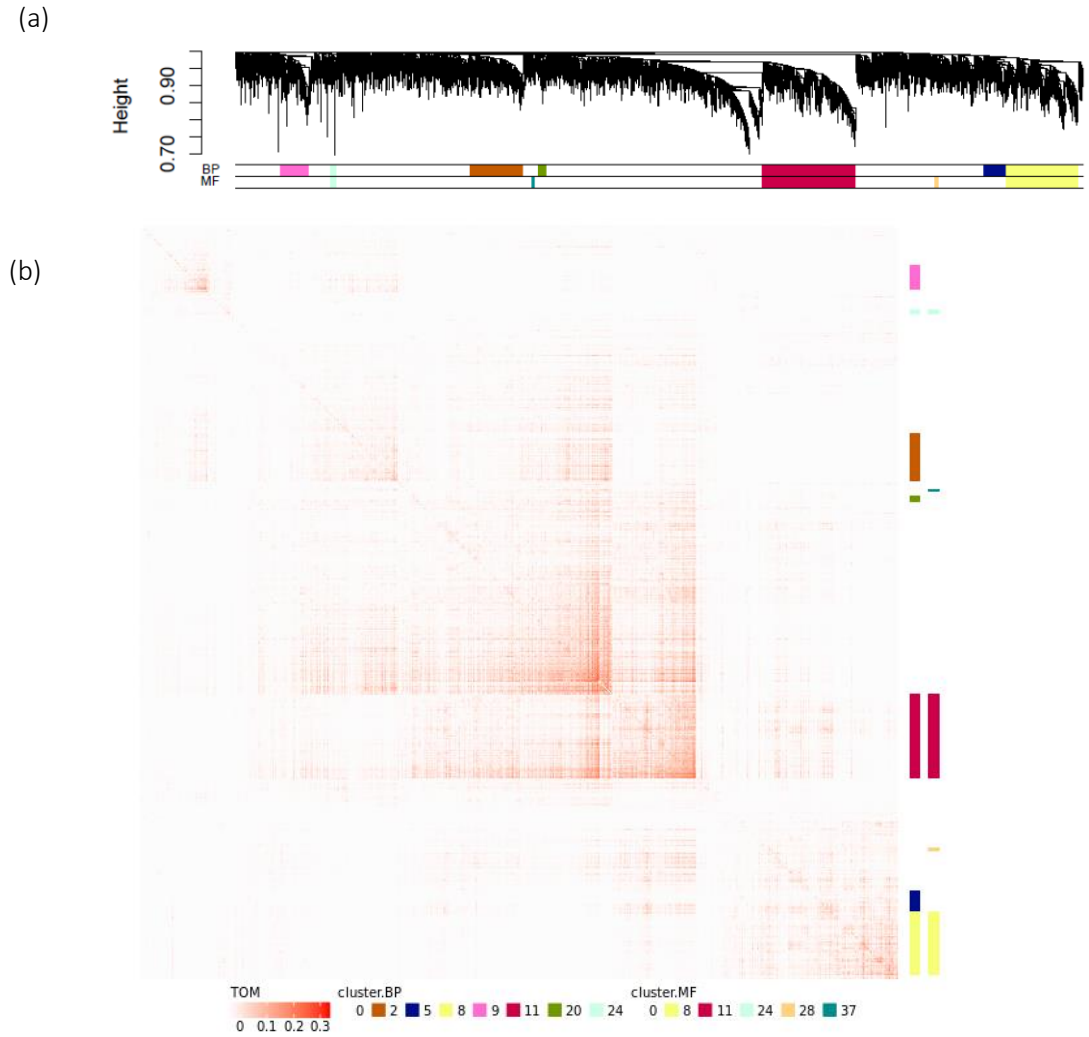

Figure 14. Cluster dendrogram and heat map for oocyte samples. (a) Dendrogram of gene co-expression modules present in oocytes created by WGCNA. (b) Heat map co-expression patterns in oocytes. Rows and columns represent pairs genes and the different shades of color present of the map correspond to the strength of the co-expression between oocyte and cumulus. White represents no correlation. The vertical bars to the side represent the clusters with significant enrichment for biological processes (BP) and molecular function (MF).

To explore the interconnectivity of oocyte genes concerning the GO term “transcription”, networks were formed according to the gene co-expression (Figure 15). These networks were built on genes expressed by the oocyte with a threshold set to absolute value of Pearson’s correlation ≥ 0.90. Within this network each node represents a gene expressed in oocytes, with colored nodes indicating genes associated with regulation of transcription. Additionally, each edge represents a correlation between the two nodes; either a positive association (Pearson’s correlation ≥ 0.90) represented by a red edge or a negative association (Pearson’s correlation ≤ -0.90) represented by a blue edge.

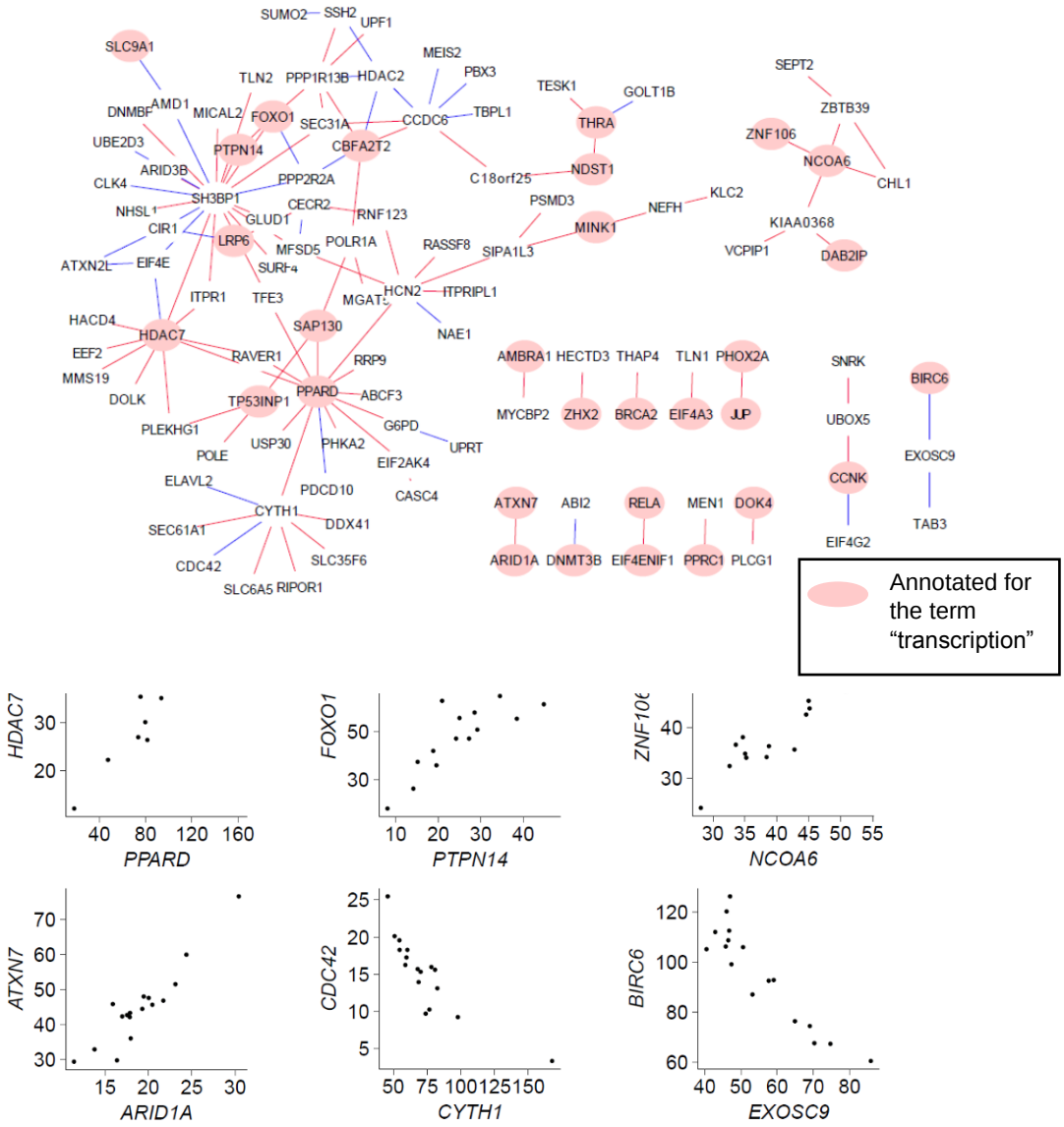

Figure 15. **Oocyte gene co-expression network.** Red ellipses represent genes annotated for the GO term “transcription”. Red edges represent a Pearson’s correlation ≥ 0.90, while the blue represent a Pearson’s correlation ≤ 0.90. Additional scatter plots of select genes representing positive or negative associations based upon Pearson’s correlation. Axes on the scatter plots represent FPKM values.

3.4.3.Functional transcriptome profiles of porcine cumulus cells through co-expression analysis

In CCs, we identified 2247 genes expressed annotated for biological process that formed six clusters (0, 1, 2, 5, 9, and 11, Figure 16 a & b). On average, the following number of genes per category occurred in each cluster: 10, 20, 36, 12, 16, and 9 in clusters 0, 1, 2, 5, 9, and 11, respectively. Additionally, the number of genes annotated for GO in each cluster were as follows: 46, 524, 1286, 138, 187, and 66, in the same corresponding clusters described above.

From these, 123 genes were expressed forming three clusters (2, 9, and 11) with significant enrichment of GO biological processes (Figure 16 a & b, FDR < 0.05). Ninety genes were annotated with the biological process “translation” (cluster 2). Followed by “cellular response to insulin stimulus” with 11 genes in cluster 9 and “regulation of gene expression” with ten genes (cluster 11, Table 3).

Additionally, there were 3915 genes in the CC samples related to molecular function across six clusters (0, 1, 2, 5, 9, and 11). On average, the number of genes per category per cluster was as follows: 10, 36, 70, 15, 22, and 17, respectively. Additionally, the number of genes annotated for GO in each cluster were as follows: 69, 522, 1277, 167, 220, and 97, in the same corresponding clusters above.

After applying an FDR filter of < 0.05, 64 genes were co-expressed forming 1 cluster (cluster 2) with significant enrichment of numerous GO terms (Figure 16 a & b). The most annotated molecular function was “structural constituent of ribosome” (64 genes in cluster 2, Table 4).

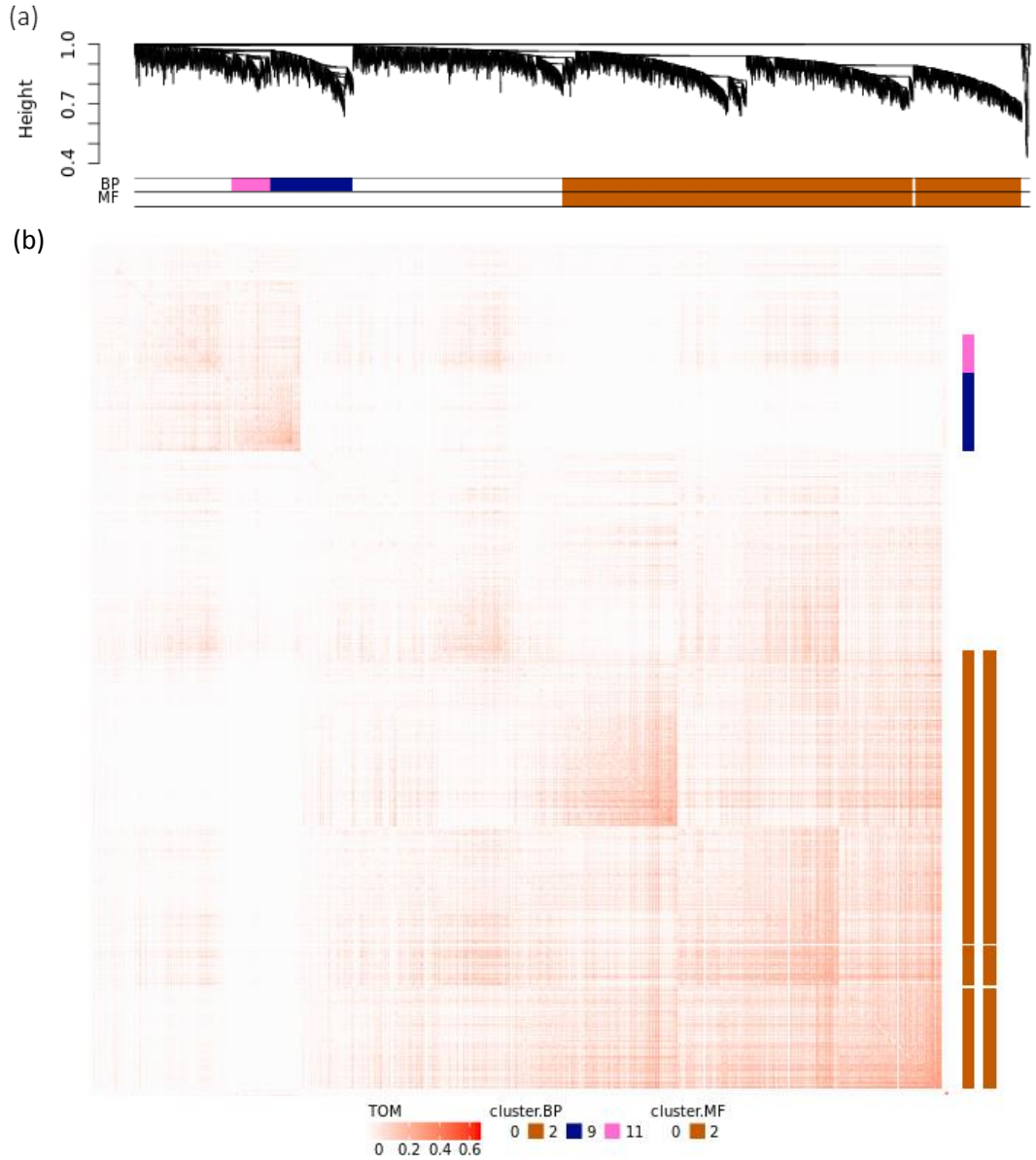

Figure 16. Cluster dendrogram and heat map for cumulus cell samples. (a) Dendrogram of gene co-expression modules present in CCs created by WGCNA.

(b) Heat map co-expression patterns in CCs. Rows and columns represent pairs genes and the different shades of color present of the map correspond to the strength of the co-expression between oocyte and cumulus. White represents no correlation. The vertical bars to the side represent the clusters showing enrichment for biological processes (BP) and molecular function (MF).

To explore the interconnectivity of CC genes concerning the GO term “transcription”, networks were formed (Figure 17). These networks were built on genes expressed by the cumulus cells with a threshold set to absolute value of Pearson’s correlation ≥ 0.90. Within this network each node represents a gene expressed in the CC samples, with a colored node indicating annotation for the term “transcription”. Additionally, each edge represents a correlation between the two nodes; with a positive association (Pearson’s correlation ≥ 0.90) represented by a red edge on a continuous scale.

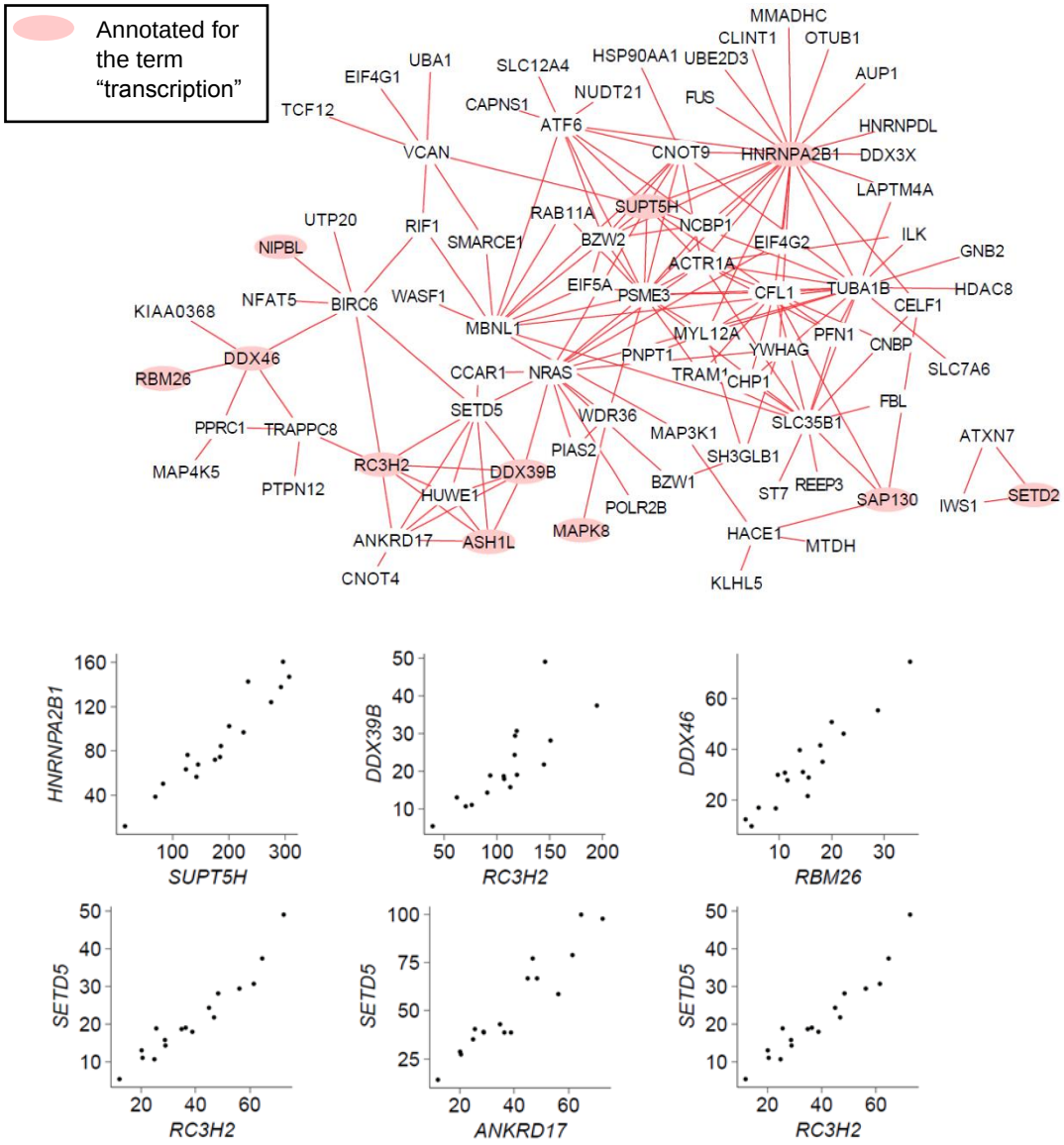

Figure 17. Cumulus cell gene co-expression network. Red ellipses represent genes annotated for the GO term "transcription". Red edges represent a Pearson's correlation ≥ 0.90. Additional scatter plots of select genes representing positive or negative associations based upon Pearson's correlation. Axes on the scatter plots represent FPKM values.

Interestingly, the oocyte displayed enrichment for terms which were not present in the CC samples, such the molecular function "translation initiation factor

activity” with 12 genes in cluster 8 and the biological process “translational initiation” with 14 genes annotated across cluster 11. On the other hand, the CC samples also contained terms not identified in the analysis of oocyte samples. For example, six genes were annotated with the biological process “Rho protein signal transduction” in cluster 9 in the CCs.

3.4.4.Differential gene expression and differential co-expression analysis

Differential gene expression analyses from both cell types showed that of the 7277 genes expressed overall, 645 were not significant in either cell type, while 1806 were upregulated (FDR < 0.05) in cumulus cells and 4826 were upregulated (FDR < 0.05) in oocytes (Figure 18).

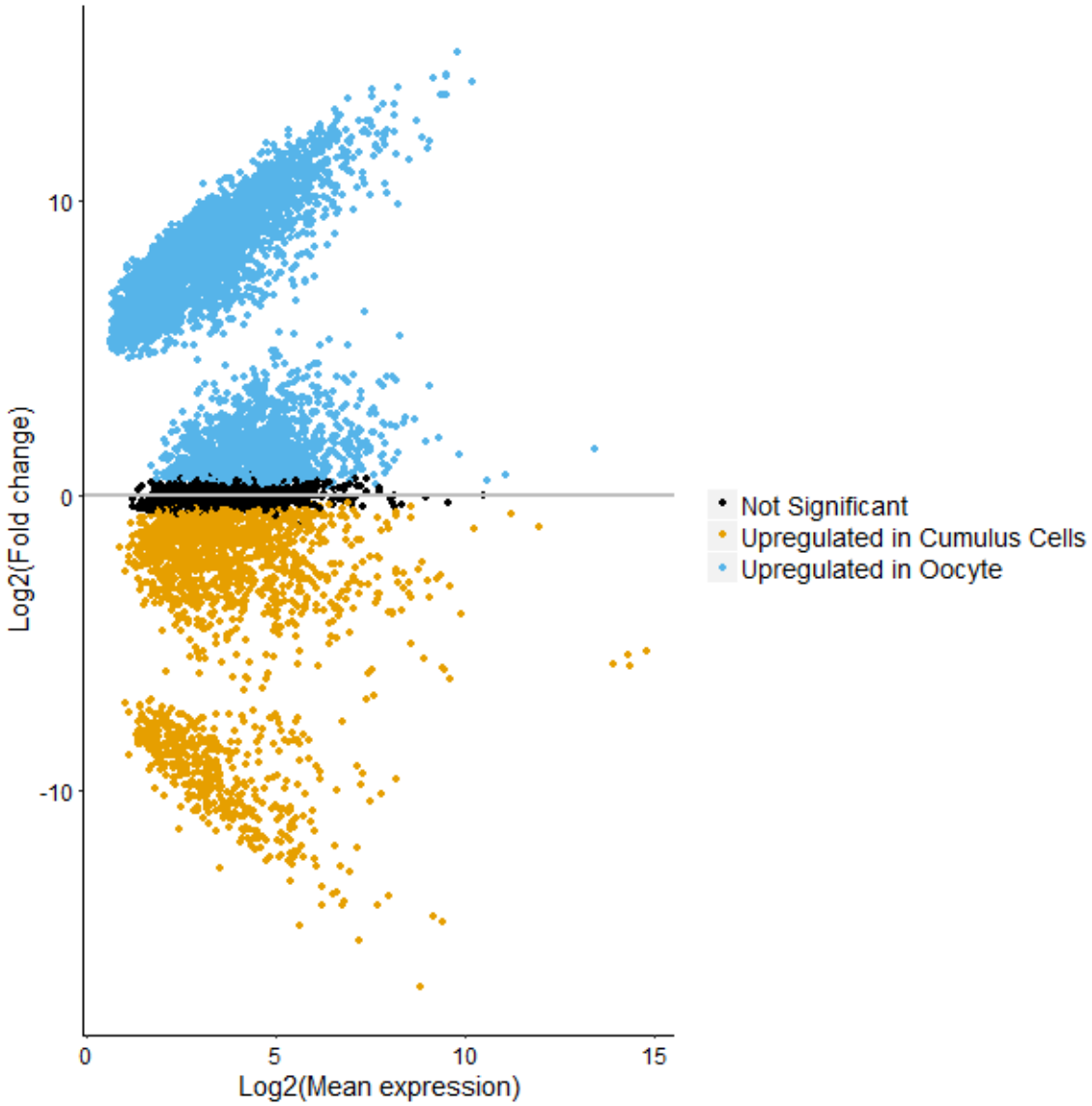

Figure 18. Scatter plot of the differential expression and overall average expression for genes transcribed in COC. (Black) Genes not differentially expressed between cell types. (Orange) Genes significantly (FDR < 0.05) upregulated in the CC samples. (Blue) Genes significantly (FDR < 0.05) upregulated in the oocyte samples.

Differential co-expression analysis was performed on the transcript levels of all genes quantified in the oocyte and cumulus cells. We identified 16 clusters (7, 10, 13, 15, 18, 22, 29, 47, 149, 181, 192, 220, 287, 320, 432, 757) containing 827 genes presenting differential co-expression between the oocyte and cumulus cells. Of those, 134 genes were present in nine clusters showing functional enrichment (FDR < 0.05) for biological processes. Within these clusters, the most represented terms were “translation” with 45 annotated genes across cluster 10, followed by "translation initiation" with 13 genes annotated across cluster 10. The next most represented terms were "ubiquitin-dependent ERAD pathway" with 10 genes across cluster 10 and “proteolysis involved in cellular protein catabolic process” also with 10 genes in cluster 10. These results demonstrated that the functional profile differences between the oocyte and cumulus cells samples are directed at the areas involving translation and post translational modifications (Tables 5 & 6, Figure 19).

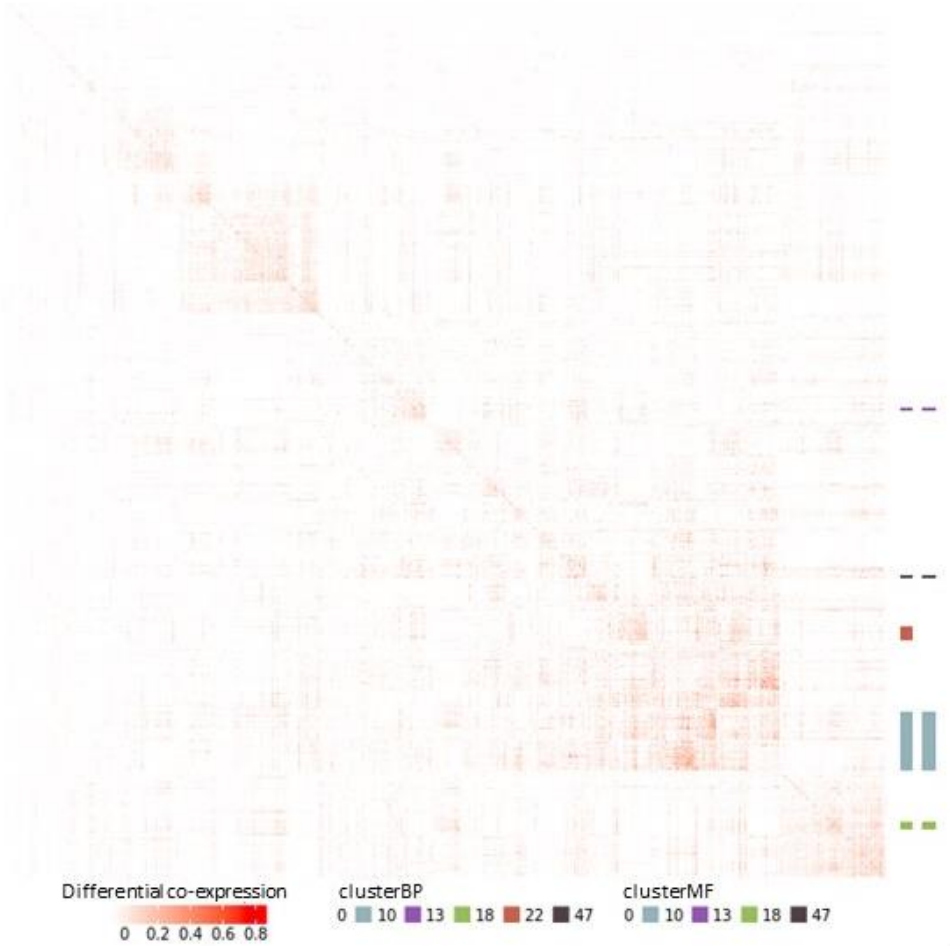

Figure 19. Heat map of the differential gene co-expression between oocytes and cumulus cells. Rows and columns represent pairs genes and the different shades of color present of the map correspond to the strength of the differential co-expression between oocyte and cumulus. White represents equivalent pair-wise gene co-expression between oocyte and cumulus cells. The vertical bars to the side represent the clusters showing enrichment for biological processes (BP) and molecular function (MF).

3.5.Discussion

In this study, we further elucidated the extensive and complex interactions that exist within oocytes and cumulus cells. By stringently separating COCs into a cleanly denuded oocyte and the corresponding cumulus cell samples, and processing them through RNA-Seq, we accurately captured a snap shot of the variable molecular state of both cell types. From the data obtained from RNA-Seq, we identified unique gene regulatory networks within and between each cell type.

It is well known that oocytes acquire and store transcripts throughout folliculogenesis**,** reaching an average of 0.6 ng of total RNA (in mice) which is approximately 20 times the amount of total RNA in any somatic cell (Sternlicht and Schultz 1981; Sanchez and Smitz 2012). These transcripts are known to originate from within the oocyte (De La Fuente and Eppig 2001) and the cumulus cells surrounding it, entering the oocyte through peripheral transzonal projections (Macaulay et al. 2014). The transcripts originating from within the oocyte are vital to the maintenance of the oocyte during meiotic arrest (Gosden and Lee 2010). The WGCNA results revealed a total of 3702 genes relating to biological process co-expressed in the oocytes. Within these, the top enriched terms (FDR < 0.05), and genes associated with such, were related to transcription and regulation of (N = 132), as well as related to protein phosphorylation (N = 32). Previous studies have shown that genes and terms associated with transcription are likely involved in the development of the follicle, and specifically involved in the FSH and prostaglandin E2 signaling cascades (Liu et al. 2010). Additionally, it has been demonstrated that the genes associated with biological process “protein

phosphorylation" are likely implicated in the regulation of oocyte meiosis (Gu et al. 2015).

The transcript population within cumulus cells varies throughout folliculogenesis and increase its levels after meiosis resumes (Feuerstein et al. 2007). Of this transcript population, a subset maintains their positions within the cumulus cells, while the other subset of the population leaves to enter the oocyte (Macaulay et al. 2016). In the WGCNA results obtained from the cumulus cells from which we derived our sample set, we demonstrated a co-expression of genes (FDR < 0.05) and GO terms (biological process) related to translation (N = 90).

The controls and mechanisms which guide genetic expression in a mature, developmentally competent COC are not yet completely understood. Likewise, the same controls and mechanisms guiding genetic expression in a prepubertal COC with decreased developmental competence are also lacking insight. Previous studies have suggested that the transcriptomes of prepubertal porcine oocytes are partly dictated by the incomplete cytoplasmic maturation (Yuan et al. 2011). The insights from this study have provided strong evidence to suggest an effect from both the PI3K-Akt signaling pathway and TGF-β/ SMAD signaling pathway on the expression of genes across the terms relating to transcription in oocytes and cumulus cells (Kaivo-oja et al. 2006; Nagyova et al. 2011; Andrade et al. 2017).

3.6.Conclusion

Our work revealed the complex transcriptomes existing within the oocyte and its accompanying cumulus cells from a prepubertal gilt. Although these results only provide a snapshot of both cell types' respective transcriptome, they provide insight into what mechanisms are regulating these cells at this stage in the mammalian ovarian cycle. We demonstrated a network formation for genes involved in the regulation of transcription in the oocyte, as well as cumulus cells. Through differential analyses we revealed distinct genetic networks, and by applying GO analyses to the genes within the networks, we indicated that, not only do follicles harbor distinct transcriptomes within its individual compartments, but it also has the potential to maintain distinct functional profiles within those compartments as well. Our findings can be used in the future to further elucidate the mechanisms governing the bi-directional communication between the cell types, as well as to further unravel what pathways come into play with key physiological events associated with the oocyte and cumulus cells, such as maintaining meiotic dormancy, re-entering meiosis, and how each cell type contributes to oocyte developmental competence.

Table 1. Enriched (FDR < 0.05) biological processes identified in co-expressing genes in oocytes.

BP Category	P Value	FDR	N Genes	Term	Cluster	Fold Enrichment	Gene Symbol
GO:0045944	4.03E-05	1.15E-02	49	positive regulation of transcription from RNA polymerase II promoter	2	1.82	EP300, LRP6, CHD8, CCNK, GSK3A, SLC9A1, CITED2, PHIP, DAB2IP, NR6A1, SETX, AGO2, NCOA2, RFX5, BCL9, JAG1, NCOA6, NCOA3, NCOA1, ATAD2B, SMAD1, FOXO1, ELF1, PPRC1, SMARCC1, ATXN7, MED12L, RELA, E2F8, DOT1L, MAML1, EGR1, PHOX2A, CDK18, NCL, NIPBL, EIF4A3, CDK12, VEZF1, WWP2, KMT2A, ZMIZ2, SREBF2, PCBP1, MAPK7, KPNA6, THRA, CNBP
GO:0042127	1.31E-04	1.87E-02	14	regulation of cell proliferation	2	3.15	PPARD, PRDM1, ABL1, JAG1, SRC, CCDC88A, BIRC6, FOXO1, BCL6, TNK2, JUP, NF1, NF2, BRCA2
GO:0000122	2.08E-04	1.99E-02	36	negative regulation of transcription from RNA polymerase II promoter	2	1.89	EP300, PPARD, CHD8, NR2F2, CNOT1, CIC, ARHGAP35, ARID1A, PRDM1, DAB2IP, NR6A1, NCOA2, RFX5, DNMT3B, CREBBP, MXD1, FOXO1, ARID5B, DCAF1, BCL6, RELA, E2F8, EGR1, MDM4, SAP130, NIPBL, ZHX2, WWP2, MEPCE, SREBF2, CBFA2T2, HDAC7, HOMEZ, SPEN, MSX2, CNBP
GO:0009887	3.42E-04	2.40E-02	7	animal organ morphogenesis	2	5.00	EP300, NOTCH2, JAG1, SMARCC1, RELA, NDST1, THRA
GO:0000165	4.18E-04	2.40E-02	10	MAPK cascade	2	3.57	MAP3K12, SETX, MAP4K3, SMAD1, NF1, MINK1, MAP3K3, ZFP36L1, DOK4, NDST1
GO:0043407	5.09E-04	2.43E-02	6	negative regulation of MAP kinase activity	2	5.55	DAB2IP, PTPN1, DUSP7, NF1, MAPK7, NUP62
GO:0008286	6.32E-04	2.52E-02	7	insulin receptor signaling pathway	2	4.59	GSK3A, PHIP, ZNF106, PTPN1, FOXO1, SMARCC1, APC
GO:0032956	7.04E-04	2.52E-02	6	regulation of actin cytoskeleton organization	2	5.24	ARHGAP35, ABL1, VANGL2, CCDC88A, CRK
GO:0017148	1.02E-03	3.23E-02	8	negative regulation of translation	2	3.81	GAPDH, CNOT1, EIF4ENIF1, ILF3, NCL, LARP1, EIF4A3

GO:0008285	1.58E-03	4.53E-02	16	negative regulation of cell proliferation	2	2.33	TNS2, DAB2IP, NOTCH2, SMAD1, BCL6, AMBRA1, APC, DRD2, PTPN14, NF1, KMT2A, NF2, TP53INP1, MSX2, PBRM1, NUP62
GO:0007017	1.61E-05	2.92E-04	6	microtubule-based process	5	10.10	TUBB3, TUBE1, TUBB2B, TUBB4B
GO:0006413	3.51E-07	9.65E-05	14	translational initiation	8	4.57	EIF3J, EIF3E, ABCE1, EIF3A, EIF1B, DDX3X, EIF1, EIF4A1, EIF2S2, EIF4E, EIF1AX, EIF2S1
GO:0000398	6.81E-05	9.37E-03	17	mRNA splicing, via spliceosome	8	2.70	SNRPC, SNRPA1, SF3B6, DHX15, METTL14, LSM3, HNRNPM, CWC15, TRA2A, PRPF40A, SNW1, SNRPE, SRSF10, HNRNPA2B1, RNPC3, LSM2
GO:0015031	1.29E-04	1.18E-02	19	protein transport	8	2.43	COPZ1, RAP1A, BBS7, VPS29, ATG3, TIMM8A, COPB1, COPG2, HIKESHI, TIMM13, KPNA3, NUP93, VPS35, TIMM9, KPNA1, GOSR1, RAB11A, SEC61B
GO:0051603	5.32E-04	2.93E-02	7	proteolysis involved in cellular protein catabolic process	8	4.33	PSMA6, CLPX, PSMB7, PSMA5, DNAJC3, PSMA4
GO:0019827	4.68E-04	2.93E-02	9	stem cell population maintenance	8	3.53	LEO1, MED27, MTF2, METTL14, SMC3, MED7, EIF4E, MED30, MED6
GO:0006357	8.62E-05	4.66E-03	17	regulation of transcription from RNA polymerase II promoter	9	2.98	MKL1, GLIS3, TADA1, PLAGL2, ARID5A, RB1, EPC1, QRICH1, MED14, MED13, CAMTA2, RBPJ, EPC2, ZNF367, ELF2, HES1, PIAS2
GO:0000122	5.86E-04	1.14E-02	22	negative regulation of transcription from RNA polymerase II promoter	9	2.21	TRIM27, SIN3A, NFATC4, RTF1, DNAJB5, ZHX1, MTDH, ARID5A, NSD2, RB1, EPC1, ZMYND11, YEATS2, USP2, RBPJ, CTCF, PTCH1, RLIM, HES1, BPTF, DMAP1
GO:0006511	6.35E-04	1.14E-02	11	ubiquitin-dependent protein catabolic process	9	3.40	UBR2, PSMA3, WWP1, USP38, USP19, USP9X, UBE4A, USP2, PSMD11, RLIM, RANBP1
GO:0006412	8.22E-06	3.61E-03	32	translation	11	2.25	EIF3L, EIF3D, RPS18, MRPL2, RPS12, RARS2, EEF1D, RPS3A, EIF2A, MRPL11, MRPL4, GFM2, LARS, RPL27A, RPL26L1,

							RARS, MARS, GFM1, MRPL9, RACK1, MRPL20, RPSA
GO:0007165	6.02E-03	1.81E-02	7	signal transduction	20	3.30	RALGDS, GNAI2, STAT1, STAT5A, STAT5B, ARRB2, GNAO1
GO:0000122	7.37E-04	7.37E-04	8	negative regulation of transcription from RNA polymerase II promoter	24	3.72	PIAS1, RBL1, LEF1, LDB1, DLG1, ZBTB1, RYBP, YY1

Table 2. Enriched (FDR < 0.05) molecular functions identified in co-expressing genes in oocytes.

MF Category	P Value	FDR	N Genes	Term	Cluster	Fold Enrichment	Gene Symbol
GO:0003723	4.6E-10	1.14E-07	113	RNA binding	8	1.70	SARNP, NAP1L1, SNRPC, SRSF3, CDC5L, PSMA6, SRP54, ERH, ZRANB2, SERBP1, HDAC2, C14orf166, KTN1, ELAVL2, SNRPA1, EIF3E, RPL30, CSDE1, ESF1, XRN2, RBM39, SRSF7, SF3B6, PUM2, DHX15, ADAD1, HMGB1, HMGB2, SFSWAP, PPP1CC, HNRNPH3, DDX50, SUPV3L1, ADK, EXOSC1, EIF3A, DYNC1LI1, EIF1B, LSM3, FXR1, MRPL39, RBBP7, DDX3X, RBMX, EIF4G2, SAFB, SAFB2, HNRNPM, HNRNPH1, BTF3, RPS3, DDX10, TRA2A, DNAJC2, TSN, NIFK, PRPF40A, SSB, MAP3K20, HNRNPA3, RBM45, ZC3H15, NABP1, BOLL, BZW1, SUMO2, EIF1, ZNF207, NSRP1, EIF4A1, STRAP, UBE2I, CHTOP, RPF1, NOP58, DAZAP1, HNRNPK, PNN, PIN4, HNRNPR, MRPL27, THUMPD1, EIF2S2, EIF4E, RBM8A, SMNDC1, METAP2, PPIG, DDX5, EIF1AX, SREK1, EIF2S1, MECP2, RPS15A, SUMO1, SRSF10, HNRNPA2B1, RPL15, RNPC3, PNISR, CPSF6, PRKRA, SEC61B, CCDC59, YWHAE, LSM2, SMARCE1, FCF1, EYA1
GO:0003743	5.94E-06	7.34E-04	12	translation initiation factor activity	8	4.41	EIF3J, EIF3E, EIF3A, EIF1B, EIF1, EIF4A1, EIF2S2, EIF4E, EIF1AX, EIF2S1
GO:0019843	3.96E-05	6.35E-03	9	rRNA binding	11	4.76	RPS18, SBDS, DDX21, MRPL11, PPAN, DIEXF, DDX28, EMG1, MRPL20
GO:0051082	2.76E-05	6.35E-03	17	unfolded protein binding	11	3.06	CCT2, HSP90AB1, NUDC, TCP1, TRAP1, CCT7, SHQ1, AIP, CALR, HSPA8, AAMP, CCT5, NUDCD2, DNAJB6, GRPEL1
GO:0003735	0.000162	1.73E-02	23	structural constituent of ribosome	11	2.33	RPS18, MRPL2, RPS12, RPS3A, MRPS31, RPLP0, MRPL11, MRPL4, RPL27A, RPL26L1, MRPL9, MRPL20, RPSA

GO:0003824	0.000272	2.18E-02	33	catalytic activity	11	1.95	TTLL12, MTHFD1, TAT, AZIN2, MTFMT, RCL1, RNF20, CKS1B, UQCRC2, HADHB, HHIP, ELP3, GOT1, GALT, APTX, HACL1, ACAA1, SUCLG2, PC, LDHC, GTF2F1, PGGT1B, ISOC1, PFKFB2, ATIC, CKB, SLC3A2, ODC1, PPCDC, FH, FEN1
GO:0003677	0.000641	5.34E-03	11	DNA binding	24	3.12	CASP8AP2, SOS1, LEF1, PDS5B, LCOR, LDB1, RCOR2, BAZ2B, RYBP, YY1, ATF2
GO:0008270	0.010324	4.30E-02	6	zinc ion binding	24	3.30	ZMYM4, PIAS1, KCMF1, TRIM24, ARIH1
GO:0042802	4.92E-05	4.92E-05	8	identical protein binding	28	4.81	FAM161A, CDC42BPA, APEH, MAPT, HEXIM2, BTK, DYNLT3, MAPRE3
GO:0046872	0.003275	3.27E-03	7	metal ion binding	37	3.60	PLAGL1, PRKCH, PRKCI, PRICKLE3, USP20, BIRC3

Table 3. Enriched (FDR < 0.05) biological processes identified in co-expressing genes in cumulus cells.

BP Category	P Value	FDR	N Genes	Term	Cluster	Fold Enrichment	Gene Symbol
GO:0006412	8.55E-15	1.76E-11	90	translation	2	1.68	EIF3L, EIF3D, RPS26, RPS18, CPEB1, RPS21, EIF3K, RPS11, EIF3I, RPS5, HBS1L, RPS12, EIF3H, EIF3E, RPL30, RPL5, EEF1D, RPS3A, RPL34, EPRS, EIF1B, EIF2A, RPS4X, EEF1G, RPS13, RPS28, RPS23, RPL27A, RPS3, RPL35A, EEF1B2, DHX29, RPL19, RPS16, MRPL27, RPL11, MRPL17, RPL13, RPL9, RPL27, RPS17, RPL26, RACK1, RPS9, RPS14, QARS, RPS15, EIF2S1, RPL37, RPL35, RPL17-C18orf32, RPL32, RPL10, RPL15, RPSA, RPS29, RPL23, RPS20
GO:0032869	3.32E-06	5.68E-04	11	cellular response to insulin stimulus	9	5.21	AKT2, GSK3A, WDTC1, MYO5A, USF1, PRKCI, MARS, IRS1, ZFP36L1, CPEB2, INHBB
GO:0006397	2.66E-04	2.28E-02	6	Rho protein signal transduction	9	5.94	HACD3, ROCK2, BCL6, PAK1, ROCK1, ARHGDIA
GO:0010468	5.47E-04	1.13E-02	7	mRNA processing	11	4.85	DDX39B, RBM26, SUPT5H, SON, PRPF3, HNRNPA2B1
GO:0007266	3.43E-04	1.13E-02	10	regulation of gene expression	11	3.75	DDX39B, RC3H2, ASH1L, MAPK8, SETD2, SAP130, NIPBL, ALKBH1, DDX46

Table 4. Enriched (FDR < 0.05) molecular function identified in co-expressing genes in cumulus cells.

MF Category	P Value	FDR	N Genes	Term	Cluster	Fold Enrichment	Gene Symbol
GO:0003735	3.69E-18	2.88E-15	64	structural constituent of ribosome	2	3.66	RPS26, RPS18, RPS21, RPS11, RPS5, RPS12, RPL30, RPL5, RPS3A, RPL34, RPLP0, RPS4X, RPLP2, RPS13, RPS28, RPS23, RPL27A, RPS3, RPL35A, RPL19, RPS16, MRPL27, RPL11, MRPL17, RPL13, RPL9, RPL27, RPS17, RPL26, RPS9, RPS15, RPL37, RPL35, RPL17-C18orf32, RPS15A, RPL32, RPL10, RPL15, RPSA, RPS29, RPL23, RPS20

Table 5. Biological processes enriched (FDR < 0.05) in clusters formed by differentially co-expressed genes between oocyte and cumulus cells.

BP Category	P value	FDR	N Genes	Term	Cluster	Gene Symbol
GO:0030433	1.91E-04	2.35E-02	10	ubiquitin-dependent ERAD pathway	10	PSMC6, VCP, AUP1, ERLEC1, STT3B, PSMC3, PSMC2, DNAJC10, 43165, PSMC5
GO:0006413	8.79E-07	2.32E-04	13	translational initiation	10	EIF3L, EIF3I, EIF3E, ABCE1, EIF1B, DDX3X, EIF1, EIF4A1, EIF2S2, EIF1AX, EIF2S1
GO:0006412	2.43E-16	2.40E-13	45	translation	10	EIF3L, RPS18, RPS11, EIF3I, RPS5, RPS12, EIF3E, RPL30, RPL5, RPS3A, EIF1B, RPS4X, EEF1G, RPS13, RPL27A, RPS3, RPL19, RPL9, RPS17, RACK1, QARS, EIF1AX, EIF2S1, RPL37, RPL17-C18orf32, RPL10, RPL15, RPSA, RPL23
GO:1901998	6.70E-06	1.32E-03	9	toxin transport	10	COPZ1, CCT2, SCFD1, TRIP4, CCT3, CCT7, DNAJA1, COPB2, CCT8
GO:0007264	3.98E-03	1.38E-02	3	small GTPase mediated signal transduction	47	CDC42, RHOA, RAP1B
GO:0060395	1.54E-04	2.08E-02	4	SMAD protein signal transduction	22	FOS, SMAD2, ROR2, VIM
GO:0006357	9.93E-03	3.65E-02	3	regulation of transcription from RNA polymerase II promoter	13	MKL1, CITED2, FOSL1
GO:0070507	7.11E-06	1.29E-04	3	regulation of microtubule cytoskeleton organization	47	PAFAH1B1, RHOA
GO:0050790	9.19E-06	2.76E-05	3	regulation of catalytic activity	432	PPP2R5C, PSMD1, PSMD2
GO:0051603	9.43E-07	2.32E-04	10	proteolysis involved in cellular protein catabolic process	10	PSMA6, CLPX, PSMB7, PSMA5, PSMB6, PSMB1, PSMB4, PSMA4, CLPP

GO:0043161	8.51E-05	1.28E-04	3	proteasome-mediated ubiquitin-dependent protein catabolic process	432	PPP2R5C, PSMD1, PSMD2
GO:0043248	2.91E-04	3.18E-02	5	proteasome assembly	10	PSMD5, POMP
GO:0045944	4.07E-03	1.99E-02	5	positive regulation of transcription from RNA polymerase II promoter	13	MKL1, CITED2, AGO2, DOT1L, ESR1
GO:0045899	5.87E-05	9.64E-03	4	positive regulation of RNA polymerase II transcriptional preinitiation complex assembly	10	PSMC6, PSMC3, PSMC2, PSMC5
GO:0008284	4.80E-03	4.80E-03	3	positive regulation of cell proliferation	757	PDGFRA, SRPK2, KITLG
GO:0007052	7.64E-04	3.48E-02	3	mitotic spindle organization	18	SBDS, POC1A
GO:0007017	5.91E-05	5.36E-04	3	microtubule-based process	47	TUBA1B, PAFAH1B1
GO:0008152	1.53E-03	1.53E-03	3	metabolic process	29	GSTA4, EDEM2, ACAT1
GO:0007156	5.46E-05	8.02E-04	3	homophilic cell adhesion via plasma membrane adhesion molecules	13	CDH2, PCDH17, DCHS1
GO:0006260	1.96E-03	4.45E-02	4	DNA replication	18	LIG1, RFC3, MCM5
GO:0007010	1.00E-04	6.06E-04	4	cytoskeleton organization	47	TUBA1B, CFL1, RHOA
GO:0002181	1.26E-04	1.78E-02	8	cytoplasmic translation	10	RPL30, RPS3A, RPL27A, RPS3, RPL9
GO:0030154	9.23E-03	2.39E-02	3	cell differentiation	47	CDC42, PAFAH1B1, RHOA
GO:0007049	8.71E-04	3.95E-03	3	cell cycle	47	PSME3, PAFAH1B1, RAB11A
GO:0007155	1.34E-03	9.86E-03	3	cell adhesion	13	CDH2, PCDH17, DCHS1
GO:0046034	7.18E-07	2.32E-04	8	ATP metabolic process	10	ATP5A1, CLPX, VCP, HSPA8, OLA1, NDUFS1, ATP6V1B2

GO:0030036	4.57E-03	1.38E-02	3	actin cytoskeleton organization	47	VEGFA, DLG1, PAK1, CDC42, PAFAH1B1, RHOA

Table 6. Molecular functions enriched (FDR < 0.05) in clusters formed by differentially co-expressed genes between oocyte and cumulus cells.

MF Category	P Value	FDR	N Genes	Term	Cluster	Gene Symbol
GO:0003723	2.55E-19	1.52E-16	123	RNA binding	10	EIF3L, SARNP, NAP1L1, NELFE, RPS18, SRSF3, HSP90AB1, CDC5L, PSMA6, SRP54, LSM14A, RPS11, FUBP1, ZRANB2, SERBP1, RPS5, HDAC2, ATP5A1, PDIA3, C14orf166, VCP, EIF3E, RPL30, CCT3, CSDE1, RALY, RBM39, TOP1, SRSF6, SRSF7, CEBPZ, SF3B6, PUM2, DHX15, EXOSC9, HMGB1, HMGB2, RAN, RSRC2, PPP1CC, HNRNPH3, EIF1B, FXR1, RBBP7, DDX3X, RPS4X, SLC25A5, RBMX, API5, RPS13, EIF4G2, SAFB, SAFB2, HNRNPM, HNRNPH1, BTF3, ETF1, CTNNA1, RPL27A, RPS3, HSPA8, DARS, TSN, PRPF40A, RBM45, CWC22, ZC3H15, BZW1, SND1, PAIP1, SUMO2, EIF1, RPL19, ZNF207, EIF4A1, STRAP, CHTOP, RPF1, NOP58, HNRNPK, PNN, HNRNPR, RPL9, EIF4H, EIF2S2, ZFR, YTHDF2, LRRC59, KPNA2, RACK1, METAP2, DDX5, RPL7, EIF1AX, SRSF5, HNRNPH2, EIF2S1, RPL37, RPS15A, SUMO1, RPL7A, RPL10, SRSF10, HNRNPA2B1, SRSF2, RPL15, HNRNPDL, PNISR, CPSF6, PUF60, YWHAE, FCF1, UBFD1, SPTBN1

GO:0003735	3.37E-13	9.99E-11	36	structural constituent of ribosome	10	RPS18, RPS11, RPS5, RPS12, RPL30, RPL5, RPS3A, RPS4X, RPS13, RPL27A, RPS3, RPL19, RPL9, RPS17, RPL37, RPL17-C18orf32, RPS15A, RPL10, RPL15, RPSA, RPL23
GO:0045296	2.68E-10	5.29E-08	35	cadherin binding	10	HSP90AB1, UNC45A, AHSA1, SERBP1, USP8, TMEM245, EIF3E, RAB1A, PAICS, RAN, ITGB1, CTNNB1, DDX3X, EEF1G, LDHA, CTNNA1, HSPA8, OLA1, ZC3H15, BZW1, SND1, PSMB6, PPME1, HNRNPK, SNX2, EIF4H, CCT8, LRRC59, RACK1, RPL7A, RPL15, PUF60, YWHAE, UBFD1, SPTBN1
GO:0004298	5.39E-07	7.99E-05	8	threonine-type endopeptidase activity	10	PSMA6, PSMB7, PSMA5, PSMB6, PSMB1, PSMB4, PSMA4
GO:0003743	2.75E-06	3.26E-04	12	translation initiation factor activity	10	EIF3L, EIF3I, EIF3E, EIF1B, EIF1, EIF4A1, EIF4H, EIF2S2, EIF1AX, EIF2S1
GO:0036402	1.78E-05	1.76E-03	4	proteasome-activating ATPase activity	10	PSMC6, PSMC3, PSMC2, PSMC5
GO:0097100	6.45E-05	5.47E-03	4	supercoiled DNA binding	10	TOP1, HMGB1, HMGB2, RPS3
GO:0046933	1.51E-04	1.12E-02	4	proton-transporting ATP synthase activity, rotational mechanism	10	ATP5A1, ATP5G3, ATP5F1
GO:0004175	3.58E-04	2.36E-02	9	endopeptidase activity	10	PSMA6, PSMB7, PSMA5, PSMB6, PSMB1, TMEM59, PSMB4, PSMA4
GO:0051082	4.08E-04	2.42E-02	12	unfolded protein binding	10	CCT2, HSP90AB1, DNAJA2, CLPX, CCT3, CCT7, ERLEC1, DNAJA1, HSPA8, HSPD1, AAMP, CCT8
GO:0047134	7.48E-04	4.04E-02	3	protein-disulfide reductase activity	10	TXNL1, PGK1
GO:0033592	1.05E-03	5.21E-02	3	RNA strand annealing activity	10	FXR1, DDX3X, EIF4H
GO:0045296	3.58E-07	3.42E-05	12	cadherin binding	13	HSP90AB1, TMEM245, EIF3E, PAICS, RAN, CTNNB1, EEF1G, LDHA, HSPA8, SNX2, RPL15, PUF60

GO:0044183	1.80E-05	8.59E-04	4	protein binding involved in protein folding	13	CCT2, CCT3, CCT7, HSPD1
GO:0051082	4.90E-05	1.56E-03	6	unfolded protein binding	13	CCT2, HSP90AB1, CCT3, CCT7, HSPA8, HSPD1
GO:0003735	3.93E-04	4.49E-03	4	structural constituent of ribosome	13	RPL5, RPS3A, RPL19, RPL37, RPL15, RPL19, RPL15
GO:0015078	5.14E-04	8.17E-03	3	hydrogen ion transmembrane transporter activity	13	ATP6V0D1, ATP5F1
GO:0000166	4.52E-04	8.17E-03	15	nucleotide binding	13	CCT2, SRP54, KARS, ATP5A1, CCT3, CCT7, RAN, TUBB4A, HSPA8, PSMC2, HSPD1, PSMC5, ACTG1, TUBB4B
GO:0097718	1.30E-03	1.77E-02	3	disordered domain specific binding	13	HSP90AB1, CTNNB1, AP2M1
GO:0005509	8.33E-03	2.29E-02	3	calcium ion binding	13	CDH2, PCDH17, DCHS1
GO:0003700	5.67E-03	2.29E-02	4	DNA binding transcription factor activity	13	MKL1, CITED2, FOSL1, ESR1
GO:0019843	9.73E-05	4.84E-03	4	rRNA binding	18	SBDS, PPAN, DIEXF, DDX28
GO:0003924	1.00E-06	2.18E-05	7	GTPase activity	47	TUBA1B, CDC42, RHOA, RAB11A, RAB5C, RAP1B
GO:0019003	4.51E-04	3.27E-03	3	GDP binding	47	TUBA1B, CDC42, RHOA, RAB11A, RAB5C, RAP1B, RHOA, RAB5C, RAP1B
GO:0003924	2.92E-06	1.61E-05	4	GTPase activity	52	TUBA1B, CDC42, RAB11A
GO:0005525	6.31E-06	1.73E-05	4	GTP binding	52	TUBA1B, CDC42, RAB11A
GO:0003924	2.64E-05	1.45E-04	4	GTPase activity	52	TUBA1B, CDC42, RAB11A
GO:0005525	5.69E-05	1.57E-04	4	GTP binding	52	TUBA1B, CDC42, RAB11A
GO:0000166	9.86E-04	1.81E-03	4	nucleotide binding	52	TUBA1B, CDC42, RAB11A
GO:0000166	6.86E-03	1.26E-02	4	nucleotide binding	52	TUBA1B, CDC42, RAB11A
GO:0003723	5.16E-03	1.55E-02	9	RNA binding	63	IPO5, UBAP2, NUP98, EIF4A3, EFTUD2, SUPT6H, THRAP3, GANAB, GOT2

4.References

Abels ER, Breakefield XO. 2016. Introduction to Extracellular Vesicles: Biogenesis, RNA Cargo Selection, Content, Release, and Uptake. *Cell Mol Neurobiol* **36**: 301-312.

Anders S, Pyl PT, Huber W. 2015. HTSeq--a Python framework to work with high-throughput sequencing data. *Bioinformatics* **31**: 166-169.

Anderson P, Kedersha N. 2009. RNA granules: post-transcriptional and epigenetic modulators of gene expression. *Nat Rev Mol Cell Biol* **10**: 430-436.

Andrade GM, da Silveira JC, Perrini C, Del Collado M, Gebremedhn S, Tesfaye D, Meirelles FV, Perecin F. 2017. The role of the PI3K-Akt signaling pathway in the developmental competence of bovine oocytes. *PLoS One* **12**: e0185045.

Aramaki S, Hayashi K, Kurimoto K, Ohta H, Yabuta Y, Iwanari H, Mochizuki Y, Hamakubo T, Kato Y, Shirahige K et al. 2013. A mesodermal factor, T, specifies mouse germ cell fate by directly activating germline determinants. *Dev Cell* **27**: 516-529.

Ashburner M, Ball CA, Blake JA, Botstein D, Butler H, Cherry JM, Davis AP, Dolinski K, Dwight SS, Eppig JT et al. 2000. Gene ontology: tool for the unification of biology. The Gene Ontology Consortium. *Nat Genet* **25**: 25-29.

Barbieri RL. 2014. The endocrinology of the menstrual cycle. *Methods Mol Biol* **1154**: 145-169.

Barragan M, Pons J, Ferrer-Vaquer A, Cornet-Bartolome D, Schweitzer A, Hubbard J, Auer H, Rodolosse A, Vassena R. 2017. The transcriptome of human oocytes is related to age and ovarian reserve. *Mol Hum Reprod* **23**: 535-548.

Benjamini Y, Hochberg Y. 1995. Controlling the False Discovery Rate: A Practical and Powerful Approach to Multiple Testing. *Journal of the Royal Statistical Society Series B (Methodological)* **57**: 289-300.

Bhattacharya S, Basu D, Ak N, Priyadarshini A. 2007. Molecular mechanism of oocyte maturation. *Soc Reprod Fertil Suppl* **63**: 45-55.

Biase FH. 2017. Oocyte Developmental Competence: Insights from Cross-Species Differential Gene Expression and Human Oocyte-Specific Functional Gene Networks. *OMICS* **21**: 156-168.

Biase FH, Cao X, Zhong S. 2014a. Cell fate inclination within 2-cell and 4-cell mouse embryos revealed by single-cell RNA sequencing. *Genome Res* **24**: 1787-1796.

Biase FH, Everts RE, Oliveira R, Santos-Biase WK, Fonseca Merighe GK, Smith LC, Martelli L, Lewin H, Meirelles FV. 2014b. Messenger RNAs in metaphase II oocytes correlate with successful embryo development to the blastocyst stage. *Zygote* **22**: 69-79.

Biase FH, Martelli L, Puga R, Giuliatti S, Santos-Biase WKF, Fonseca Merighe GK, Meirelles FV. 2010. Messenger RNA expression of Pabpnl1 and Mbd3l2 genes in oocytes and cleavage embryos. *Fertil Steril* **93**: 2507-2512.

Caixeta ES, Ripamonte P, Franco MM, Junior JB, Dode MA. 2009. Effect of follicle size on mRNA expression in cumulus cells and oocytes of Bos indicus: an approach to identify marker genes for developmental competence. *Reprod Fertil Dev* **21**: 655-664.

Chomczynski P, Sacchi N. 2006. The single-step method of RNA isolation by acid guanidinium thiocyanate-phenol-chloroform extraction: twenty-something years on. *Nat Protoc* **1**: 581-585.

Chouinard LA. 1971. A light- and electron-microscope study of the nucleolus during growth of the oocyte in the prepubertal mouse. *J Cell Sci* **9**: 637-663.

Cirera S. 2013. Highly efficient method for isolation of total RNA from adipose tissue. *BMC Res Notes* **6**: 472.

Clarke H. 2017. Control of Mammalian Oocyte Development by Interactions with the Maternal Follicular Environment. *Results Probl Cell Differ* **63**: 17-41.

Clarke HG, Hope SA, Byers S, Rodgers RJ. 2006. Formation of ovarian follicular fluid may be due to the osmotic potential of large glycosaminoglycans and proteoglycans. *Reproduction* **132**: 119-131.

Clarke HJ. 2018. Regulation of germ cell development by intercellular signaling in the mammalian ovarian follicle. *Wiley Interdiscip Rev Dev Biol* **7**.

Cline MS, Smoot M, Cerami E, Kuchinsky A, Landys N, Workman C, Christmas R, Avila-Campilo I, Creech M, Gross B et al. 2007. Integration of biological networks and gene expression data using Cytoscape. *Nat protoc* **2**: 2366-2382.

Cummins J. 1998. Mitochondrial DNA in mammalian reproduction. *Rev Reprod* **3**: 172-182.

Da Silva-Buttkus P, Jayasooriya GS, Mora JM, Mobberley M, Ryder TA, Baithun M, Stark J, Franks S, Hardy K. 2008. Effect of cell shape and packing density on granulosa cell proliferation and formation of multiple layers during early follicle development in the ovary. *J Cell Sci* **121**: 3890-3900.

De La Fuente R, Eppig JJ. 2001. Transcriptional activity of the mouse oocyte genome: companion granulosa cells modulate transcription and chromatin remodeling. *Dev Biol* **229**: 224-236.

De Lesegno CV, Reynaud K, Pechoux C, Thoumire S, Chastant-Maillard S. 2008. Ultrastructure of canine oocytes during in vivo maturation. *Mol Reprod Dev* **75**: 115-125.

De los Reyes M, Palomino J, Jofre S, Villarroel A, Moreno R. 2012. Golgi apparatus and endoplasmic reticulum dynamic during meiotic development in canine oocytes. *Reprod Domest Anim* **47 Suppl 6**: 93-97.

Diaz FJ, Wigglesworth K, Eppig JJ. 2007. Oocytes are required for the preantral granulosa cell to cumulus cell transition in mice. *Dev Biol* **305**: 300-311.

Dickinson SE, Griffin BA, Elmore MF, Kriese-Anderson L, Elmore JB, Dyce PW, Rodning SP, Biase FH. 2018. Transcriptome profiles in peripheral white blood cells at the time of artificial insemination discriminate beef heifers with different fertility potential. *BMC Genomics* **19**: 129.

Dorji, Ohkubo Y, Miyoshi K, Yoshida M. 2012. Gene expression differences in oocytes derived from adult and prepubertal Japanese Black cattle during in vitro maturation. *Reprod Domest Anim* **47**: 392-402.

Edwards RG. 2007. The significance of parthenogenetic virgin mothers in bonnethead sharks and mice. *Reprod Biomed Online* **15**: 12-15.

Elvin JA, Clark AT, Wang P, Wolfman NM, Matzuk MM. 1999. Paracrine actions of growth differentiation factor-9 in the mammalian ovary. *Mol Endocrinol* **13**: 1035-1048.

Elvin JA, Matzuk MM. 1998. Mouse models of ovarian failure. *Rev Reprod* **3**: 183-195.

Emori C, Sugiura K. 2014. Role of oocyte-derived paracrine factors in follicular development. *Anim Sci J* **85**: 627-633.

Eppig JJ, Wigglesworth K, Pendola FL. 2002. The mammalian oocyte orchestrates the rate of ovarian follicular development. *Proc Natl Acad Sci U S A* **99**: 2890-2894.

Erickson GF. 1983. Primary cultures of ovarian cells in serum-free medium as models of hormone-dependent differentiation. *Mol Cell Endocrinol* **29**: 21-49.

Fair T, Hulshof SC, Hyttel P, Greve T, Boland M. 1997a. Nucleus ultrastructure and transcriptional activity of bovine oocytes in preantral and early antral follicles. *Mol Reprod Dev* **46**: 208-215.

Fair T, Hulshof SC, Hyttel P, Greve T, Boland M. 1997b. Oocyte ultrastructure in bovine primordial to early tertiary follicles. *Anat Embryol* **195**: 327-336.

Ferreira EM, Vireque AA, Adona PR, Meirelles FV, Ferriani RA, Navarro PA. 2009. Cytoplasmic maturation of bovine oocytes: structural and biochemical modifications and acquisition of developmental competence. *Theriogenology* **71**: 836-848.

Feuerstein P, Cadoret V, Dalbies-Tran R, Guerif F, Bidault R, Royere D. 2007. Gene expression in human cumulus cells: one approach to oocyte competence. *Hum Reprod* **22**: 3069-3077.

Flicek P, Amode MR, Barrell D, Beal K, Billis K, Brent S, Carvalho-Silva D, Clapham P, Coates G, Fitzgerald S et al. 2013. Ensembl 2014. *Nucleic Acids Res* **42**: D749 – 755.

Fulka H, Langerova A. 2014. The maternal nucleolus plays a key role in centromere satellite maintenance during the oocyte to embryo transition. *Development* **141**: 1694-1704.

Georges A, Auguste A, Bessiere L, Vanet A, Todeschini AL, Veitia RA. 2014. FOXL2: a central transcription factor of the ovary. *J Mol Endocrinol* **52**: R17-33.

Gertz J, Varley KE, Davis NS, Baas BJ, Goryshin IY, Vaidyanathan R, Kuersten S, Myers RM. 2012. Transposase mediated construction of RNA-seq libraries. *Genome Res* **22**: 134-141.

Gilchrist RB. 2011. Recent insights into oocyte-follicle cell interactions provide opportunities for the development of new approaches to in vitro maturation. *Reprod Fertil Dev* **23**: 23-31.

Gilchrist RB, Lane M, Thompson JG. 2008. Oocyte-secreted factors: regulators of cumulus cell function and oocyte quality. *Hum Reprod Update* **14**: 159-177.

Goodenough DA, Paul DL. 2009. Gap junctions. *Cold Spring Harb Perspect Biol* **1**: a002576.

Gosden R, Lee B. 2010. Portrait of an oocyte: our obscure origin. *J Clin Invest* **120**: 973-983.

Griffin J, Emery BR, Huang I, Peterson CM, Carrell DT. 2006. Comparative analysis of follicle morphology and oocyte diameter in four mammalian species (mouse, hamster, pig, and human). *J Exp Clin Assist Reprod* **3**: 2.

Grondahl ML, Yding Andersen C, Bogstad J, Nielsen FC, Meinertz H, Borup R. 2010. Gene expression profiles of single human mature oocytes in relation to age. *Hum Reprod* **25**: 957-968.

Gu L, Liu H, Gu X, Boots C, Moley KH, Wang Q. 2015. Metabolic control of oocyte development: linking maternal nutrition and reproductive outcomes. *Cell Mol LIfe Sciences* **72**: 251-271.

Gu Z, Eils R, Schlesner M. 2016. Complex heatmaps reveal patterns and correlations in multidimensional genomic data. *Bioinformatics* **32**: 2847-2849.

Gulyas BJ. 1980. Cortical granules of mammalian eggs. *Int Rev Cytol* **63**: 357-392.

Guthrie HD, Bolt DJ, Cooper BS. 1990. Effects of gonadotropin treatment on ovarian follicle growth and granulosal cell aromatase activity in prepuberal gilts. *J Anim Sci* **68**: 3719-3726.

Hamatani T, Falco G, Carter MG, Akutsu H, Stagg CA, Sharov AA, Dudekula DB, VanBuren V, Ko MS. 2004. Age-associated alteration of gene expression patterns in mouse oocytes. *Hum Mol Genet* **13**: 2263-2278.

Han SJ, Conti M. 2006. New pathways from PKA to the Cdc2/cyclin B complex in oocytes: Wee1B as a potential PKA substrate. *Cell Cycle* **5**: 227-231.

Hatzirodos N, Irving-Rodgers HF, Hummitzsch K, Rodgers RJ. 2014. Transcriptome profiling of the theca interna from bovine ovarian follicles during atresia. *PLoS One* **9**: e99706.

Hayashi K, Hikabe O, Obata Y, Hirao Y. 2017. Reconstitution of mouse oogenesis in a dish from pluripotent stem cells. *Nat Protoc* **12**: 1733-1744.

Hickey TE, Marrocco DL, Amato F, Ritter LJ, Norman RJ, Gilchrist RB, Armstrong DT. 2005. Androgens augment the mitogenic effects of oocyte-secreted factors and growth differentiation factor 9 on porcine granulosa cells. *Biol Reprod* **73**: 825-832.

Holt JE, Jackson A, Roman SD, Aitken RJ, Koopman P, McLaughlin EA. 2006. CXCR4/SDF1 interaction inhibits the primordial to primary follicle transition in the neonatal mouse ovary. *Dev Biol* **293**: 449-460.

Hsueh AJ, Kawamura K, Cheng Y, Fauser BC. 2015. Intraovarian control of early folliculogenesis. *Endocr Rev* **36**: 1-24.

Hyttel P. 2012. Electron Microscopy of Mammalian Oocyte Development, Maturation, and Fertilization. In *Oocyte Maturation and Fertilization: A Long History for a Short Event*, pp. 1-37. Bentham Science Publishers.

Hyttel P, Fair T, Callesen H, Greve T. 1996. Oocyte Growth, Capacitation, and Final Maturation in Cattle. *Theriogenology* **47**: 23-32.

Hyttel P, Viuff D, Fair T, Laurincik J, Thomsen PD, Callesen H, Vos PL, Hendriksen PJ, Dieleman SJ, Schellander K et al. 2001. Ribosomal RNA gene expression and chromosome aberrations in bovine oocytes and preimplantation embryos. *Reproduction* **122**: 21-30.

Ihaka R, Gentleman. 2012. R: A Language and Environment for Statistical Computing. *J Comput Graph Stats* **5**: 299-214.

Jones GM, Cram DS, Song B, Magli MC, Gianaroli L, Lacham-Kaplan O, Findlay JK, Jenkin G, Trounson AO. 2008. Gene expression profiling of human oocytes following in vivo or in vitro maturation. *Hum Reprod* **23**: 1138-1144.

Joyce IM, Pendola FL, O'Brien M, Eppig JJ. 2001. Regulation of prostaglandin-endoperoxide synthase 2 messenger ribonucleic acid expression in mouse granulosa cells during ovulation. *Endocrinology* **142**: 3187-3197.

Joyce IM, Pendola FL, Wigglesworth K, Eppig JJ. 1999. Oocyte regulation of kit ligand expression in mouse ovarian follicles. *Dev Biol* **214**: 342-353.

Kaivo-oja N, Jeffery LA, Ritvos O, Mottershead DG. 2006. Smad signalling in the ovary. *Reprod Biol Endocrinol* **4**: 21.

Kanitz W, Brussow K-P, Becker F, Torner H, Schneider F, Kubelka M, Tomek W. 2001. Comparative Aspects of Follicular Development, Follicular and Oocyte Maturation and Ovulation in Cattle and Pigs. *Arch Tierz, Dummerstorf* **44**: 9-23.

Katz-Jaffe MG, McCallie BR, Preis KA, Filipovits J, Gardner DK. 2009. Transcriptome analysis of in vivo and in vitro matured bovine MII oocytes. *Theriogenology* **71**: 939-946.

Kidder GM, Mhawi AA. 2002. Gap junctions and ovarian folliculogenesis. *Reproduction* **123**: 613-620.

Kidder GM, Vanderhyden BC. 2010. Bidirectional communication between oocytes and follicle cells: ensuring oocyte developmental competence. *Can J Physiol Pharmacol* **88**: 399-413.

Kim D, Langmead B, Salzberg SL. 2015. HISAT: a fast spliced aligner with low memory requirements. *Nat Methods* **12**: 357-360.

Kim JH, Richter JD. 2006. Opposing polymerase-deadenylase activities regulate cytoplasmic polyadenylation. *Mol Cell* **24**: 173-183.

Kimble KM, Dickinson SE, Biase FH. 2018. Extraction of total RNA from single-oocytes and single-cell mRNA sequencing of swine oocytes. *BMC Res Notes* **11**: 155.

Kinsella RJ, Kähäri A, Haider S, Zamora J, Proctor G, Spudich G, Almeida-King J, Staines D, Derwent P, Kerhornou A et al. 2011. Ensembl BioMarts: a hub for data retrieval across taxonomic space. *Database* **2011**: bar030.

Kline D. 2000. Attributes and dynamics of the endoplasmic reticulum in mammalian eggs. *Curr Top Dev Biol* **50**: 125-154.

Klinger FG, De Felici M. 2002. In vitro development of growing oocytes from fetal mouse oocytes: stage-specific regulation by stem cell factor and granulosa cells. *Dev Biol* **244**: 85-95.

Knight PG, Glister C. 2006. TGF-beta superfamily members and ovarian follicle development. *Reproduction* **132**: 191-206.

Kreeger PK, Fernandes NN, Woodruff TK, Shea LD. 2005. Regulation of mouse follicle development by follicle-stimulating hormone in a three-dimensional in vitro culture system is dependent on follicle stage and dose. *Biol Reprod* **73**: 942-950.

Kruip TAM, Cran DG, van Beneden TH, Dieleman SJ. 1983. Structural changes in bovine oocytes during final maturation in vivo. *Gamete Res* **8**: 29-47.

Kussano NR, Leme LO, Guimaraes AL, Franco MM, Dode MA. 2016. Molecular markers for oocyte competence in bovine cumulus cells. *Theriogenology* **85**: 1167-1176.

Kyogoku H, Kitajima TS, Miyano T. 2014. Nucleolus precursor body (NPB): a distinct structure in mammalian oocytes and zygotes. *Nucleus* **5**: 493-498.

Langfelder P, Horvath S. 2008. WGCNA: an R package for weighted correlation network analysis. *BMC bioinformatics* **9**: 559.

Langfelder P, Horvath S. 2012. Fast R Functions for Robust Correlations and Hierarchical Clustering. *J Stat Softw* **46**: i11.

Langfelder P, Zhang B, Horvath S. 2008. Defining clusters from a hierarchical cluster tree: the Dynamic Tree Cut package for R. *Bioinformatics* **24**: 719-720.

Langmead B, Salzberg SL. 2012. Fast gapped-read alignment with Bowtie 2. *Nat methods* **9**: 357-359.

Law CW, Alhamdoosh M, Su S, Smyth GK, Ritchie ME. 2016. RNA-seq analysis is easy as 1-2-3 with limma, Glimma and edgeR. *F1000Res* **5**: 1408.

Li GP, Liu Y, Bunch TD, White KL, Aston KI. 2005. Asymmetric division of spindle microtubules and microfilaments during bovine meiosis from metaphase I to metaphase III. *Mol Reprod Dev* **71**: 220-226.

Li R, Albertini DF. 2013. The road to maturation: somatic cell interaction and self-organization of the mammalian oocyte. *Nat Rev Mol Cell Biol* **14**: 141-152.

Lingenfelter BM, Dailey RA, Inskeep EK, Vernon MW, Poole DH, Rhinehart JD, Yao J. 2007. Changes of maternal transcripts in oocytes from persistent follicles in cattle. *Mol Reprod Dev* **74**: 265-272.

Liu M. 2011. The biology and dynamics of mammalian cortical granules. *Reprod Biol Endocrinol* **9**: 149.

Liu Q, Li Y, Feng Y, Liu C, Ma J, Li Y, Xiang H, Ji Y, Cao Y, Tong X et al. 2016. Single-cell analysis of differences in transcriptomic profiles of oocytes and cumulus cells at GV, MI, MII stages from PCOS patients. *Sci Rep* **6**: 39638.

Liu Z, Fan HY, Wang Y, Richards JS. 2010. Targeted disruption of Mapk14 (p38MAPKalpha) in granulosa cells and cumulus cells causes cell-specific changes in gene expression profiles that rescue COC expansion and maintain fertility. *Mol Endocrinol* **24**: 1794-1804.

Lodde V, Modina S, Maddox-Hyttel P, Franciosi F, Lauria A, Luciano AM. 2008. Oocyte morphology and transcriptional silencing in relation to chromatin remodeling during the final phases of bovine oocyte growth. *Mol Reprod Dev* **75**: 915-924.

Love MI, Huber W, Anders S. 2014. Moderated estimation of fold change and dispersion for RNA-seq data with DESeq2. *Genome Biol* **15**: 550.

Lucas X, Martinez EA, Roca J, Vazquez JM, Gil MA, Pastor LM, Alabart JL. 2002. Relationship between antral follicle size, oocyte diameters and nuclear maturation of immature oocytes in pigs. *Theriogenology* **58**: 871-885.

Ma JY, Li M, Luo YB, Song S, Tian D, Yang J, Zhang B, Hou Y, Schatten H, Liu Z et al. 2013. Maternal factors required for oocyte developmental competence in mice: transcriptome analysis of non-surrounded nucleolus (NSN) and surrounded nucleolus (SN) oocytes. *Cell Cycle* **12**: 1928-1938.

Macaulay AD, Gilbert I, Caballero J, Barreto R, Fournier E, Tossou P, Sirard MA, Clarke HJ, Khandjian EW, Richard FJ et al. 2014. The gametic synapse: RNA transfer to the bovine oocyte. *Biol Reprod* **91**: 90.

Macaulay AD, Gilbert I, Scantland S, Fournier E, Ashkar F, Bastien A, Saadi HA, Gagne D, Sirard MA, Khandjian EW et al. 2016. Cumulus Cell Transcripts Transit to the Bovine Oocyte in Preparation for Maturation. *Biol Reprod* **94**: 16.

Machaca K. 2007. Ca2+ signaling differentiation during oocyte maturation. *J Cell Physiol* **213**: 331-340.

Magoffin DA. 2005. Ovarian theca cell. *Int J Biochem Cell Biol* **37**: 1344-1349.

Mao L, Lou H, Lou Y, Wang N, Jin F. 2014. Behaviour of cytoplasmic organelles and cytoskeleton during oocyte maturation. *Reprod Biomed Online* **28**: 284-299.

McLaughlin EA, McIver SC. 2009. Awakening the oocyte: controlling primordial follicle development. *Reproduction* **137**: 1-11.

Mehlmann LM, Kalinowski RR, Ross LF, Parlow AF, Hewlett EL, Jaffe LA. 2006. Meiotic resumption in response to luteinizing hormone is independent of a Gi family G protein or calcium in the mouse oocyte. *Dev Biol* **299**: 345-355.

Melo EO, Cordeiro DM, Pellegrino R, Wei Z, Daye ZJ, Nishimura RC, Dode MA. 2017. Identification of molecular markers for oocyte competence in bovine cumulus cells. *Anim Genet* **48**: 19-29.

Memili E, Dominko T, First NL. 1998. Onset of transcription in bovine oocytes and preimplantation embryos. *Mol Reprod Dev* **51**: 36-41.

Meric F, Searfoss AM, Wormington M, Wolffe AP. 1996. Masking and unmasking maternal mRNA. The role of polyadenylation, transcription, splicing, and nuclear history. *J Biol Chem* **271**: 30804-30810.

Molyneaux K, Wylie C. 2004. Primordial germ cell migration. *Int J Dev Biol* **48**: 537-544.

Monniaux D. 2016. Driving folliculogenesis by the oocyte-somatic cell dialog: Lessons from genetic models. *Theriogenology* **86**: 41-53.

Moore MJ. 2005. From birth to death: the complex lives of eukaryotic mRNAs. *Science* **309**: 1514-1518.

Mtango NR, Potireddy S, Latham KE. 2008. Oocyte quality and maternal control of development. *Int Rev Cell Mol Biol* **268**: 223-290.

Nagyova E, Camaioni A, Scsukova S, Mlynarcikova A, Prochazka R, Nemcova L, Salustri A. 2011. Activation of cumulus cell SMAD2/3 and epidermal growth factor receptor pathways are involved in porcine oocyte-cumulus cell expansion and steroidogenesis. *Mol Reprod Dev* **78**: 391-402.

Nilsson E, Rogers N, Skinner MK. 2007. Actions of anti-Mullerian hormone on the ovarian transcriptome to inhibit primordial to primary follicle transition. *Reproduction* **134**: 209-221.

Nivet AL, Vigneault C, Blondin P, Sirard MA. 2013. Changes in granulosa cells' gene expression associated with increased oocyte competence in bovine. *Reproduction* **145**: 555-565.

Noguchi M, Yoshioka K, Itoh S, Suzuki C, Arai S, Wada Y, Hasegawa Y, Kaneko H. 2010. Peripheral concentrations of inhibin A, ovarian steroids, and gonadotropins associated with follicular development throughout the estrous cycle of the sow. *Reproduction* **139**: 153-161.

Norris RP, Freudzon M, Mehlmann LM, Cowan AE, Simon AM, Paul DL, Lampe PD, Jaffe LA. 2008. Luteinizing hormone causes MAP kinase-dependent phosphorylation and closure of connexin 43 gap junctions in mouse ovarian follicles: one of two paths to meiotic resumption. *Development* **135**: 3229-3238.

Norris RP, Ratzan WJ, Freudzon M, Mehlmann LM, Krall J, Movsesian MA, Wang H, Ke H, Nikolaev VO, Jaffe LA. 2009. Cyclic GMP from the surrounding somatic cells regulates cyclic AMP and meiosis in the mouse oocyte. *Development* **136**: 1869-1878.

Nunes C, Silva JV, Silva V, Torgal I, Fardilha M. 2015. Signalling pathways involved in oocyte growth, acquisition of competence and activation. *Hum Fertil* **18**: 149-155.

Oh JS, Han SJ, Conti M. 2010. Wee1B, Myt1, and Cdc25 function in distinct compartments of the mouse oocyte to control meiotic resumption. *J Cell Biol* **188**: 199-207.

Ohinata Y, Payer B, O'Carroll D, Ancelin K, Ono Y, Sano M, Barton SC, Obukhanych T, Nussenzweig M, Tarakhovsky A et al. 2005. Blimp1 is a critical determinant of the germ cell lineage in mice. *Nature* **436**: 207-213.

Palermo R. 2007. Differential actions of FSH and LH during folliculogenesis. *Reprod Biomed Online* **15**: 326-337.

Pan H, Ma P, Zhu W, Schultz RM. 2008. Age-associated increase in aneuploidy and changes in gene expression in mouse eggs. *Dev Biol* **316**: 397-407.

Pan H, O'Brien M J, Wigglesworth K, Eppig JJ, Schultz RM. 2005. Transcript profiling during mouse oocyte development and the effect of gonadotropin priming and development in vitro. *Dev Biol* **286**: 493-506.

Panigone S, Hsieh M, Fu M, Persani L, Conti M. 2008. Luteinizing hormone signaling in preovulatory follicles involves early activation of the epidermal growth factor receptor pathway. *Mol Endocrinol* **22**: 924-936.

Patel OV, Bettegowda A, Ireland JJ, Coussens PM, Lonergan P, Smith GW. 2007. Functional genomics studies of oocyte competence: evidence that reduced transcript abundance for follistatin is associated with poor developmental competence of bovine oocytes. *Reproduction* **133**: 95-106.

Pepling ME. 2006. From primordial germ cell to primordial follicle: mammalian female germ cell development. *Genesis* **44**: 622-632.

Pepling ME, Spradling AC. 2001. Mouse ovarian germ cell cysts undergo programmed breakdown to form primordial follicles. *Dev Biol* **234**: 339-351.

Perez-Armendariz EM, Saez JC, Bravo-Moreno JF, Lopez-Olmos V, Enders GC, Villalpando I. 2003. Connexin43 is expressed in mouse fetal ovary. *Anat Rec A Discov Mol Cell Evol Biol* **271**: 360-367.

Persani L, Rossetti R, Di Pasquale E, Cacciatore C, Fabre S. 2014. The fundamental role of bone morphogenetic protein 15 in ovarian function and its involvement in female fertility disorders. *Hum Reprod Update* **20**: 869-883.

Petry S, Vale RD. 2015. Microtubule nucleation at the centrosome and beyond. *Nat Cell Biol* **17**: 1089-1093.

Picelli S, Faridani OR, Bjorklund AK, Winberg G, Sagasser S, Sandberg R. 2014a. Full-length RNA-seq from single cells using Smart-seq2. *Nat Protoc* **9**: 171-181.

Przygrodzka E, Kaczmarek MM, Kaczynski P, Ziecik AJ. 2016. Steroid hormones, prostanoids, and angiogenic systems during rescue of the corpus luteum in pigs. *Reproduction* **151**: 135-147.

Racedo SE, Rawe VY, Niemann H. 2012. Dynamic changes of the Golgi apparatus during bovine in vitro oocyte maturation. *Reproduction* **143**: 439-447.

Read CC, Willhelm G, Dyce PW. 2018. Connexin 43 coupling in bovine cumulus cells, during the follicular growth phase, and its relationship to in vitro embryo outcomes. *Mol Reprod Dev* doi:10.1002/mrd.22993.

Reader KL, Stanton J-AL, Juengel JL. 2017. The Role of Oocyte Organelles in Determining Developmental Competence. *Biology* **6**: 35.

Reyes JM, Chitwood JL, Ross PJ. 2015. RNA-Seq profiling of single bovine oocyte transcript abundance and its modulation by cytoplasmic polyadenylation. *Mol Reprod Dev* **82**: 103-114.

Richter JD. 2007. CPEB: a life in translation. *Trends Biochem Sci* **32**: 279-285.

Rimon-Dahari N, Yerushalmi-Heinemann L, Alyagor L, Dekel N. 2016. Ovarian Folliculogenesis. *Results Probl Cell Differ* **58**: 167-190.

Ritter LJ, Sugimura S, Gilchrist RB. 2015. Oocyte induction of EGF responsiveness in somatic cells is associated with the acquisition of porcine oocyte developmental competence. *Endocrinology* **156**: 2299-2312.

Rivera-Perez JA, Magnuson T. 2005. Primitive streak formation in mice is preceded by localized activation of Brachyury and Wnt3. *Dev Biol* **288**: 363-371.

Robinson MD, McCarthy DJ, Smyth GK. 2010a. edgeR: a Bioconductor package for differential expression analysis of digital gene expression data. *Bioinformatics* **26**: 139-140.

Robinson MD, Oshlack A. 2010. A scaling normalization method for differential expression analysis of RNA-seq data. *Genome Biol* **11**: R25.

Rodgers RJ, Irving-Rodgers HF. 2010. Morphological classification of bovine ovarian follicles. *Reproduction* **139**: 309-318.

Russell DL, Gilchrist RB, Brown HM, Thompson JG. 2016. Bidirectional communication between cumulus cells and the oocyte: Old hands and new players? *Theriogenology* **86**: 62-68.

Russell DL, Robker RL. 2007. Molecular mechanisms of ovulation: co-ordination through the cumulus complex. *Hum Reprod Update* **13**: 289-312.

Saitou M, Payer B, O'Carroll D, Ohinata Y, Surani MA. 2005. Blimp1 and the emergence of the germ line during development in the mouse. *Cell Cycle* **4**: 1736-1740.

Sanchez F, Smitz J. 2012. Molecular control of oogenesis. *Biochim Biophys Acta* **1822**: 1896-1912.

Sato Y, Cheng Y, Kawamura K, Takae S, Hsueh AJ. 2012. C-type natriuretic peptide stimulates ovarian follicle development. *Mol Endocrinol* **26**: 1158-1166.

Scaramuzzi RJ, Baird DT, Campbell BK, Driancourt MA, Dupont J, Fortune JE, Gilchrist RB, Martin GB, McNatty KP, McNeilly AS et al. 2011. Regulation of folliculogenesis and the determination of ovulation rate in ruminants. *Reprod Fertil Dev* **23**: 444-467.

Schrader C, Schielke A, Ellerbroek L, Johne R. 2012. PCR inhibitors - occurrence, properties and removal. *J Appl Microbiol* **113**: 1014-1026.

Schwarz T, Kopyra M, Nowicki J. 2008. Physiological mechanisms of ovarian follicular growth in pigs--a review. *Acta Vet Hung* **56**: 369-378.

Sirard MA. 2001. Resumption of meiosis: mechanism involved in meiotic progression and its relation with developmental competence. *Theriogenology* **55**: 1241-1254.

Sirard MA, Florman HM, Leibfried-Rutledge ML, Barnes FL, Sims ML, First NL. 1989. Timing of nuclear progression and protein synthesis necessary for meiotic maturation of bovine oocytes. *Biol Reprod* **40**: 1257-1263.

Smirnov AV, Entelis NS, Krasheninnikov IA, Martin R, Tarassov IA. 2008. Specific Features of 5S rRNA Structure - Its Interactions with Macromolecules and Possible Functions. *Biochemistry-Moscow* **73**: 1418-1437 .

Soede N, Hazeleger W, Kemp B. 1998. Follicle Size and the Process of Ovulation in Sows as Studied with Ultrasound *Reprod Dom Anim* **33**.

Soede NM, Langendijk P, Kemp B. 2011. Reproductive cycles in pigs. *Anim Reprod Sci* **124**: 251-258.

Stebler J, Spieler D, Slanchev K, Molyneaux KA, Richter U, Cojocaru V, Tarabykin V, Wylie C, Kessel M, Raz E. 2004. Primordial germ cell migration in the chick and mouse embryo: the role of the chemokine SDF-1/CXCL12. *Dev Biol* **272**: 351-361.

Steffen W, Karki S, Vaughan KT, Vallee RB, Holzbaur EL, Weiss DG, Kuznetsov SA. 1997. The involvement of the intermediate chain of cytoplasmic dynein in binding the motor complex to membranous organelles of Xenopus oocytes. *Mol Biol Cell* **8**: 2077-2088.

Sternlicht AL, Schultz RM. 1981. Biochemical studies of mammalian oogenesis: kinetics of accumulation of total and poly(A)-containing RNA during growth of the mouse oocyte. *J Exp Zool* **215**: 191-200.

Steuerwald N, Cohen J, Herrera RJ, Sandalinas M, Brenner CA. 2001. Association between spindle assembly checkpoint expression and maternal age in human oocytes. *Mol Hum Reprod* **7**: 49-55.

Steuerwald NM, Bermudez MG, Wells D, Munne S, Cohen J. 2007. Maternal age-related differential global expression profiles observed in human oocytes. *Reprod Biomed Online* **14**: 700-708.

Stojkovic M, Machado SA, Stojkovic P, Zakhartchenko V, Hutzler P, Goncalves PB, Wolf E. 2001. Mitochondrial distribution and adenosine triphosphate content of bovine oocytes before and after in vitro maturation: correlation with morphological criteria and developmental capacity after in vitro fertilization and culture. *Biol Reprod* **64**: 904-909.

Sugiura K, Su YQ, Diaz FJ, Pangas SA, Sharma S, Wigglesworth K, O'Brien MJ, Matzuk MM, Shimasaki S, Eppig JJ. 2007. Oocyte-derived BMP15 and FGFs cooperate to promote glycolysis in cumulus cells. *Development* **134**: 2593-2603.

Sugiura K, Su YQ, Li Q, Wigglesworth K, Matzuk MM, Eppig JJ. 2010. Estrogen promotes the development of mouse cumulus cells in coordination with oocyte-derived GDF9 and BMP15. *Mol Endocrinol* **24**: 2303-2314.

Sun QY. 2003. Cellular and molecular mechanisms leading to cortical reaction and polyspermy block in mammalian eggs. *Microsc Res Tech* **61**: 342-348.

Sun QY, Schatten H. 2006. Regulation of dynamic events by microfilaments during oocyte maturation and fertilization. *Reproduction* **131**: 193-205.

Takeo S, Kawahara-Miki R, Goto H, Cao F, Kimura K, Monji Y, Kuwayama T, Iwata H. 2013. Age-associated changes in gene expression and developmental competence of bovine oocytes, and a possible countermeasure against age-associated events. *Mol Reprod Dev* **80**: 508-521.

Tang F, Barbacioru C, Wang Y, Nordman E, Lee C, Xu N, Wang X, Bodeau J, Tuch BB, Siddiqui A et al. 2009. mRNA-Seq whole-transcriptome analysis of a single cell. *Nat methods* **6**: 377-382.

Tarazona AM, Rodriguez JI, Restrepo LF, Olivera-Angel M. 2006. Mitochondrial activity, distribution and segregation in bovine oocytes and in embryos produced in vitro. *Reprod Domest Anim* **41**: 5-11.

Tesfaye D, Ghanem N, Carter F, Fair T, Sirard MA, Hoelker M, Schellander K, Lonergan P. 2009. Gene expression profile of cumulus cells derived from cumulus-oocyte complexes matured either in vivo or in vitro. *Reprod Fertil Dev* **21**: 451-461.

Tesson BM, Breitling R, Jansen RC. 2010. DiffCoEx: a simple and sensitive method to find differentially coexpressed gene modules. *BMC Bioinformatics* **11**: 497.

Timmons JA, Szkop KJ, Gallagher IJ. 2015. Multiple sources of bias confound functional enrichment analysis of global -omics data. *Genome Biol* **16**: 186.

Tripathi A, Kumar KV, Chaube SK. 2010. Meiotic cell cycle arrest in mammalian oocytes. *J Cell Physiol* **223**: 592-600.

Tsai PS, van Haeften T, Gadella BM. 2011. Preparation of the cortical reaction: maturation-dependent migration of SNARE proteins, clathrin, and complexin to the porcine oocyte's surface blocks membrane traffic until fertilization. *Biol Reprod* **84**: 327-335.

Tsuda M, Sasaoka Y, Kiso M, Abe K, Haraguchi S, Kobayashi S, Saga Y. 2003. Conserved role of nanos proteins in germ cell development. *Science* **301**: 1239-1241.

Vaccari S, Weeks JL, 2nd, Hsieh M, Menniti FS, Conti M. 2009. Cyclic GMP signaling is involved in the luteinizing hormone-dependent meiotic maturation of mouse oocytes. *Biol Reprod* **81**: 595-604.

Wang JJ, Ge W, Liu JC, Klinger FG, Dyce PW, De Felici M, Shen W. 2017. Complete in vitro oogenesis: retrospects and prospects. *Cell Death Differ* **24**:1845-1852.

Watson AJ. 2007. Oocyte cytoplasmic maturation: a key mediator of oocyte and embryo developmental competence. *J Anim Sci* **85**: E1-3.

Wear HM, McPike MJ, Watanabe KH. 2016. From primordial germ cells to primordial follicles: a review and visual representation of early ovarian development in mice. *J Ovarian Res* **9**: 36.

Wigglesworth K, Lee KB, Emori C, Sugiura K, Eppig JJ. 2015. Transcriptomic diversification of developing cumulus and mural granulosa cells in mouse ovarian follicles. *Biol Reprod* **92**: 23.

Wilhelm D, Englert C. 2002. The Wilms tumor suppressor WT1 regulates early gonad development by activation of Sf1. *Genes Dev* **16**: 1839-1851.

Wilhelm D, Palmer S, Koopman P. 2007. Sex determination and gonadal development in mammals. *Physiol Rev* **87**: 1-28.

Williams CJ, Erickson GF. 2000. Morphology and Physiology of the Ovary. In *Endotext*, (ed. LJ De Groot, et al.), South Dartmouth (MA).

Wilmut I, Bai Y, Taylor J. 2015. Somatic cell nuclear transfer: origins, the present position and future opportunities. *Philos Trans R Soc Lond B Biol Sci* **370**: 20140366.

Wright CS, Hovatta O, Margara R, Trew G, Winston RM, Franks S, Hardy K. 1999. Effects of follicle-stimulating hormone and serum substitution on the in-vitro growth of human ovarian follicles. *Hum Reprod* **14**: 1555-1562.

Xu M, West-Farrell ER, Stouffer RL, Shea LD, Woodruff TK, Zelinski MB. 2009. Encapsulated three-dimensional culture supports development of nonhuman primate secondary follicles. *Biol Reprod* **81**: 587-594.

Xue Z, Huang K, Cai C, Cai L, Jiang C-Y, Feng Y, Liu Z, Zeng Q, Cheng L, Sun YE et al. 2013. Genetic programs in human and mouse early embryos revealed by single-cell RNA sequencing. *Nature* **500**: 593-597.

Yin XY, Cheng GH, Guo HY, Wang Q, Li YJ, Zhang H. 2017. Single cell transcriptome profiling revealed differences in gene expression during oocyte maturation in Haimen white goats. *Genet Mol Res* **16** (1).

Young JM, McNeilly AS. 2010. Theca: the forgotten cell of the ovarian follicle. *Reproduction* **140**: 489-504.

Young MD, Wakefield MJ, Smyth GK, Oshlack A. 2010. Gene ontology analysis for RNA-seq: accounting for selection bias. *Genome biol* **11**: R14.

Yu J, Russell JE. 2001. Structural and functional analysis of an mRNP complex that mediates the high stability of human beta-globin mRNA. *Mol Cell Biol* **21**: 5879-5888.

Yuan Y, Ida JM, Paczkowski M, Krisher RL. 2011. Identification of developmental competence-related genes in mature porcine oocytes. *Mol Reprod Dev* **78**: 565-575.

Zhang T, Li Y, Li H, Ma XS, Ouyang YC, Hou Y, Schatten H, Sun QY. 2017. RNA-associated protein LSM family member 14 controls oocyte meiotic maturation through regulating mRNA pools. *J Reprod Dev* **63**: 383-388.